DEPOSITIONAL CHARACTERIZATION OF THE EAU CLAIRE FORMATION AT THE ILLINOIS BASIN – DECATUR PROJECT: FACIES, MINERALOGY AND GEOCHEMISTRY

BY

MARTIN J. PALKOVIC

THESIS

Submitted in partial fulfillment of the requirements
for the degree of Master of Science in Geology
in the Graduate College of the
University of Illinois at Urbana-Champaign, 2015

Urbana, Illinois

Advisers:

Professor Craig C. Lundstrom
Assistant Geologist Jared T. Freiburg

ABSTRACT

The Cambrian-age Eau Claire Formation serves as the primary seal at the Illinois Basin – Decatur Project (IBDP), a one million tonne carbon capture and storage demonstration project located in Decatur, Illinois. The Eau Claire Formation conformably overlies the Mt. Simon Sandstone, the reservoir for the IBDP. At the IBDP site, analysis of drill core and geophysical logs reveals the Eau Claire consists of two major lithostratigraphic units: a siliciclastic dominant lower unit and a carbonate dominant upper unit. Within the Eau Claire, four major depositional facies exist within a tidally influenced, shallow marine depositional environment. These include (Unit A) intertidal mixed sand/mud flats and tidal channels of the foreshore environment; (Unit B) subtidal deposits of the offshore transition zone; (Unit C) subtidal deposits of the upper shoreface environment; and (Unit D) subtidal mixed carbonate/siliciclastic deposits. An approximately +8‰ $\delta^{13}C$ excursion ($R^2 = 0.97$) defines the Eau Claire at the IBDP site, possibly correlative with the Steptoean positive carbon isotope excursion (SPICE) found worldwide 500–495 Ma ago. This study aims to elucidate the depositional environment, seal quality, age and provenance of the Eau Claire Formation in central Illinois.

The mineralogy of the four depositional facies varies widely throughout the Eau Claire, with a persistently high K-feldspar content. The K-feldspar mode averages 8.7% for the formation and reaches an average of 20.3% in Unit C. Unit A is approximately 30 ft. (9.1 m) thick and exhibits intense bioturbation, ripple beds, and flaser/lenticular bedding, with an average porosity and permeability (n = 20) of 6.7% and 8.6 mD. Unit B is an approximately 40 ft. (12.2 m) thick tight shale sequence, with thin siltstones interbedded throughout. Unit B represents the most desirable seal facies in the formation with an average porosity (n=9) and permeability (n=4) of 5.6% and 2.0×10^{-5} mD. Unit C is the largest siliciclastic unit in the formation, spanning an average of 95 ft. (29 m) in all three wells at the IBDP. Unit C exhibits the classic tidalite signature of rhythmically interbedded siltstones and shales, with an average porosity and permeability (n = 50) of 9.4% and 0.9 mD. Unit D spans approximately 345 ft. (105.2 m) and begins as a mixed siliciclastic/carbonate environment, slowly becoming a dolomitized carbonate shelf dominated by oolitic packstone and grainstone.

ACKNOWLEDGEMENTS

I would like to express deep gratitude to Jared Freiburg for giving me the opportunity to work on this project, and providing me with hours of meaningful discussion, feedback and guidance. I have vastly expanded my knowledge of geology as a result of the remarkable experience I have had at the University of Illinois at Urbana-Champaign (UIUC) and am eternally grateful for this opportunity. I would also like to thank Craig Lundstrom for opening my eyes to the exciting world of isotope geochemistry. I very much enjoyed that portion of the project and loved working with the data. Many thanks to both Jared and Craig whose edits significantly strengthened this document. Thank you to Sallie Greenberg and Rob Finley at the Illinois State Geological Survey (ISGS) for awarding me a Graduate Research Assistantship for two consecutive years, which funded me during my time at the UIUC. Thank you to Scott Frailey for providing me with the opportunity work at the ISGS as a student assistant. Thank you to Qina Yan for conducting grain size analyses for this project. Thank you to Dana Labotka for engaging discussion of isotope geochemistry in regards to this project. And lastly, thank you to my girlfriend Elizabeth, my parents, the Advanced Energy Technology Division at the ISGS, and all of the graduate students at UIUC who offered support and feedback along the way, it has been an incredible journey.

TABLE OF CONTENTS

CHAPTER 1: INTRODUCTION

1.1 Carbon Capture and Storage

Meeting the energy demands of the future while simultaneously decreasing greenhouse gas emissions (GHG) is one of the greatest challenges we face in the twenty-first century. The average annual surface temperature may increase 1-6 °Celsius (C) by 2070 if atmospheric concentrations of CO_2 continue to increase at their current rate, causing major implications worldwide (Shukla et al. 2010). Carbon capture and storage (CCS), the process of capturing and storing anthropogenic CO_2 in geological formations, promises to be an excellent climate mitigation technique (Pacala and Socolow 2004; Bachu et al. 2008; Oelkers and Cole 2008; Liu et al. 2012). Storage options include deep saline reservoirs, depleted oil and gas reservoirs, and unmineable coal beds (Benson and Cole 2008; Shukla et al. 2010). Deep geologic formations in sedimentary basins offer several advantages over other options. Often, these reservoirs contain abundant interconnected pore networks, suitable for storing vast quantities of CO_2 (Bachu 2003). Waters deep in the crust are hypersaline with high total dissolved solids (TDS) concentrations, unfit for human consumption or industrial/agricultural use. High pressures within formations deeper than 2,560 ft. (800 m) ensure that CO_2 will remain in the supercritical phase (pressures greater than 7.38 MPa, temperatures greater than 31.1 °C) (Bachu 2000; Benson and Cole 2008). Candidates for CCS reservoirs should meet all the above criteria, be adequately permeable so injection can occur at high flow rates, and possess at least one thick, impermeable sealing unit overlying the reservoir (Benson and Cole 2008). Because CO_2 is buoyant, a caprock of high integrity is necessary to contain the sequestered CO_2. The most current estimates for storage capacity in North America range from 1160 to 3500 Billion tons of CO_2, encompassing storage in saline reservoirs, depleted oil and gas reservoirs, and deep unmineable coal beds (DOE 2007).

Numerous CCS demonstration-scale projects (for the purpose of research, and verification of technology) and commercial-scale projects (for the purpose of reducing GHG emissions) currently operate worldwide. The Illinois Basin – Decatur Project (IBDP), located in Macon County, Illinois, is part of the Midwest Geological Sequestration Consortium's (MGSC) effort to demonstrate large-scale CCS. The IBDP is a joint project between the Illinois State Geological Survey (ISGS) Advanced Energy Technology Initiative division, Schlumberger Carbon Services, and Archer Daniels Midland (ADM). The IBDP injected 1,000 metric tons per day into the Cambrian-age Mt. Simon Sandstone, operating over a 3-year period with injection concluding on November 24th 2014. The

Cambrian-age Eau Claire Formation conformably overlies the Mt. Simon, serving as the primary sealing unit for the IBDP. Additionally, the Ordovician-age Maquoketa Shale and the Devonian/Mississippian-age New Albany Shale serve as back up seals. ADM's corn-processing facility in Decatur, Illinois, hosts four wells at the IBDP's sequestration site **(Fig. 1.1)**. The injection well (CCS#1) reaches a maximum depth of 7,236 ft. (2,205 m). The CCS#1 well has three perforation zones for CO_2 injection at 6977 to 6978 ft. (2126 m), 6982 to 7012 ft. (2128-2137 m), and 7025 to 7050 ft. (2141-2149 m). The second well, the Verification #1 well (VW#1), is located approximately 1,008 ft. (307 m) north of the CCS#1 well, and is used to monitor the CO_2 plume. The third well, the Verification #2 well (VW#2), also functions as a monitoring well, and is located approximately 1 mi (1.6 km) north of the CCS #1 well. (Freiburg et al. 2014). A second injection well (CCS#2) is being drilled at the time of writing. Initial site characterization in Decatur revealed that the Eau Claire contains a thick shale zone near its base, which could effectively serve as the primary sealing unit for a carbon sequestration project. This study aims to characterize the seal quality of the thick shale zone, and ultimately characterize all depositional facies within the Eau Claire to determine the sealing quality of the unit.

1.2 Objectives

The objective of this research is to study the depositional environments, mineralogy, and geochemistry of the Eau Claire Formation, the primary seal at the IBDP, and to assess its viability as a CCS caprock. This is a site-specific study at the IBDP site with the larger goal of serving as a framework for regional correlation and characterization beyond the IBDP site. This study uses detailed correlations between drill cores, wireline logs and laboratory data to determine which Eau Claire facies have the highest potential of containing CO_2 within the underlying Mt. Simon Sandstone. CCS seals require impermeable rock with sufficiently low porosity to prevent buoyant CO_2 from migrating upwards into shallow groundwater aquifers. An additional requirement is chemical stability; the caprock must remain near chemical equilibrium with CO_2 rich brines for millions of years, engaging in as few chemical reactions as possible. Isotopic analyses will be used for establishing a framework to interpret CO_2-H_2O-rock interaction, with the added goal of interpreting provenance and the age of the formation.

Lastly, a laterally extensive formation capable of serving numerous CCS projects in a single basin is desirable. This study puts the largest emphasis on interpreting the depositional environments and facies within the

Eau Claire to build a conceptual framework for interpreting quantitative data for the formation. This includes petrophysical, textural, and mineralogical analyses to classify facies and determine which have the highest sealing capacity. All facies are put in context architecturally into larger depositional models to imply lateral continuity.

Numerous investigators have characterized the Mt. Simon throughout the Illinois Basin and Midwestern United States (Hoholick et al 1984; Duffin 1989; Morse and Leetaru 2005; Leetaru et al. 2008; Fischietto 2009; Medina et al. 2010, 2011; Bowen et al. 2011; Medina and Rupp 2012; Freiburg et al. 2014). Comparatively, work on the Eau Claire formation has been minimal, focused largely in Indiana, Kentucky, Wisconsin, or outside of the Illinois Basin (Walcott 1914; Aswasereelrt et al. 2008; Bandy 2012; Neufelder et al. 2012; Lahann et al. 2014). No previous study has utilized such a comprehensive suite of core to study the Eau Claire formation in the central part of the Illinois Basin. Previous unpublished commercial laboratory data, including routine core analysis (porosity/permeability), X-ray diffraction (XRD), and permeability estimated from mercury injection – capillary pressure (MICP) data is presented in addition to the author's work.

Fig. 1.1. Aerial site photo of the IBDP. CO_2 is compressed into the supercritical state, transported 1 mile along a pipeline, and injected into the CCS#1 well at a depth of ~7,000 ft. (2,134 m) into the Lower Mt. Simon Sandstone.

CHAPTER 2: GEOLOGIC SETTING

2.1 Illinois Basin

The IBDP resides within the north central portion of the Illinois Basin, a 285,000 km^2 (110,000 mi^2) structural and depositional basin in the North American craton (Laurentia) filled with a thick succession of Paleozoic sedimentary rocks (Collinson et al. 1988; Kolata and Nelson 1991). The Illinois Basin covers most of Illinois, a large portion of southwestern Indiana, western Kentucky, and small areas of Missouri and Tennessee (Collinson et al. 1988) **(Fig. 2.1)**. Precambrian crystalline basement underlies these sedimentary rocks, composed predominantly of granite, granodiorite or rhyolite (Bradbury and Atherton, 1965). Basement rocks underneath the Illinois Basin are part of the Eastern Granite-Rhyolite Province (EGRP), a 1.48-1.38 billion year (Ga) old igneous complex that covers a large swath of the Midwestern United States (Bickford et al. 1986; Lidiak 1996; Van Schmus et al. 1996). The contact between the lowermost sedimentary unit (Mt. Simon) and the Precambrian basement is a nonconformity, often referred to as the 'great unconformity' or the 'sub-sauk unconformity', encompassing 600 to 900 Million years (Ma) of missing time in the rock record (Wilman et al. 1975; Yochelson 2006). Initial basin subsidence formed the proto-Illinois Basin in the Neoproterozoic to late Cambrian, resulting in deposition of the Mt Simon Sandstone over northeastern Illinois (Kolata and Nelson 2010). The cause of the initial subsidence is uncertain. A rifting origin, commonly observed in intracratonic basins, seems unlikely due to the absence of mafic rocks in the basement, which are typically a component of rift systems (Bickford et al. 1986). Rift basins typically exhibit some degree of linearity, whereas the proto-Illinois Basin exhibits an elliptical shape. McBride et al. (2003, 2010) suggested that the proto-Illinois Basin formed due to caldera collapse, citing the similarities of the basin geometry to calderas in the nearby St. Francois Mountains of east central Missouri. Arcuate faults also bind the flanks of the proto – Illinois Basin, a typical component of calderas (Kolata and Nelson 2010).

North America was part of the supercontinent Rodinia in the Neoproterozoic, which began to break up around 750 Ma due to rifting along Laurentia's western margin (Li et al. 2008). The New Madrid Rift System, one of numerous rift systems that developed along Laurentian margins over the next 200 Ma, exhibits a large control on the geometry of the Illinois Basin's southern border. The northeast trending Realfoot Rift extends from the paleocratonic margin of Rodinia into southern Illinois, where it turns sharply eastward into western Kentucky, forming the Rough Creek Graben. By late Cambrian time lithospheric thinning had largely concluded, and the New

Madrid Rift System gradually changed to a slowly subsiding cratonic trough or embayment plunging southwest towards the deeper ocean (Kolata and Nelson 2010). Rates of subsidence and sedimentation were greatest in the Rough Creek Graben, where the basin attains a maximum thickness of 30,000 ft. (9,100 m), comprising the depocenter of the Illinois Basin (Nelson 2010). The Ozark Dome was uplifted from the middle Silurian through Early Devonian, creating the present day western margin of the basin (Nelson and Marshak 1996). Subsidence continued through the remainder of the Paleozoic, until continental collision with the African and South American plates caused the Ouachita Orogeny, forming Pangea (Kolata and Nelson 2010). The formation of Pangea cut the Illinois Basin off from the ocean, but it remained a shallow epeiric sea until the early Permian, where elevation of the Pascola Arch in the south gave the basin its present shape (Nelson 2010).

2.2 Mt. Simon Sandstone

The Cambrian age Mt. Simon Sandstone serves as the reservoir unit for the IBDP. Fine- to coarse-grained, partly pebbly, poorly sorted, arenaceous to arkosic sandstone primarily composes the Mt. Simon, with lenses of mudstone found throughout (Kolata 2010; Freiburg et al. 2014). The Mt. Simon is approximately 1,500 ft. (457 m) thick at the IBDP site, and reaches a maximum thickness of 2,600 ft. (792 m) in northeastern Illinois. This area does not correspond to the depocenter of all other overlying strata in the Illinois Basin, which reach their maximum thickness in southeastern Illinois (Nelson 2010; Freiburg et al. 2014). Besides trace fossils in the Upper Mt. Simon (Morse and Leetaru 2005), the Mt. Simon is devoid of fossils, such that constraining a relative age is difficult. Stratigraphic correlation with the overlying Eau Claire Formation, which contains late Cambrian fossils, indicates an age of middle to late Cambrian (Kolata 2010). The Mt. Simon is part of the Potsdam supergroup, and represents the lowermost member of the Sauk transgressive sequence (Sloss 1963; Wilman 1975). The Mt. Simon exists in almost all of Illinois and parts of Wisconsin, Indiana, Iowa, Michigan, and Ohio, with correlative units in Missouri (Lamotte Sandstone), and Minnesota (Fond du Lac Sandstone) (Buschbach, 1964; Bowen et al. 2011). No outcrop exposures of the Mt. Simon Sandstone exist within Illinois (Bowen et al. 2011; Freiburg et al. 2014). Historically, most Illinois Basin researchers have interpreted the Mt. Simon as a shallow, subtidal marine environment based on outcrop studies in southern Wisconsin and core from the Illinois Basin (Droste and Shaver 1983; Driese et al. 1981; Sargent and Lasemi 1993; Morse and Leetaru 2005). Specifically, Morse and Leetaru (2005) mentioned the presence

of *Skolithos* and *Planolites* burrows within intertidal Mudstones in the Upper Mt. Simon, indicative of a shallow marine nearshore environment. Previous work centered entirely on the Upper Mt. Simon, and until the IBDP project, no core was available from the Lower and Middle Mt. Simon within the Illinois Basin. Freiburg et al. (2014) studied the Lower and Middle Mt. Simon at the IBDP, interpreting them as dominantly fluvial braided river deposits with occasional eolian influence. Evidence includes lack of marine indicators such as body or trace fossils, fining upward channel and bar sequences, abundant coarse grains and polycrystalline granules and pebbles, all of which are typical in braided rivers and alluvial fan deposits (Miall 1977).

2.3 Eau Claire Formation

C.D. Walcott, a famous invertebrate paleontologist, first described the Eau Claire Formation near Eau Claire, Wisconsin, noting a 100 ft. outcrop of thinly bedded, partly shaly, fossiliferous sandstone (Walcott 1914). In the Illinois Basin, the lower Eau Claire consists of siltstones, shales, and sandstones (very fine to fine grained), and is variably arkosic, clayey, glauconitic, dolomitic, and micaceous (Gutstadt 1958; Wilman et al. 1975; Becker et al. 1978; Palmer 1982; Ostrom 1978; Neufelder et al. 2012; Lahann et al. 2014). The upper Eau Claire consists of dolomite and siltstone, and correlates with the Bonneterre Formation of eastern Missouri (Buschbach 1975; Treworgy et al. 1997). At the IBDP site, siltstone and shale dominate the lithology of the Eau Claire's lower half, with siltstone and dolomitic limestone comprising the upper half. The Eau Claire spans the entire state of Illinois in the subsurface, and no outcrop exposures exist within the state (Kolata 2010). Thickness of the formation ranges from approximately 100 ft. (61 m) in western Illinois (Buschbach 1975) to more than 1,200 ft. (370 m) in southernmost Illinois **(Fig. 2.2)** (Sargent 1991). The Eau Claire reaches a maximum thickness of approximately 2,750 ft. (838 m) in the Rough Creek Graben of western Kentucky, corresponding with the Illinois basin depocenter (Wilman et al. 1975; Sargent 1991). In northeastern Iowa, Eau Claire outcrops contain *Cedaria*, *Crepicephalus*, *Aphelaspis*, and *Dunderbergia* Zone trilobite faunas (Mckay 1988). The laterally equivalent Bonneterre Formation also contains the *Crepicephalus* and *Aphelaspis* Zone trilobite faunas (Thompson 1995), confirming that the Eau Claire/Bonneterre in Iowa and Missouri is Dresbachian (501-497 Ma) in age (Kolata 2010). In the Illinois Basin, poorly defined faunal zones for the Eau Claire have made absolute age constraints difficult. The Knox Supergroup

overlies the Eau Claire in the Illinois Basin, and some authors consider the Eau Claire to be a member of the Knox (Wilman et al. 1975).

The Eau Claire exists in numerous Midwestern states, including Indiana, Wisconsin, Missouri, Iowa, Kentucky and Ohio, and is considered to be middle to late Cambrian in age (Avila 1981; Palmer, 1982; Mckay 1988; Babcock 1994; Thompson 1995; Kolata 2010). In Indiana, the Eau Claire conformably overlies the Mt. Simon Sandstone. It reaches a maximum depth of 1000 ft. (305 m) in southwest Indiana and thins to 393 ft. (120 m) in the northeast (Becker et al. 1978). In Indiana the Eau Claire exhibits the entire range of clastic compositions, ranging from shale to quartz arenite. Major lithologies include pink, variably glauconitic, dolomitic, K-feldspar rich sandstone or siltstone; green, maroon, and dark grey glauconitic mica rich shales; and tan, variably glauconitic silty or sandy dolostone (Gustadt 1958, Becker et al. 1978). Liu et al. (2012) conducted a review of Eau Claire literature, noting a unit of heterogeneous lithology in Indiana dominated by siltstones and shales. Concurrent with the Eau Claire of Illinois, the Eau Claire of Indiana contains abundant glauconite and K-feldspar. Becker et al. (1978) reports XRD data from six wells in Indiana averaging 20% K-feldspar with a maximum of 35%. Lahann et al. (2014) conducted a lithofacies analysis and log correlation of the Eau Claire throughout Indiana and found the southwestern and northern portions of the state to contain significant amounts of silty or dolomitic shale. Log correlations into Kentucky and Ohio revealed the Eau Claire becomes more carbonaceous to the east and southeast of Indiana (Lahann et al. 2014).

In Missouri, the Eau Claire is referred to as the Bonneterre formation, and hosts world class Mississippi Valley Type (MVT) Pb-Zn deposits (Gregg 1985; Gregg and Shelton 1990). It conformably overlies the Lamotte Sandstone and in some places lies directly on the Mesoproterozoic EGRP. The Bonneterre thickens to the southeast towards the depocenter of the Eau Claire in the Illinois Basin (Larsen 1977). The Bonneterre of Missouri is dominantly dolostone that is variably glauconitic or shale rich (Howe and Koenig 1961) deposited on a carbonate shelf that nucleated around the early Cambrian topography of southeast Missouri (Larsen 1977). Gerdemann and Myers (1972) noted the occurrence of MVT ore deposits shared a close association with a stromatolite reef facies found throughout the Bonneterre in Southeast Missouri.

The Eau Claire Formation is exposed at the surface in central Wisconsin as thinly bedded shaly sandstone (Walcott 1914). In this region, the Eau Claire conformably overlies the Mt. Simon and underlies the Womewoc Formation (Huber 1975). Recent studies of drill cores and outcrop indicate the Eau Claire of Wisconsin is very fine to medium grained, moderately to well-sorted glauconitic and dolomitic K-feldspar rich sandstone containing thinly interbedded siltstones and shales (Aswasereelert et al. 2008). The Eau Claire is thickest in southern Wisconsin and thins towards the northern part of the state (Ostrom 1978). Aswasereelert et al. (2008) noted coarser grained, less arkosic samples in southern Wisconsin and finer grained more arkosic sediments in central Wisconsin outcrops.

In Kentucky, the Eau Claire Formation overlies the Mt. Simon Sandstone in the west, while the laterally equivalent Conasauga group overlies the Mt. Simon in the eastern portion of the state (Bandy 2012). The Eau Claire reaches a maximum thickness of 2,750 ft. (840 m) in the Illinois Basin depocenter of western Kentucky and thins towards the east end of the state to a minimum thickness of 250 ft. (75 m) (Grebs and Solis 2009). Bandy (2012) cites many features of the Eau Claire in Kentucky that are concurrent with the Eau Claire of Illinois, such as the lithologic dominance of shale and siltstone, abundant glauconite, soft sediment deformation, flat pebble conglomerate beds, and a carbonaceous member at the top of the Eau Claire in western Kentucky. Burrows and trilobite fragments are found in the Eau Claire of Kentucky, although they are not well constrained due to their poor resolution (Bandy 2012).

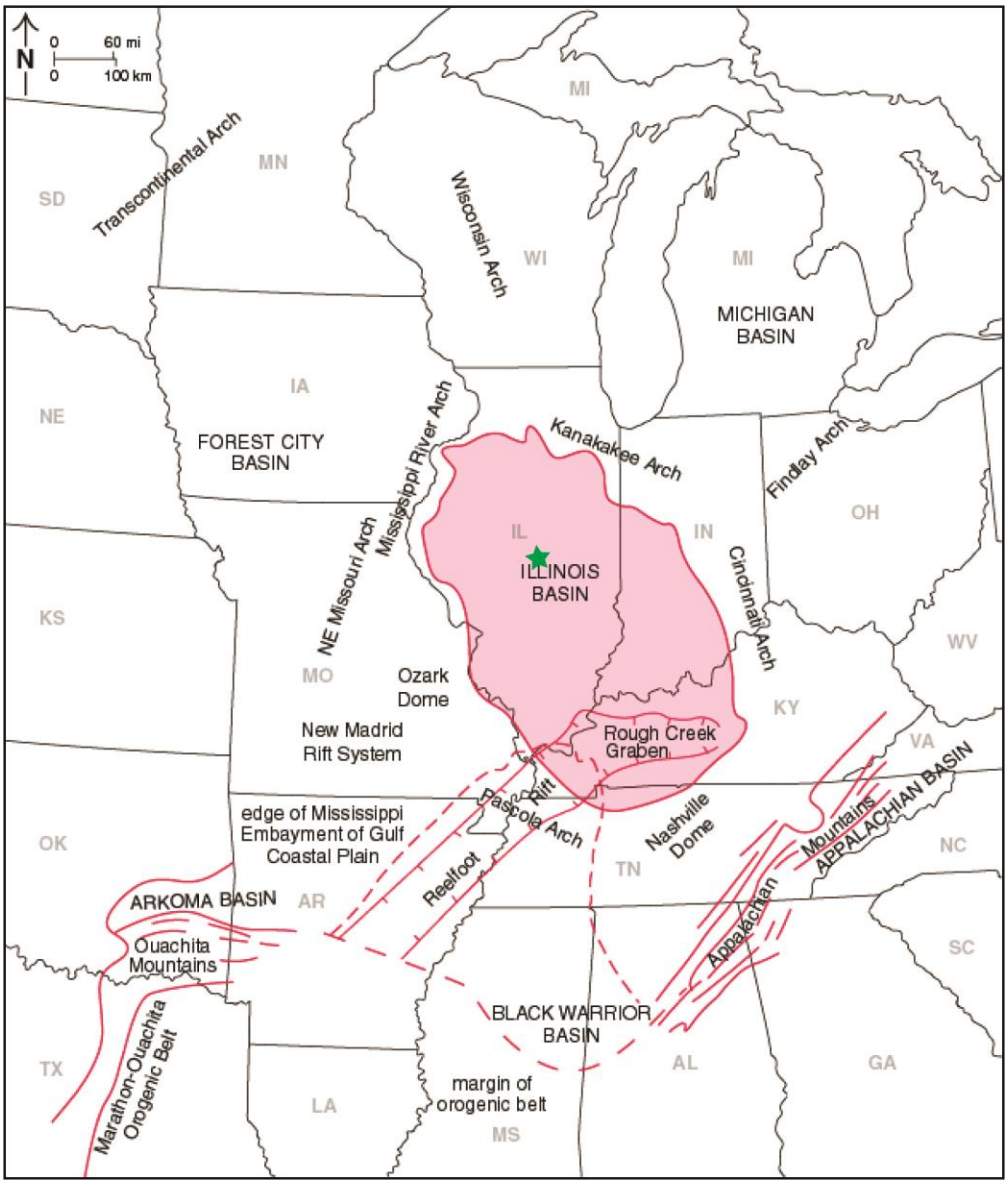

Fig. 2.1. Regional map of the United States Midcontinent. The Illinois basin is the spoon shaped feature outlined and shaded in red. Green star represents the location of the Illinois Basin – Decatur Project.

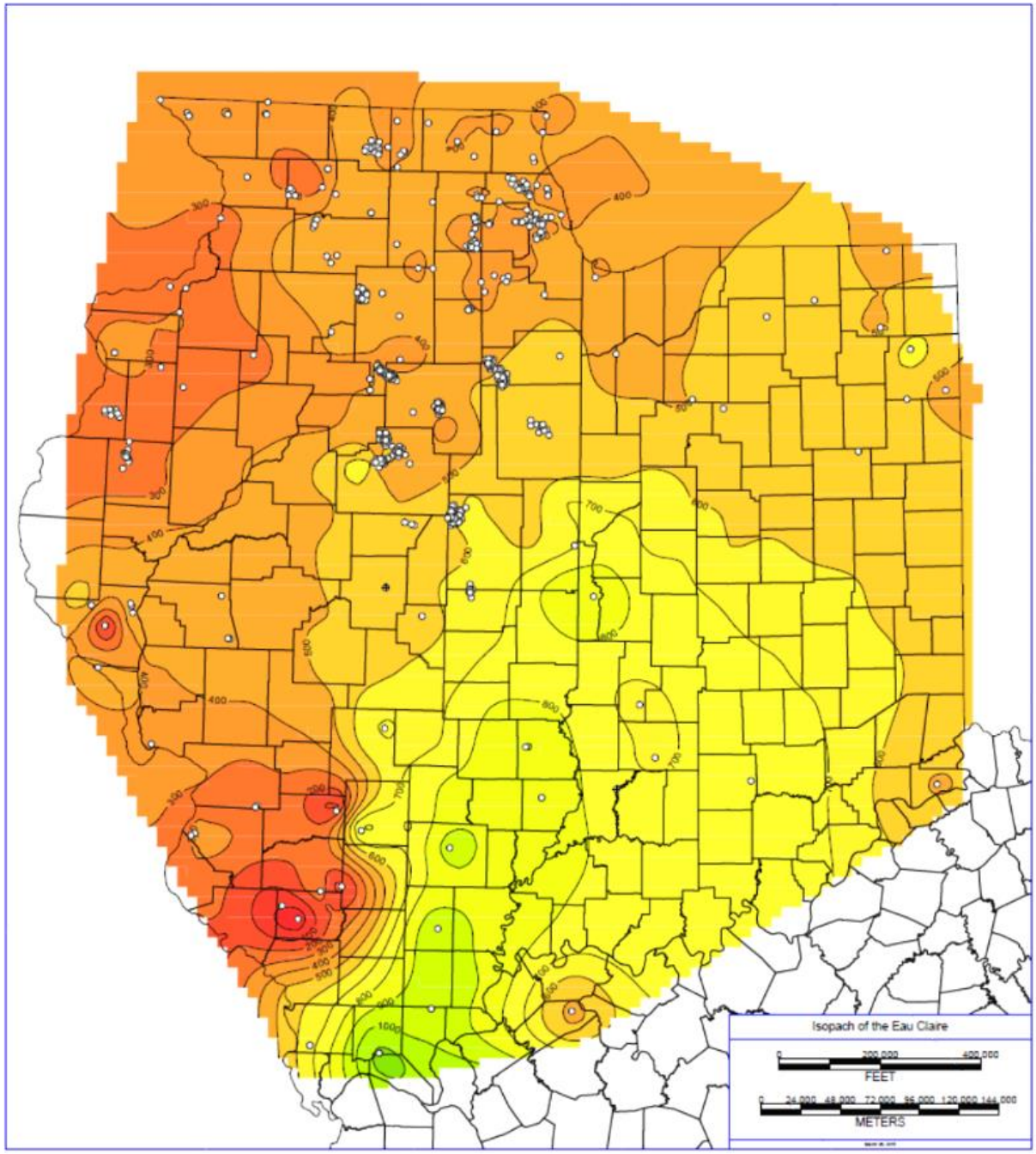

Fig. 2.2. Isopach map for the Eau Claire Formation in the Illinois Basin from Leetaru (2015, unpublished).

CHAPTER 3: METHODS

The Illinois Basin – Decatur Project (IBDP) in Macon County, IL provides the most comprehensive suite of drill core through the Cambrian aged succession in the central part of the Illinois Basin, creating a state of the art laboratory for studying CCS. The VW#1 well provides 101 ft. (31 m) of four-inch (10-cm) diameter core through the Lower Eau Claire formation, including the conformable contact with the underlying Mt. Simon Sandstone. Eight 1.5 in. diameter x 2.5 in. long (3.8 cm diameter x 6.4 cm long) rotary sidewall cores (RSWC) were cut in the Eau Claire from the VW#1 well above the cored interval. Thirty feet (9 m) of whole core and 14 RSWCs were recovered from the CCS#1 well, while 43 ft. (13 m) of whole core and 5 RSWCs were recovered from the VW#2 well. Sampling for thin sections occurred in regular intervals in an attempt to representatively sample all lithologies, facies, and diagenetic features. This study employs core descriptions from all three wells, facies analysis on the VW#1 well, petrographic analyses on 101 thin sections, carbon and oxygen isotope ratios on 17 samples, X-ray diffraction data from 4 samples, strontium isotope analysis on 27 samples, as well as commercial petrophysical and X-ray diffraction data.

3.1 Sedimentological Descriptions

Petrologic observations were made on all Eau Claire drill cores from the CCS#1 well and VW#2 well for this study. Researchers at the ISGS completed core descriptions on the VW#1 well prior to this study; however, a facies analysis was not completed on Eau Claire core from the VW#1 well. Depositional/litho- facies analysis was performed on the VW#1 well core because it contains the largest suite of core for the Eau Claire, 102 ft. (31.1 m). Unless otherwise mentioned, all facies observations listed in the results are from the VW#1 well. Color, texture, composition, sedimentary structures, ichnology, fossils, and diagenesis comprised observations from the cores. Samples with greater than 75% clay were characterized either as shales (fissile) or mudstones (no fissility). Correlation of wireline logs to observations made from drill core yielded three well-defined depositional facies. Closer to the surface, wireline logs and rotary sidewall cores revealed an additional depositional facies above the cored interval. Additionally, nine lithofacies were chosen based on the same criteria, creating more specific interpretations within the broader depositional regimes **(Fig. A1-A2)**. The upper 345 ft. (105 m) is characterized

entirely from wireline logs and rotary sidewall cores. Depositional block models were constructed using observations made from the VW#1 drill core in conjunction with the gamma ray log **(Fig. E.1)**.

3.2 Point Counting

Thin sections from VW#1(*n*=23), VW#2(*n*=16), and CCS#1(*n*=31) were prepared by Wagner Petrographic (Lindon, UT) and analyzed at the Illinois State Geological Survey petrography laboratory with a Zeiss Axiophot polarizing microscope. Thin sections were polished, vacuum impregnated with blue epoxy to reveal pore space, and half stained with sodium cobaltinitrite to aid in identification of potassium feldspars. Both plane-polarized and cross-polarized light were used in the characterization of sample composition. Standard point counting methods were used to quantify modal mineralogy and porosity, using a 5x objective and 494 points per photomicrograph. In thin sections with widely varying lithology, more than one count was necessary per thin section to assess composition. Samples were classified using the classification schemes of Dott (1964) and Folk (1980) where 0-15% clay matrix in a clastic rock is an arenite, 15–75% is a wacke, and >75% is a mudstone.

To quantify grain size, point counts were conducted under 2.5x magnification with 529 points per photomicrograph using a Zeiss Axiophot polarizing microscope and the Olympus Stream Essentials 'arbitrary line' function. The arbitrary line function allows measurement of grain diameter calibrated to µm. Point counts proceed in a similar fashion to that of mineralogy, where a grain diameter will receive more than 1 measurement if it falls on more than one grid intersection. All data was collected and reported in µm and phi (φ) units, and sigma (σ), or the degree of sorting was also calculated:

$$\varphi = -\log_2(grain\ size, mm) \tag{1}$$

$$\sigma = \frac{\varphi_{84} - \varphi_{16}}{4} + \frac{\varphi_{95} - \varphi_{5}}{6.6} \tag{2}$$

Where φ_{84} is the 84th percentile of grain sizes for a sample, φ_{16} is the 16th percentile of grain sizes for a sample, φ_{95} is the 95th percentile of grain sizes for a sample, and φ_{5} is the 5th percentile of grain sizes for a sample.

3.3 Scanning Electron Microscopy

Scanning electron microscopy (SEM) – energy dispersive x-ray spectroscopy (EDS) was used to determine the composition of select mineral grains and fossil fragments in thin sections throughout the Eau Claire. Samples were analyzed on a JEOL 6060 low vacuum SEM coupled to an iXRF 550i EDS system at the Frederick Seitz Materials Research Laboratory (MRL) on the University of Illinois at Urbana – Champaign (UIUC) campus. All samples were analyzed in low vacuum mode (20 Pa) using the back scattered electron (BSE) detector with an accelerating voltage of 20 keV, a 50 µm spot size and a 10 mm working distance. Samples were photographed and analyzed using the EDS system to determine the elemental composition, and ultimately define the mineralogy of select grains. Mineral mapping was performed on entire photomicrographs, and select points on these photomicrographs were analyzed. An algorithm in the Iridium Ultra EDS software produces color coded maps which correlate to different elements, whereas spectral analysis must be performed for individual points. Additionally, Weatherford Laboratories provided SEM photomicrographs of the Eau Claire Formation from the CCS#1 well.

3.4 Carbon/Oxygen Isotopes

Eighteen samples were collected from the VW#1 (n=13) whole core and CCS#1(n=5) rotary sidewall cores to analyze for Carbon ($^{13}C/^{12}C$) and Oxygen ($^{18}O/^{16}O$) isotope ratios. A drill was used to pulverize a small amount of sample from the core, and the resulting powder was collected into a vial. Drill bits were cleaned with ethyl alcohol and acetone between samples to avoid contamination. Samples were weighed in the range of 75-90 µg using a Mettler Toledo AT21 Comparator scale. Samples were run at the ISGS stable isotope laboratory using a Kiel III automated carbonate device coupled to a Finnegan MAT 252 isotope ratio mass spectrometer (IRMS). All samples were standardized to the Vienna Pee Dee Belemnite (VPDB) for both $\delta^{13}C$ and $\delta^{18}O$, as well as Vienna Standard Mean Ocean Water (VSMOW) for $\delta^{18}O$. All values are reported in delta notation.

3.5 Strontium

Samples were prepared for strontium isotope ratio analysis using a NaOH fusion method (n=15) or a HNO_3 digestion method (n=12). The HNO_3 method involved partial digestion/leaching of soluble Sr from the rock whereas the NaOH fusion provided an isotopic ratio of the whole rock. Approximately 20 mg of sample was placed inside a silver crucible along with 250 mg of NaOH. Samples were then heated in a furnace for 10 minutes at 725 °C. After the fusion, samples were removed from the oven and the outside of the crucible was washed off with H_2O and placed inside a Teflon beaker with 20 mL of H_2O. Samples sat overnight on a hot plate, and were placed in a sonic bath for 45 minutes the following day and shaken every 15 minutes. Samples were then transferred to a 50 mL centrifuge tube, while 8 mL H_2O and enough concentrated HNO_3 to make 3N HNO_3 were added to the Teflon beakers. Teflon beakers were shaken, and then added to the mother solution in the 50 mL centrifuge tubes. Prior to the development of the NaOH fusion methodology, 12 samples were digested in 3N HNO_3 overnight on a hotplate prior to column chromatography. Samples were then run through columns following a typical strontium column chromatography procedure using strontium spec resin to remove other elements from the solution. Samples were then run at the University of Illinois isotope geochemistry laboratory using a Nu Plasma multi collector-inductively coupled plasma-mass spectrometer (MC-ICP-MS). Samples were introduced as 2% nitric acid into a DSN-100 desolvator. All samples were analyzed for $^{87}Sr/^{86}Sr$. Selected samples were analyzed for $^{87}Rb/^{86}Sr$ by isotope dilution methods to apply an age correction to the samples.

3.6 Core Analysis

Schlumberger Carbon Services (SCS), a collaborator on the IBDP, conducted routine core analysis on whole core samples from all three wells. Thirty six samples were analyzed by SCS from the VW#2 well, while Weatherford Laboratories analyzed seven samples from the CCS#1 well and six samples from the VW#1 well. Measurements on samples from the VW#2 well were made on the 4 in. diameter whole core, while core plugs or RSWCs were used for CCS#1 and VW#1. Whole core measurements produce more accurate data than measurements on core plugs because the larger sample size is a more accurate representation of the heterogeneity encountered in an expansive geologic formation.

Twelve core plugs were also sampled in the Eau Claire from the VW#1 well and analyzed for porosity at the ISGS core analysis laboratory on the UIUC campus using a helium porosimeter, Temco model HP-1. The porosimeter operates on the principle of Boyles Law ($P_1V_1 = P_2V_2$; P = pressure, V = volume) and measures the pressure in chambers of known volume against those of the rock sample to obtain a value for porosity. Permeability measurements were attempted at the ISGS core lab as well, although low permeability measurements were impossible due to equipment limitations.

Due to poor sample resolution in the shales, permeability was estimated from mercury injection capillary pressure (MICP) data. Dastidar (2007) presents an empirical equation to calculate permeability for tight clastic rocks that takes advantage of permeability's relationship to pore throat radius and porosity:

$$\log K\ (mD) = -2.51+3.06 \log(\phi)+1.64 \log (R_{WGM}) \quad (3)$$

Where ϕ is the porosity (%) and R_{WGM} is the weighted geometric mean of pore throat radii (microns). Porosity obtained from MICP is true porosity and not an estimation.

3.7 X-Ray Diffraction

Mineralogical analyses of four samples were performed at the Illinois State Geological Survey (ISGS) using x-ray diffraction (XRD) methods following the methodology described by Moore & Reynolds (1997). For the XRD procedure, the samples were micronized in a McCrone micronizing mill with deionized water for 10 minutes. Then they were transferred to 50 mL centrifuge tubes which were placed in the centrifuge for 20 minutes at 2000 rpm. The clear supernatant was poured off and the remaining material dried overnight at 80 °C. When completely dried the material was mixed lightly with a mortar and pestle and then packed into an end-loading sample holder as a random powder bulk-pack. The random powder bulk-pack was analyzed with a Scintag XDS 2000 diffractometer. Step-scanned data was collected from 2° to 60° 2θ with a fixed rate of 2° per minute with a step size of 0.05°2θ. All resulting traces were analyzed using the semi-quantitative data reduction software from Materials Data Inc. (MDI) known as Jade 9.

The clay mineral composition was determined using oriented slides of the clay size < 2 μm fraction with semi-quantitative values of the clay mineral assemblage calculated from ethylene glycol (EG) solvated slides (Hughes and Warren 1989, Hughes et al, 1994, Moore and Reynolds 1997). In preparation for XRD, 20 to 30 g of each sample was soaked for about 10 to 12 hours in deionized water and protected from external agents. As water interacts with the sample, small clay particles are released into the solution. Further stirring of the solution mechanically induced clay release from the sample. After settling, about 1/3 of the water was removed from the beaker. The beaker is then refilled with deionized water and two drops of sodium hexametaphospate is added as a dispersant. The mixture was stirred and then allowed to settle for 15 minutes. The generated supernatant was pipetted and several drops were added onto a glass slide and let to dry overnight.

CHAPTER 4: RESULTS

4.1 Unit A (VW#1 5,487-5,527 ft.) Depositional Environment

Across the Mt. Simon Sandstone – Eau Claire Formation boundary the gamma ray signature increases **(Fig. E.1)**, grain size gradually decreases, and the color changes from maroon/pink (Upper Mt. Simon) to pink, grey and light tan (Eau Claire Unit A). Otherwise, the depositional environment does not change between the top of the Mt. Simon and Unit A of the Eau Claire. Pink and grey/tan siltstones, grey/dark grey mudstones, very fine-grained grey/tan sandstones, and interbedded siltstones/mudstones comprise the basal facies in VW1 (**Fig. 4.1**). Above the Mt. Simon – Eau Claire contact at 5527 ft. (1684.6 m) in the VW#1 well, sediments are heavily bioturbated for approximately 20 ft. and lack glauconite. Flaser and lenticular bedding are common throughout this sequence. These bioturbated beds consist predominantly of grey/tan siltstone and dark grey mudstone. Bioturbation occurs within planar to low angle cross bedding across the interval. One foot thick beds of light grey well sorted, well rounded, and very fine grained sandstones exist within the bioturbated zone, which are planar to cross bedded and quartz to subarkosic arenite in composition. A few lenses of these quartz arenites are iron oxidized or pyritized. Above the bioturbated zone, sedimentary structures are more commonly preserved. Siltstones and shales are planar laminated to low angle cross-bedded with some ripple beds. Brachiopod fragments are commonly concentrated in laminae. Possible *planolites* trace fossils and syneresis cracks exist in the bioturbated zone. Glauconite rich beds, as well as disseminated pyrite, soft sediment deformation, and a flat pebble conglomerate lens also appear above the bioturbated zone. Clasts within the flat pebble conglomerate are brachiopod rich lithic fragments, rimmed by halos of iron oxide. The flat pebble conglomerate is heavily cemented with secondary quartz infilling all pore space. From point counts, Unit A exhibits an average mineralogy of 69% quartz, 14% clay, 12% feldspar, 2% carbonate, 2% pore space, and <1% of hematite and pore space. The average grain size of Unit A is 124 μm (very fine sand) (**Table 4.1**).

4.1.1 Unit A Petrography

Unit A is characterized by sandstones, mudstones and siltstones which are commonly bioturbated in the basal 20 ft. (6.1 m) **(Table 4.1)** and planar to ripple bedded in the upper 15 ft. (4.6 m)**.** Quartz arenites found in the basal 20 ft. (6.1 m) are most commonly composed of well rounded, well sorted and fine to medium grains, and are heavily cemented with authigenic quartz occluding pore space. Siltstones are subarkosic to arkose arenite in composition **(Fig. 4.2A)**, and some beds contain concentrated intervals of brachiopod fragments **(Fig. 4.2B)**. The bioturbation of interbedded siltstones and mudstones is evident at the petrographic scale in some samples **(Fig. 4.2C).** Bioturbated siltstones and mudstones are commonly K-feldspar rich and contain a poorly sorted distribution of grains (**Fig. 4.2D)**. Most quartz cement occurs as an intergranular cement occluding nearly all primary porosity **(Fig. 4.2E).** However, some quartz cement occurs as syntaxial overgrowths on detrital grains which results in a partial preservation of primary porosity (**Fig. 4.2F**). Some polycrystalline grains exist, but most detrital grains in Unit A are monocrystalline.

4.1.2 Unit A Petrophysics

Unit A exhibits helium porosity and air permeability values (*n*=20) of 6.7% and 8.6 mD (**Figs. 4.3-4.4; Table D.1**). Porosity values range from 2.3% to 13.2%, while permeability values range from 0.2 mD to 21.4 mD. Unit A's gamma ray log signature exhibits a large increase in potassium and thorium relative to the Mt. Simon, while uranium only exhibits a slight increase (**Fig. E.1).**

4.2 Unit B (VW#1 5,448-5,487 ft.) Depositional Environment

Unit B shows a slight increase in gamma ray (GR) signature, and is predominantly composed of dark grey shale with interbedded maroon/pink siltstones and tan/grey clayey siltstones **(Fig. 4.5)**. Some of the interbedded siltstones/clayey siltstones are wavy to planar laminated. Dark grey shale is highly fissile, contains trace detritus, and is otherwise largely absent of any sedimentary structure. Trace rip up clasts, bioturbation, pyrite nodules, convoluted laminae and possible *cruziana* trace fossils exist throughout the unit. Thin glauconite-rich beds exist periodically throughout the sequence. A 1 ft. (0.3 m) thick silty glauconitic dolostone bed (referred to as 'mixed

carbonate/siltstone in **Fig. A.2**) dominates the lithology near the base of Unit B (5475-5475.75 ft.). A small segment of the bed is brecciated, and the overall texture is mottled/distorted. The base of the bed has a sharp contact with the underlying shale, and the upper boundary slowly grades into a siltstone. Above the glauconitic dolostone bed, siltstone interbeds are minimal, and the lithology is comprised almost entirely of fissile shale. Oblique slickensides (5462.6 ft., 5465.6 ft., 5468.3 ft., 5468.6 ft., and 5472.9 ft.) exist within some fractures of Unit B shales. Wavy/ripple beds appear near the top of this unit, defining the upper boundary of this facies. The shale is heavily fractured as a result of the coring process. Unit B has an average point count mineralogy of 43% clay, 26% quartz, 19% carbonate, 9% K-feldspar, 2% lithics, and 1% glauconite (**Table 4.2)**.

4.2.1 Unit B Petrography

Unit B is dominated by thick shale deposits, interbedded siltstones, and a large glauconitic dolostone bed (**Table 4.2)**. Unit B contains numerous interbedded siltstones (**Fig. 4.6A-B**), however 30.3 ft. (~75%) of the Unit is shale **(Fig. 4.6C-E)**. The average point count mineralogy is 72% clay, 13% quartz, 13% feldspar, and <2% carbonate, glauconite, hematite, lithics and pore space. A 1 ft. (0.3 m) thick silty glauconitic dolostone bed exists near the base of the unit, containing 88% carbonate, 5% lithics, 4% glauconite, 1% quartz, 1% K-feldspar and <1% of clay, hematite and pore space from point count mineralogy **(Fig. 4.6F-G)**. Dissolution of fossils and glauconite grains is common within the glauconitic dolostone bed. Primary porosity is nonexistent, with minor secondary porosity as a result of dissolution. Pyrite and hematite otherwise appear to be absent from Unit B hand samples. Parting is commonly seen throughout along clay laminae, alluding to the fissile nature of the shale (**Fig. 4.6H).** Siltstone beds that exist throughout contain abundant clay laminae, trace brachiopod fragments, and trace glauconite. Under SEM, the Eau Claire's Unit B can be seen as having an extensive clay matrix with detrital material throughout (**Fig. 4.7**).

4.2.2 Unit B Petrophysics

Unit B contains helium porosity values, however all permeability values are estimated from MICP data. The average porosity and permeability of Unit B is 5.8% and 2.0×10^{-5} mD (20 nD). Porosity ranges from 0.9% to

13.5%, while permeability ranges from $1.0x10^{-5}$ mD to $3.4x10^{-5}$ mD (**Figs. 4.3-4.4; Table D.1**). Unit B's gamma ray log signature is similar to Unit A's and remains relatively high, with a sharp decrease observed at the location of the glauconitic dolostone bed (**Fig. E.1**). Potassium and thorium are also much higher than uranium in Unit B's gamma ray signature.

4.3 Unit C (VW#1 5350-5448 ft.) Depositional Environment

Unit C contains interlaminated maroon/pink to grey/tan siltstones, grey/dark grey shales, and tan/grey clayey siltstones and is predominantly planar laminated to homogeneous, however some wavy, ripple, and cross beds are present (**Fig. 4.8**). Maroon/pink – grey/tan siltstones are predominantly arenaceous – arkosic, but may be clay-rich. Tan/gray clayey siltstones contain variable quartz/feldspar detritus. Grey/dark grey shales are clay rich, and contain variable quartz/feldspar detritus. Trace bioturbation, glauconite, brecciation, flaser/lenticular laminations and clastic dikes exist within this facies. Some Unit C burrows are simple and appear to be *skolithos*. Some burrows are more complex and the ichnofacies remains unknown. Bioturbation is primarily limited to the more clay-rich rocks in this unit and is largely absent in the siltstones. Approximately 1 inch (2.54 cm) glauconitic/dolomitic (greensand) beds occur in a relatively rhythmic pattern every 1-6 ft. Overall, this sequence is well consolidated. Shales present are highly fissile, which have been aggravated from the coring process. Unit C has an average point count mineralogy of 46% quartz, 22% clay, 20% K-feldspar, 7% carbonate, 2% glauconite, 2% pore space and 1% lithics (**Table 4.3).**

4.3.1 Unit C Petrography

Unit C consists largely of interbedded siltstones, clayey siltstones and shales. Petrography reveals this unit is considerably arkosic, with an average potassium feldspar content of 20.3% **(Fig. 4.9A-B).** Some siltstone beds contain trace brachiopod fragments and glauconite (**Fig. 4.9C).** One inch (2.54 cm) thick glauconitic to dolomitic siltstone beds also exist in Unit C, which are similar to Unit B's glauconitic dolostone bed but are much smaller (**Fig. 4.9D).** The glauconitic dolostone beds in Unit C contain 58% quartz, 23% dolomite, 9% clay, 5% glauconite, 2% lithics, 2% K-feldspar and <1% hematite and pore space from point count mineralogy.

4.3.2 Unit C Petrophysics

Unit C has an average core analysis porosity and permeability (*n*=50) of 9.4% and 0.9 mD with most of the samples coming from the VW#2 well on the north end of the IBDP site. Porosity values range from 2.7% to 16.3%, and permeability values range from 0.004 mD to 12.3 mD. (**Figs. 4.3-4.4**; **Table D.1)**. Unit C's spectral gamma ray log signature shows a slight decrease in uranium and thorium with a relatively steady potassium signature (**Fig. E.1).**

4.4 Unit D (VW#1 5010-5350 ft.) Depositional Environment

Near its base in the VW#1 well, Unit D is largely conformable with unit C in terms of its deposition, beginning as a silty quartz/K-feldspar-rich lithology with periodic pulses of carbonate deposition occurring in the first 150 ft. (45.7 m). By 5200 ft. (1585 m), limestone/dolostone deposits become the primary lithology in Unit D across all three wells. Clay is a major component of Unit D's basal 150 ft. (45.7 m) as well, with VW#1 and VW#2 exhibiting dominantly illite while CCS#1 contains a significant chlorite component. In VW#2, limestone and dolostone production begins dominating the stratigraphy within 40 ft. (12.2 m) of its base at 5360 ft. (1633.7 m) and continues as the primary lithology until its contact with the overlying Ironton-Galesville Sandstone at 5015 ft. (1528.6 m). In all three wells, siliciclastic input begins to reappear within 100 ft. (30.5 m) of the Ironton-Galesville contact **(Fig. E.1)**.

RSWCs for Unit D are drilled in the upper 250 ft. (76.2 m) of the formation and reveal siltstone, silty carbonates, oolitic packstone to grainstone, and well sorted, very fine grained sandstone near the upper contact (**Fig. 4.10A-D**). Some ooids are replaced with dolomite. Thin sections from RSWCs at depths of 5120 ft. (1560.6 m), 5132 ft. (1564.2 m) and 5140 ft. (1566.7 m) contain calcite with less dolomite cement, while thin sections from 5180 ft. (1578.9 m), 5190 ft. (1581.9 m), and 5206 ft. (1586.8 m) contain abundant oolitic packstone with dolomite rhombs replacing some of the ooids. The average point count mineralogy of the unit is 47% quartz, 36% carbonate, 12% clay, 3% porosity and 2% K-feldspar (**Fig. 4.11-4.13; Table 4.4**).

4.5 Grain Size and Sorting

The grain size of the Eau Claire Formation ranges from <4 µm to 531 µm, with an average value of 73.4 µm in the very fine grained sand size range (**Fig. 4.14-4.15)**. Grain sizes are reported in µm and ϕ units, and grain sorting is calculated as σ where raw grain size data was available. Sigma values are available for most of Unit A, two samples in Unit C and 3 in Unit D. The average σ value is 0.8, corresponding to moderately sorted.

4.6 Isotopes

Carbon, oxygen, and strontium isotope ratios are reported as $\delta^{13}C$, $\delta^{18}O$ and $^{87}Sr/^{86}Sr$ **(Table 4.5).** $\delta^{13}C$ values range from -4.8‰ to +4.6‰ and become isotopically lighter with greater depth. Units A-C plot within a range of -4.8‰ to –2.8‰, while Unit D plots between +0.5‰ to +4.6‰. $\delta^{18}O$ shows a similar relationship with depth, although the correlation is not as strong as depth vs. $\delta^{13}C$. $\delta^{18}O$ ranges from -11‰ to -6‰, coinciding with a typical early Paleozoic $\delta^{18}O$ value (Veizer et al. 1997). $^{87}Sr/^{86}Sr$ range from 0.709208 to 0.771930, with measurements from both siliciclastic and carbonate lithologies. $^{87}Sr/^{86}Sr$ ratios are also reported for the basement rock at the IBDP site and from the felsic igneous rock in EGRP outcrops of southeast Missouri **(Table 4.5)**.

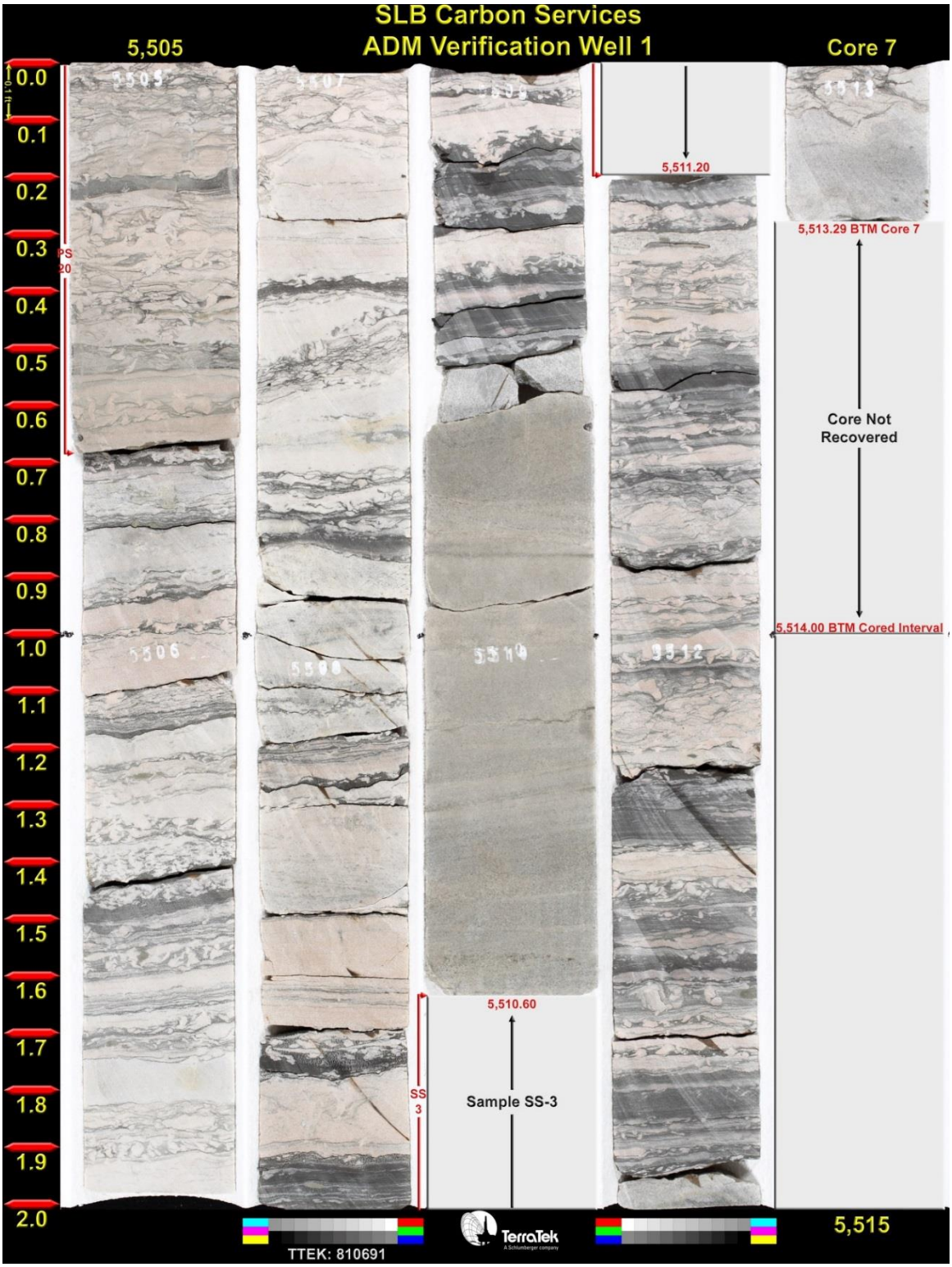

Fig. 4.1. Core photo of the Eau Claire Formation Unit A, from 5,505 ft. to 5,515 ft. in the VW#1 well. Heavy bioturbation and flaser/lenticular bedding define this depositional facies. Well sorted, well-rounded, homogeneous to planar bedded sandstones occur between the bioturbated interval. Photograph by Terratek.

Depth (ft)	Quartz	K-Feldspar	Pore	Glauc	Clay	Iron Oxide	Lithics	Carbonate	Total	Mean Grain Size (um)	Lithofacies	Depositional Environment
5491.97	53.4%	37.2%	0.4%	0.0%	7.9%	0.0%	0.0%	1.0%	1.0	40.2	Homogenous Siltstone	Subtidal Channel
5494.19	46.0%	46.8%	0.0%	0.0%	6.5%	0.0%	0.8%	0.0%	1.0	47.1	Planar-Bedded Siltstone	Subtidal Channel
5501.3	98.4%	0.6%	0.0%	0.0%	0.8%	0.0%	0.2%	0.0%	1.0	195.0	Bioturbated Siltstone-Sandstone	Subtidal Flat
5501.3	92.3%	0.8%	0.0%	4.7%	1.2%	0.0%	0.0%	1.0%	1.0		Bioturbated Siltstone-Sandstone	Subtidal Flat
5502.9	81.6%	2.0%	0.0%	0.0%	16.4%	0.0%	0.0%	0.0%	1.0	149.3	Flat Pebble Conglomerate	Subtidal Flat
5503.27	77.9%	10.1%	3.0%	0.0%	6.1%	0.0%	0.0%	2.8%	1.0	52.9	Bioturbated Siltstone-Sandstone	Tidal Flat
5503.9	39.9%	33.4%	1.0%	0.0%	24.7%	0.0%	0.8%	0.2%	1.0	56.2	Bioturbated Siltstone-Sandstone	Tidal Flat
5512.1	63.8%	31.6%	1.0%	0.0%	2.6%	0.2%	0.8%	0.0%	1.0	81.0	Bioturbated Siltstone-Sandstone	Tidal Flat
5513.2	99.6%	0.4%	0.0%	0.0%	0.0%	0.0%	0.0%	0.0%	1.0	168.4	Bioturbated Siltstone-Sandstone	Tidal Flat
5515.8	59.7%	3.2%	8.1%	0.0%	27.7%	0.0%	1.2%	0.0%	1.0	192.1	Homogenous Sandstone	Tidal Channel
5515.8	93.9%	0.2%	1.0%	0.0%	4.3%	0.6%	0.0%	0.0%	1.0		Homogenous Sandstone	Tidal Channel
5516.4	91.9%	0.4%	2.8%	0.0%	4.3%	0.0%	0.6%	0.0%	1.0	201.2	Bioturbated Siltstone-Sandstone	Tidal Flat
5516.4	79.4%	5.3%	8.5%	0.0%	5.1%	0.4%	1.4%	0.0%	1.0		Bioturbated Siltstone-Sandstone	Tidal Flat
5518.8	87.4%	2.2%	1.4%	0.0%	8.1%	0.0%	0.8%	0.0%	1.0	183.1	Cross-Bedded Sandstone	Tidal Channel
Average	**76.1%**	**12.4%**	**2.0%**	**0.3%**	**8.3%**	**0.1%**	**0.5%**	**0.4%**	**100%**	**124.2**		

Table 4.1. Point Count mineralogy, grain size, lithofacies and depositional environment for Unit A for the Eau Claire Formation from the VW#1 well. Average composition as indicated by the mineralogy data is a subarkosic arenite, with an average grain size of 124 µm. Glauc=Glauconite.

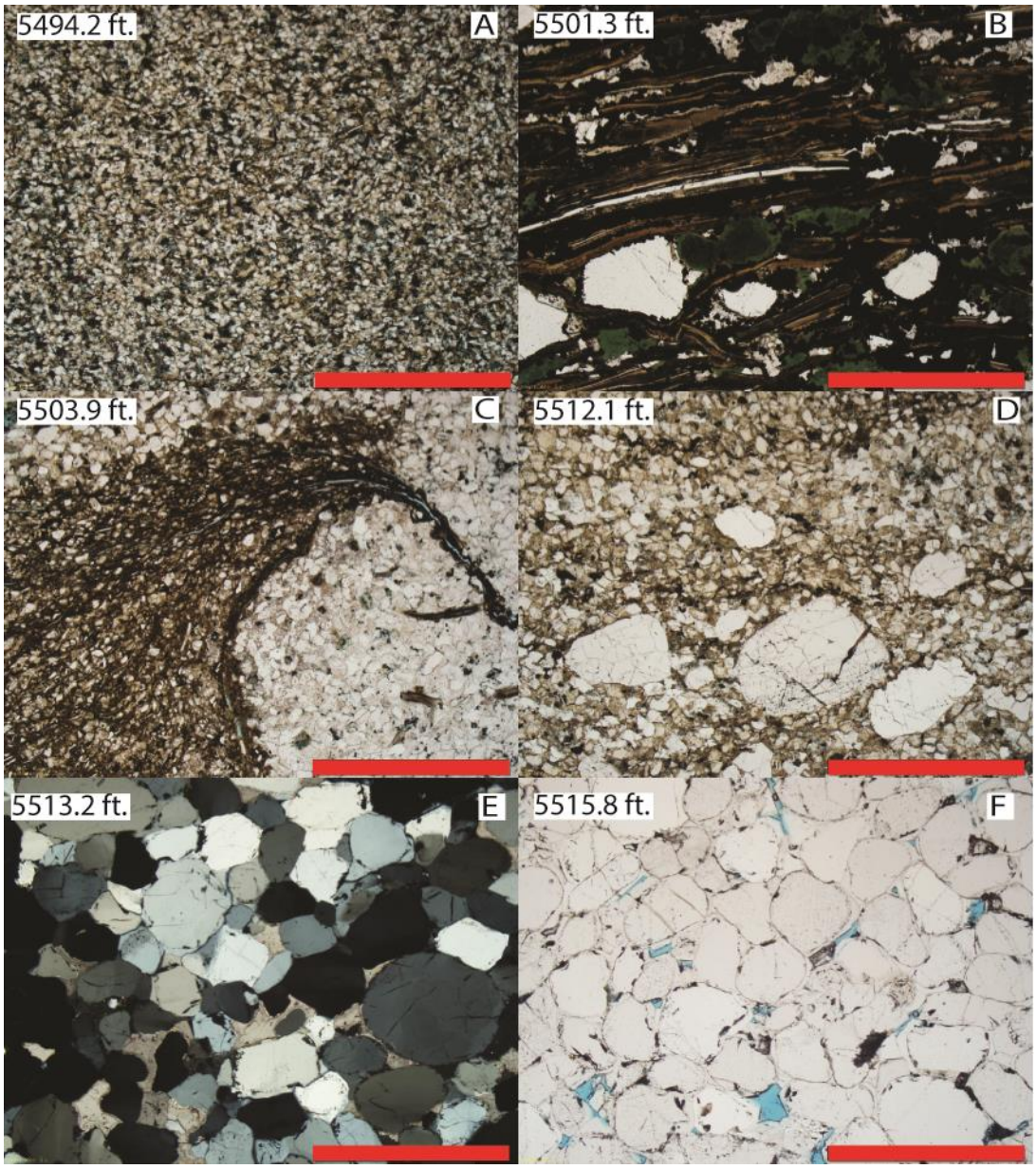

Fig. 4.2. Photomicrographs of the Eau Claire Formation for Unit A from the VW#1 well. All scale bars (red) are equal to 1 mm. Photos are in plane-polarized light unless otherwise mentioned. Fig. 4.2A (depth=5494.2 ft.) displays an arkosic siltstone, a common composition within the Eau Claire Formation. Fig. 4.2B (depth=5501.3 ft.) shows a concentration of brachiopod fragments and glauconite within a siltstone bed. Fig. 4.2C (depth=5503.9 ft.) is a heavily bioturbated clayey siltstone sample. Fig. 4.2D (depth=5512 ft.) displays a bioturbated arkosic siltstone, where larger quartz grains have been reworked into a silty K-feldspar-rich matrix. Fig. 4.2E (cross polarized light, depth=5513.2 ft.) shows a heavily cemented quartz arenite. Fig. 4.2F (depth=5515.8 ft.) shows a quartz arenite with authigenic overgrowths and some primary porosity preservation.

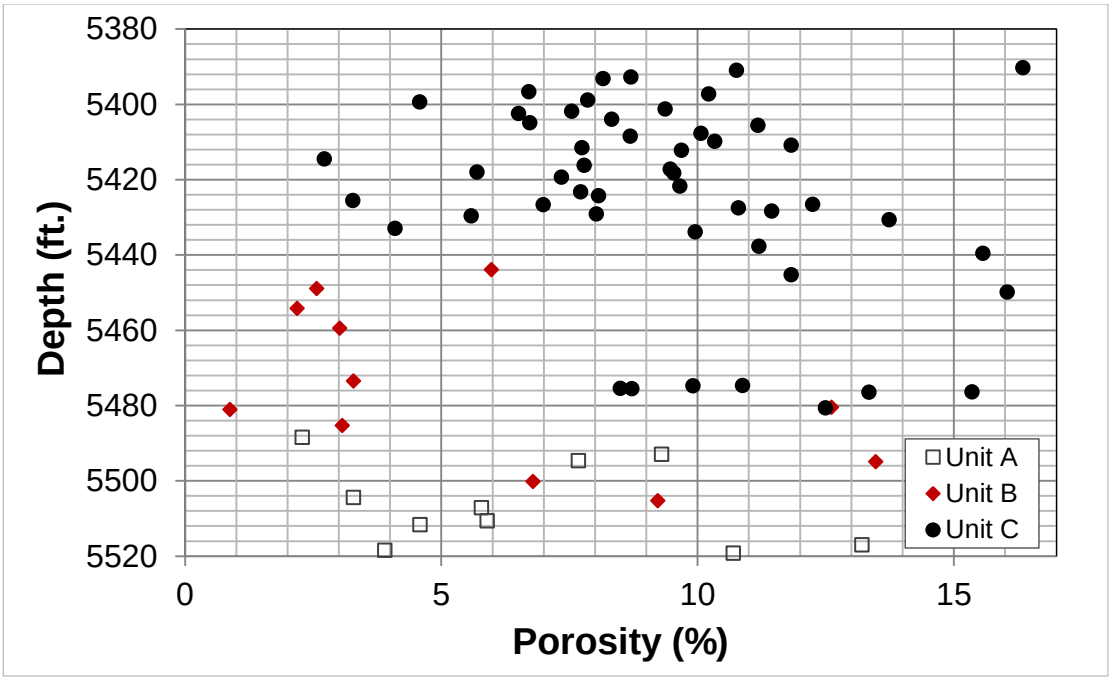

Fig. 4.3. Depth (ft.) vs. porosity (%) for the Eau Claire Formation obtained with helium porosimetry by Schlumberger Carbon Services, Weatherford International and the author (See Table D.1 for details).

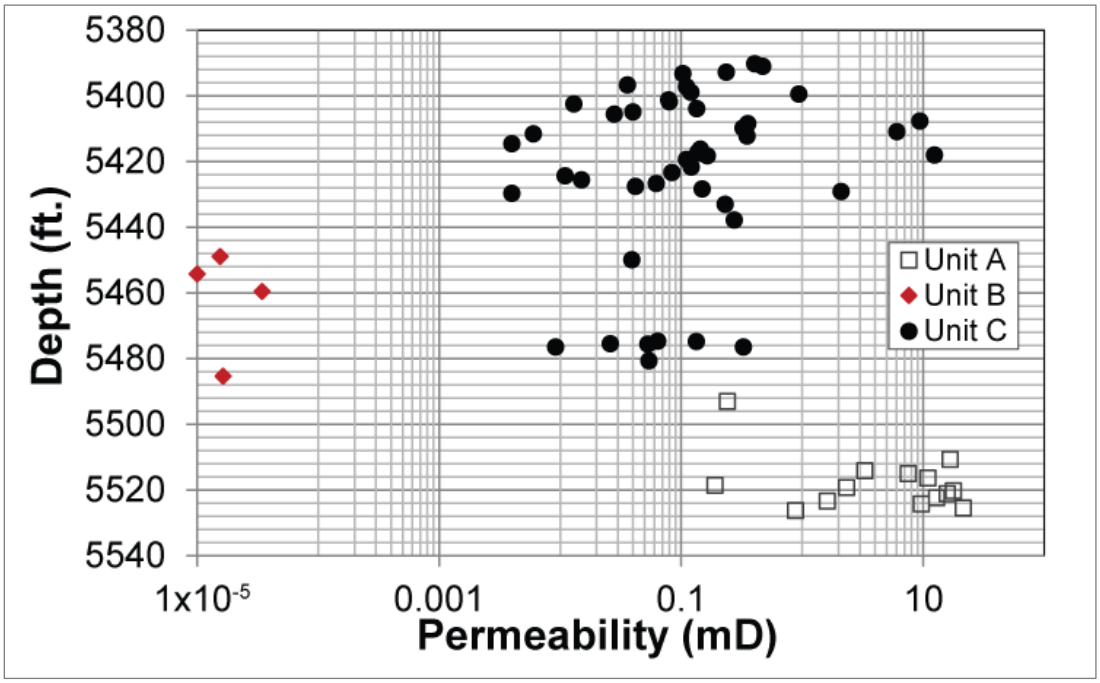

Fig. 4.4. Depth (ft.) vs. air permeability (mD) for the Eau Claire Formation at the IBDP. Unit B permeabilities are estimated from MICP data using an empirical equation from Dastidar (2007) while Units A and C were measured with a nitrogen permeameter by Schlumberger Carbon Services and Weatherford international (See Table D.1 for details).

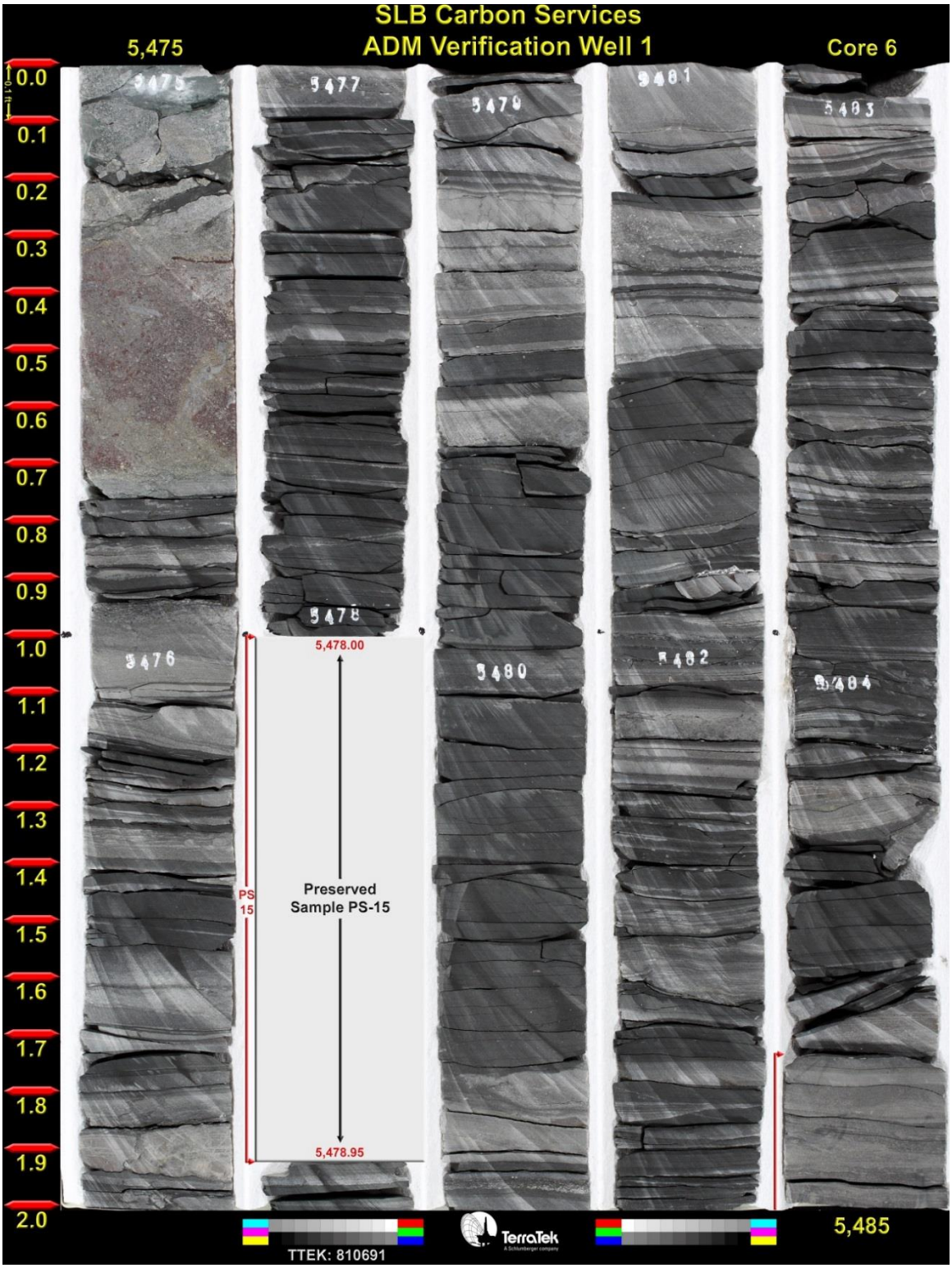

Fig. 4.5. Core photo of the Eau Claire Formation Unit B, from 5,475 ft. to 5,485 ft. in the VW#1 well. Grey to dark grey fissile shale dominates this facies, with lesser amounts of interbedded siltstone and a glauconitic dolostone deposit near 5,475 ft. (1,668.78 m) to 5,475.75 ft. (1,668.93 m). Photograph by Terratek.

Depth (ft)	Quartz	K-Feldspar	Pore	Glauc	Clay	Iron Oxide	Lithics	Carbonate	Total	Mean Grain Size (um)	Lithofacies	Depositional Environment
5452	87.85%	4.05%	0.0%	0.0%	5.67%	0.0%	1.21%	1.21%	1.0	51.5	Interbedded Siltstone/Shale	Continental Shelf-above SWB
5452	0.77%	6.92%	0.0%	0.8%	91.54%	0.0%	0.00%	0.00%	1.0	<4	Shale	Continental Shelf-above SWB
5452	45.34%	13.16%	0.0%	0.4%	39.47%	0.0%	1.62%	0.00%	1.0	<4	Shale	Continental Shelf-above SWB
5452.3	33.00%	58.91%	0.0%	0.4%	6.48%	0.2%	1.01%	0.00%	1.0	43.4	Homogenous Siltstone	Continental Shelf-above SWB
5454.6	5.06%	2.43%	0.2%	0.2%	92.11%	0.0%	0.00%	0.00%	1.0	21.6	Shale	Continental Shelf-above SWB
5459.9	5.06%	2.83%	0.2%	0.0%	90.89%	0.0%	1.01%	0.00%	1.0	14.5	Shale	Continental Shelf-above SWB
5464.8	2.23%	3.04%	0.0%	0.0%	94.74%	0.0%	0.00%	0.00%	1.0	<4	Shale	Continental Shelf-above SWB
5468.6	1.21%	0.20%	0.0%	0.0%	95.34%	0.0%	0.00%	3.24%	1.0	<4	Shale	Continental Shelf-above SWB
5474	79.55%	9.72%	0.2%	0.2%	4.05%	0.0%	6.28%	0.00%	1.0	53.1	Planar-Bedded Siltstone	Continental Shelf-above SWB
5474	80.36%	6.88%	0.4%	1.4%	6.07%	2.8%	1.42%	0.61%	1.0	<4	Planar-Bedded Siltstone	Continental Shelf-above SWB
5474.4	2.23%	2.02%	0.0%	0.2%	3.04%	0.2%	2.23%	90.08%	1.0	47.8	Packstone (Dolomite)	Storm Deposit
5474.9	0.00%	0.00%	0.0%	3.0%	0.00%	1.8%	10.12%	85.02%	1.0	<4	Packstone (Dolomite)	Storm Deposit
5475.35	2.02%	2.23%	0.2%	4.7%	0.40%	0.0%	0.00%	90.49%	1.0	<4	Packstone (Dolomite)	Storm Deposit
5486.4	13.4%	20.0%	0.0%	0.8%	65.8%	0.0%	0.0%	0.0%	1.0	26.8	Shale	Subtidal Channel
Average	**26.52%**	**8.65%**	**0.09%**	**0.87%**	**40.75%**	**0.39%**	**1.92%**	**20.82%**		**21.2**		

Table 4.2. Point count mineralogy, grain size, lithofacies and depositional environment for Unit B of the Eau Claire Formation, from the VW#1 well. The average lithology is arkosic wacke (15-75% clay, greater than 5% K-feldspar; Dott 1964) with a mean grain size of 21.2 µm. Glauc = Glauconite.

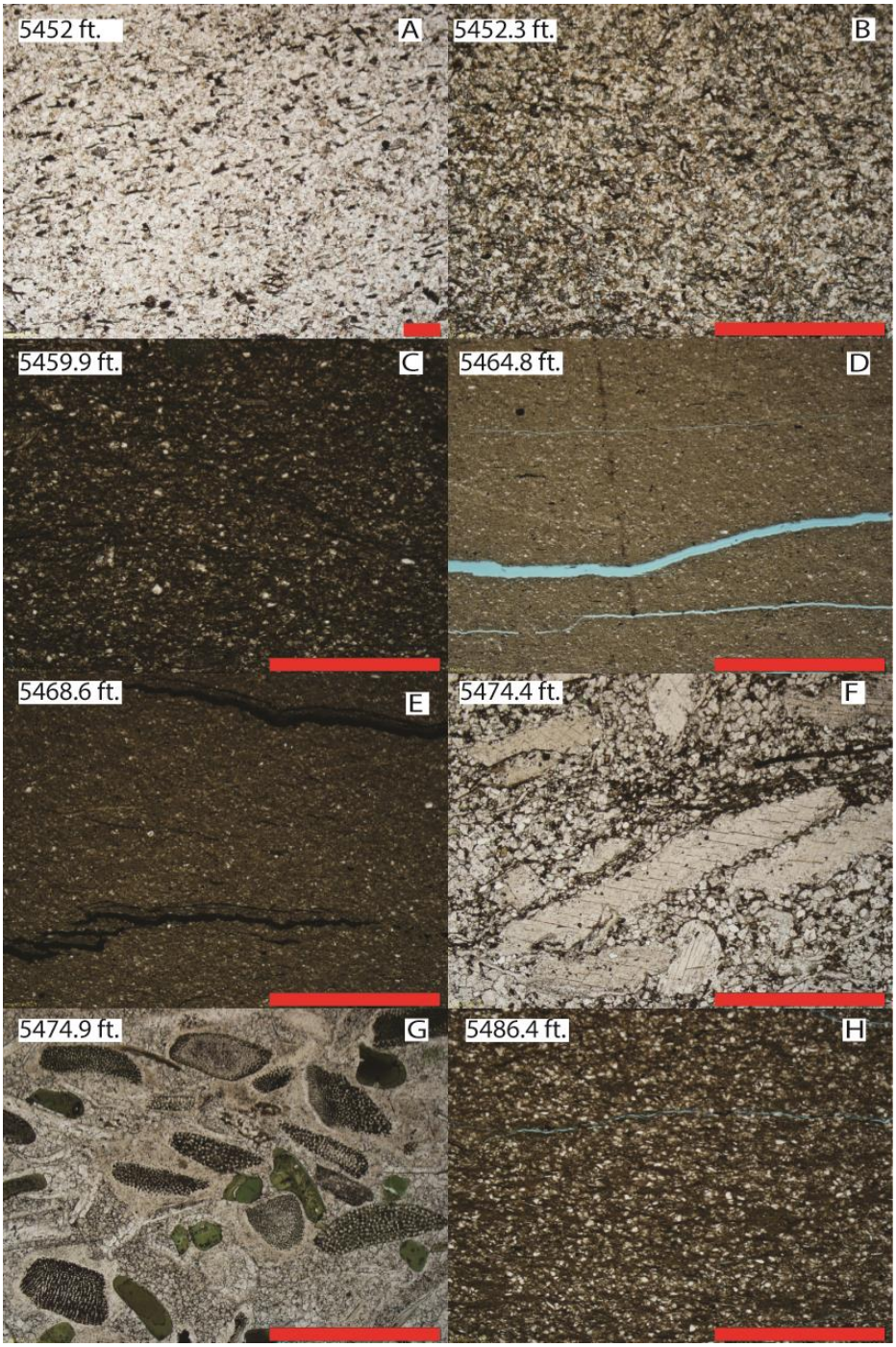

Fig. 4.6. Photomicrographs of the Eau Claire Formation for Unit B from the VW#1 well. Fig. 4.4A Scale bar (red) equals 0.2 mm, Fig.4.4B-H scale bars are equal to 1 mm. All photomicrographs are in plane-polarized light. Fig. 4.4A-B (Fig. 4.4A depth=5452 ft., Fig. 4.4B depth=5452.3 ft.) show siltstones that are feldspar rich, which occur interbedded with Unit B shales. Fig. 4.4C-E (Fig. 4.4C depth=5459.9 ft., Fig. 4.4D depth=5464.8 ft., Fig. 4.4E=5468.6 ft.) show 3 different types shales in the Eau Claire, each a slightly different color with variable amounts of detritus. Figures 4.4F (depth=5474.4 ft.) displays a glauconitic dolostone with large calcite grains in a silty clay-rich matrix. Fig. 4.4G (depth=5474.9 ft.) shows a glauconitic dolostone deposit with partially dissolved echidoderm and brachiopod fragments and secondary dolomite cementation. Fig. 4.4H (depth=5486.4 ft.) shows a shale near the base of Unit B with substantial quartz detritus throughout.

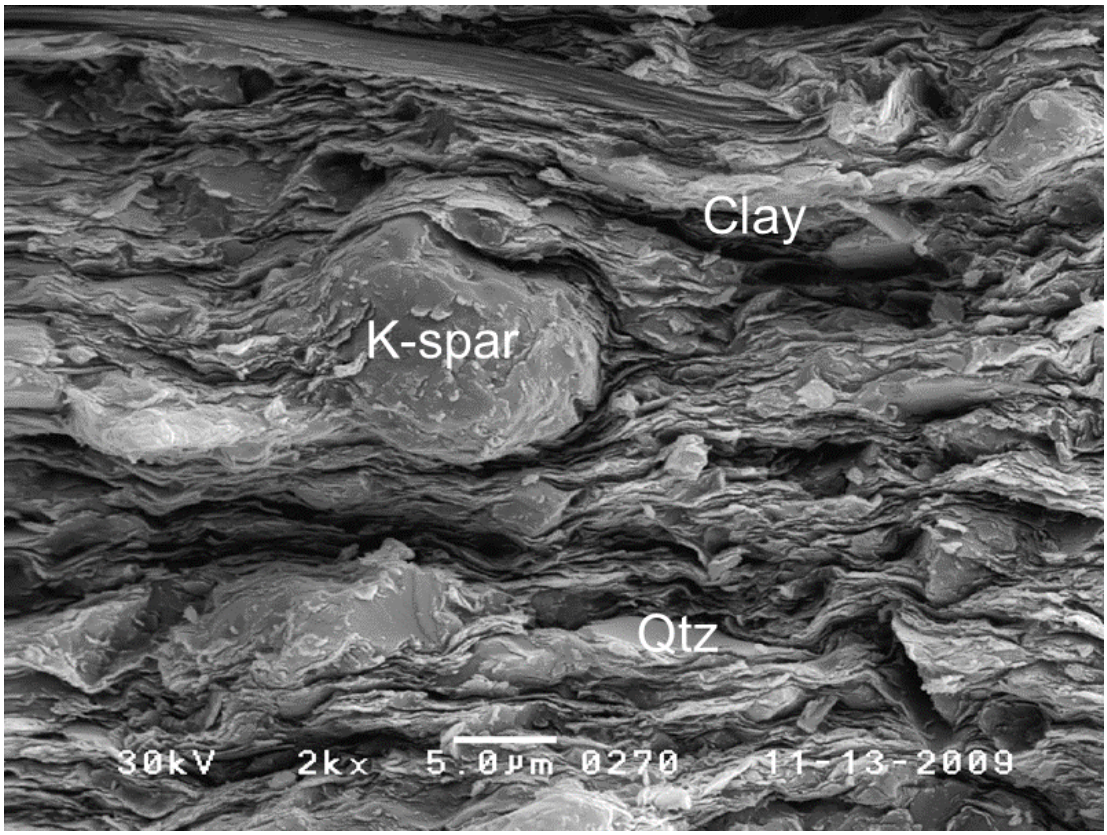

Fig. 4.7. SEM photomicrograph of the Eau Claire Unit B from CCS#1 5502.7 ft. at 2000x magnification. Photomicrograph shows a shale with quartz and K-feldspar detritus in a clay rich matrix. Photograph by Weatherford Laboratories.

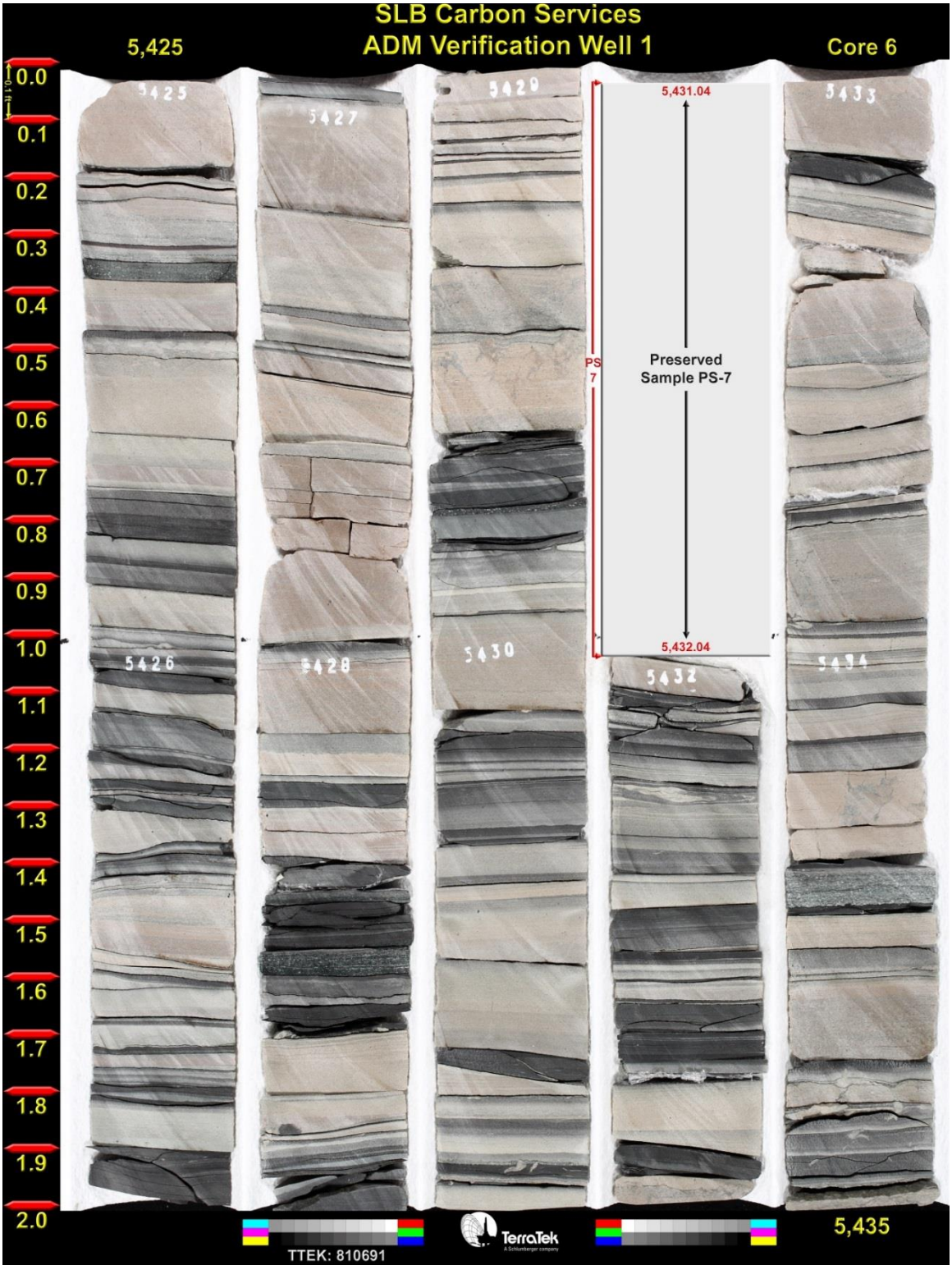

Fig. 4.8. Core photo of the Eau Claire Formation Unit C from 5,425 ft. to 5,435 ft. in the VW#1 well. Planar-bedded siltstones, clayey siltstones, shales and glauconitic siltstones interbed in a rhythmic fashion. Photograph by Terratek.

Depth (ft)	Quartz	K-Feldspar	Pore	Glauc	Clay	Iron Oxide	Lithics	Carbonate	Total	Mean Grain Size (um)	Lithofacies	Depositional Environment
5350	38.46%	52.02%	4.25%	0.00%	4.86%	0.00%	0.00%	0.40%	1.000	62.6		
5367	36.44%	32.59%	4.25%	0.20%	27.53%	0.00%	1.01%	0.00%	1.020	63.4		
5378	64.98%	10.12%	6.68%	0.81%	2.23%	0.00%	1.21%	13.97%	1.000	58.1		
5378	27.33%	20.65%	1.01%	0.00%	47.57%	0.00%	0.40%	3.04%	1.000			
5418	43.52%	36.44%	3.24%	0.40%	13.16%	0.00%	2.63%	0.61%	1.000	42.4		
5425.2	76.72%	2.43%	0.00%	1.21%	16.80%	0.40%	2.02%	0.40%	1.000	53.9	Planar-Bedded Siltstone	Upper shoreface-above FWWB
5425.2	74.70%	4.05%	1.21%	5.47%	3.24%	0.00%	2.83%	8.50%	1.000		Planar-Bedded Siltstone	Upper shoreface-above FWWB
5430.6	51.01%	21.46%	0.00%	0.00%	23.48%	0.00%	0.20%	3.85%	1.000	31.2	Planar-Bedded Siltstone	Upper shoreface-above FWWB
5432.4	75.71%	7.09%	2.23%	0.20%	14.37%	0.00%	0.00%	0.40%	1.000		Interbedded Siltstone/Shale	Upper shoreface-above FWWB
5432.4	4.62%	1.54%	0.00%	3.08%	90.77%	0.00%	0.00%	0.00%	1.000		Interbedded Siltstone/Shale	Upper shoreface-above FWWB
5434.1	60.53%	20.24%	0.00%	0.20%	15.38%	0.00%	0.00%	3.64%	1.000	42.0	Interbedded Siltstone/Shale	Upper shoreface-above FWWB
5434.1	22.06%	24.29%	1.21%	0.40%	50.61%	0.00%	1.01%	0.00%	0.996		Interbedded Siltstone/Shale	Upper shoreface-above FWWB
5434.5	0.00%	0.00%	0.00%	13.36%	11.34%	0.00%	0.00%	75.30%	1.000		Greensand	Upper shoreface-above FWWB
5434.5	81.17%	1.82%	0.61%	0.20%	5.47%	0.00%	4.25%	6.48%	1.000	42.0	Greensand	Upper shoreface-above FWWB
5435.5	48.18%	39.07%	0.00%	2.43%	9.11%	0.00%	1.21%	0.00%	1.000		Greensand	Upper shoreface-above FWWB
5441.4	28.95%	51.42%	0.40%	0.00%	16.19%	0.00%	1.01%	0.20%	0.982	48.8	Interbedded Siltstone/Shale	Upper shoreface-above FWWB
Average	**45.90%**	**20.33%**	**1.57%**	**1.75%**	**22.01%**	**0.03%**	**1.11%**	**7.30%**		**49.38**		

Table 4.3. Point count mineralogy, grain size, lithofacies and depositional environment for Unit C of the Eau Claire Formation, from the VW#1 well. Unit C has an average composition of arkose wacke (15-75% clay, greater than 5% K-feldspar; Dott 1964) and an average grain size of 49.4 µm. Glauc = Glauconite.

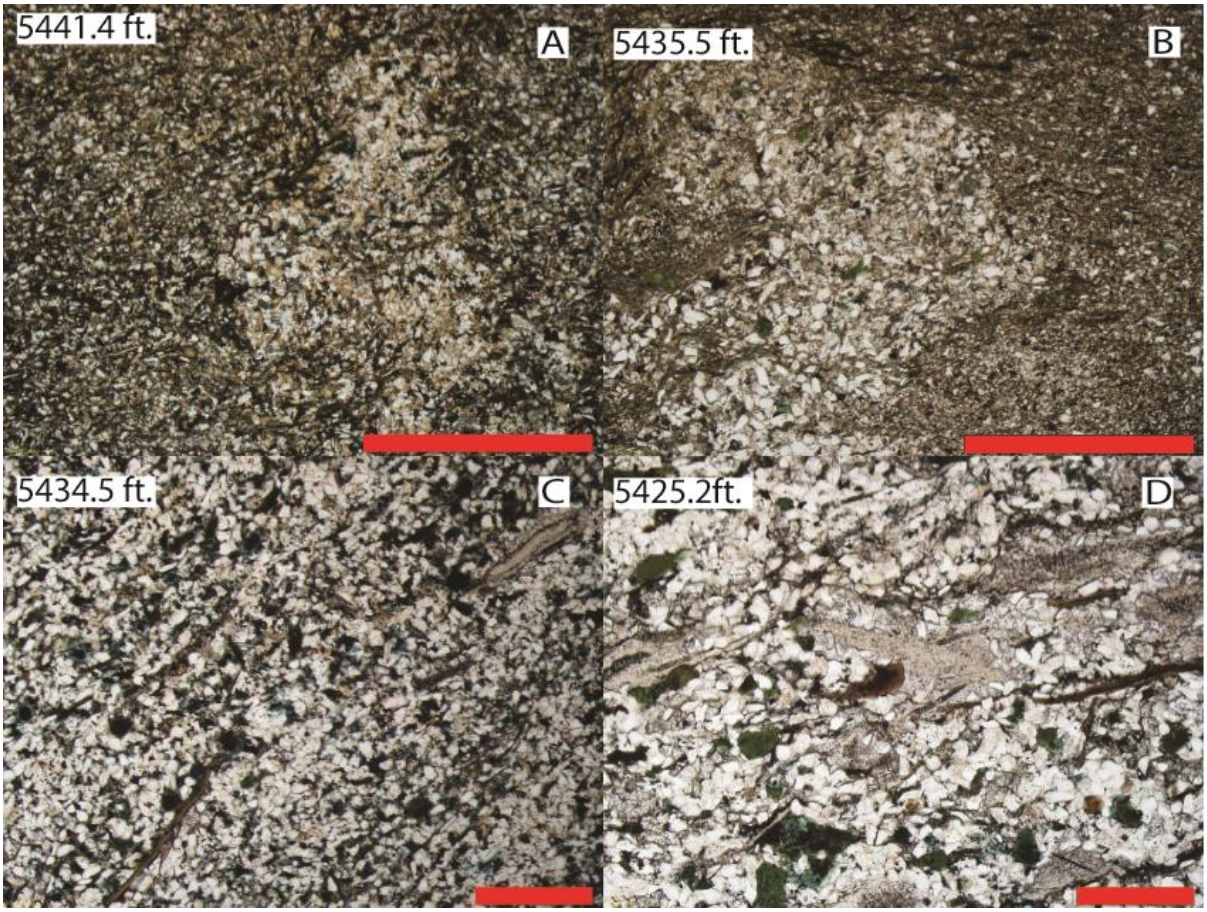

Fig. 4.9. Photomicrographs of the Eau Claire Formation for Unit C from the VW#1 well. Scale bar (red) for Fig. 4.9 A/B is 1 mm and 0.5 mm for Fig. 4.9C/D. Figs. 4.9A-B are arkosic siltstones and represent the type lithology of Unit C. Fig. 4.9C shows a siltstone containing trace glauconite, echinoderm and brachiopod fragments. Fig. 4.9D is a glauconitic-dolomitic siltstone, with brachiopod fragments and a phosphatic fragment in the middle of the sample.

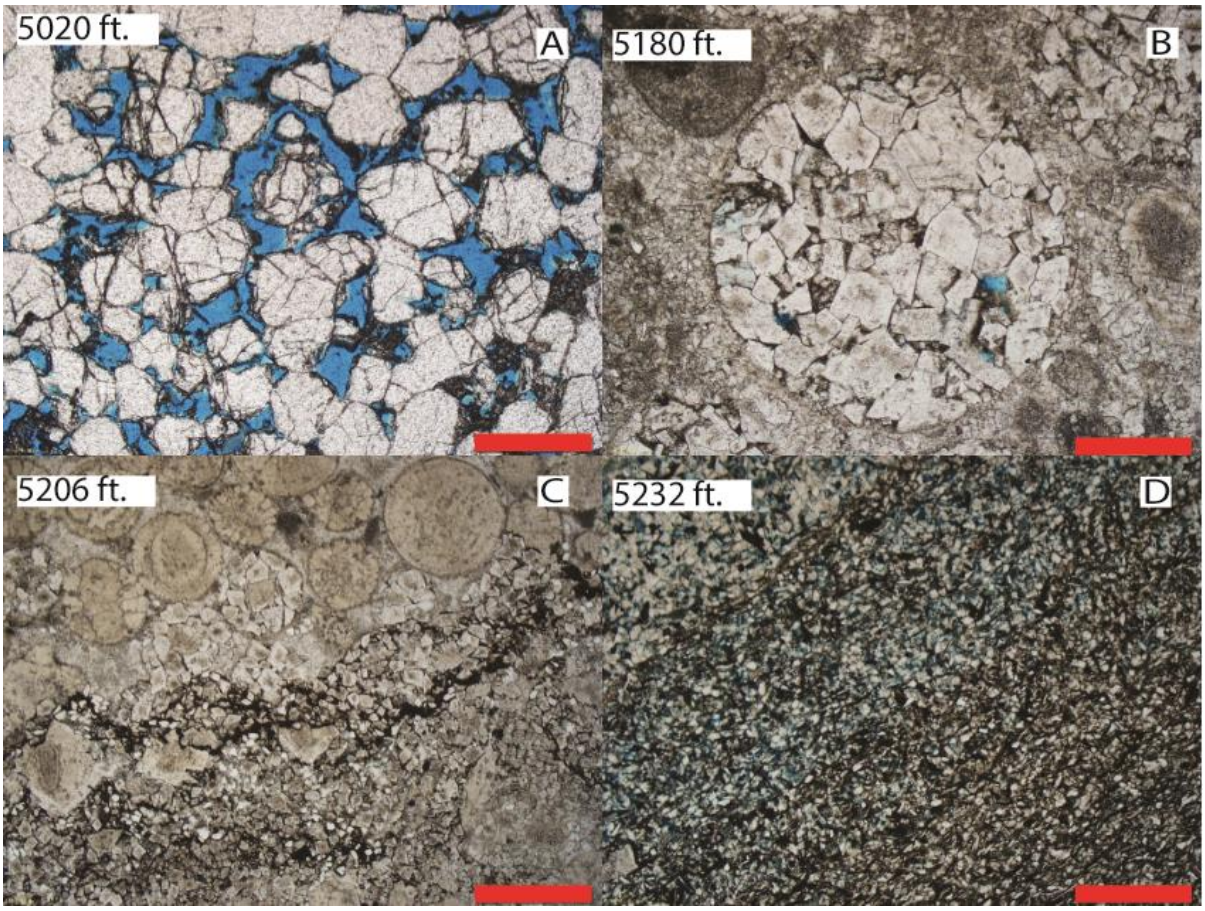

Fig. 4.10. Photomicrographs of the Eau Claire Formation for Unit D from the CCS#1 well. Fig. 4.10 A,B and D scale bar equals 0.5 mm, Fig. 4.10 C scale bar equals 1 mm. All photomicrographs are in plane polarized light. Fig. 4.10A displays a clean quartz sandstone at the top of the Eau Claire Formation near the overlying Ironton-Galesville Sandstone. Fig. 4.10B displays an oolitic packstone with secondary dolomite, while Fig. 4.10C displays an oolitic packstone with clay laminae. Fig. 4.10D shows a clayey siltstone with 2.6% porosity.

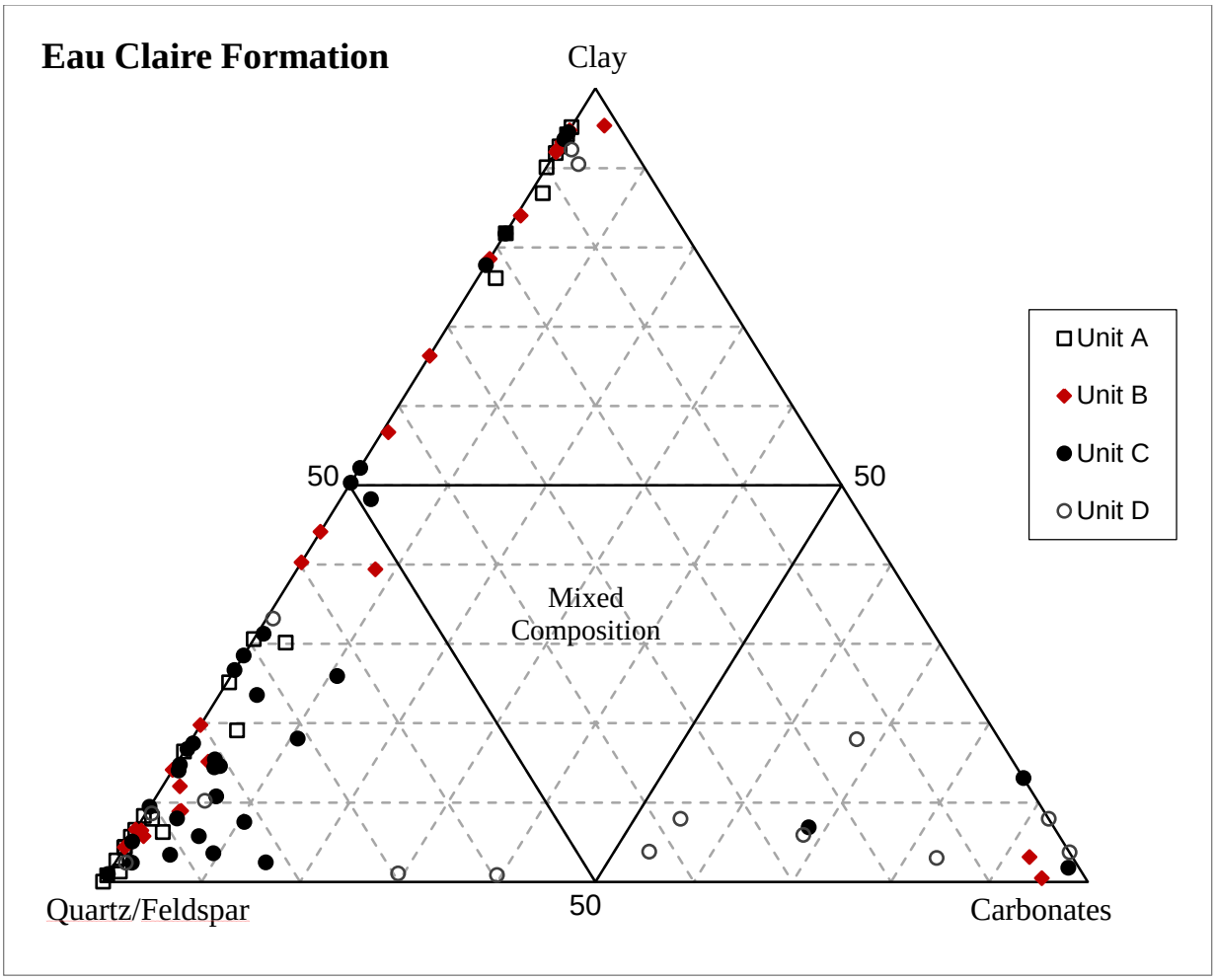

Fig. 4.11. Ternary Diagram for the Eau Claire Formation at the IBDP with axes of clay, quartz/feldspar and carbonate.

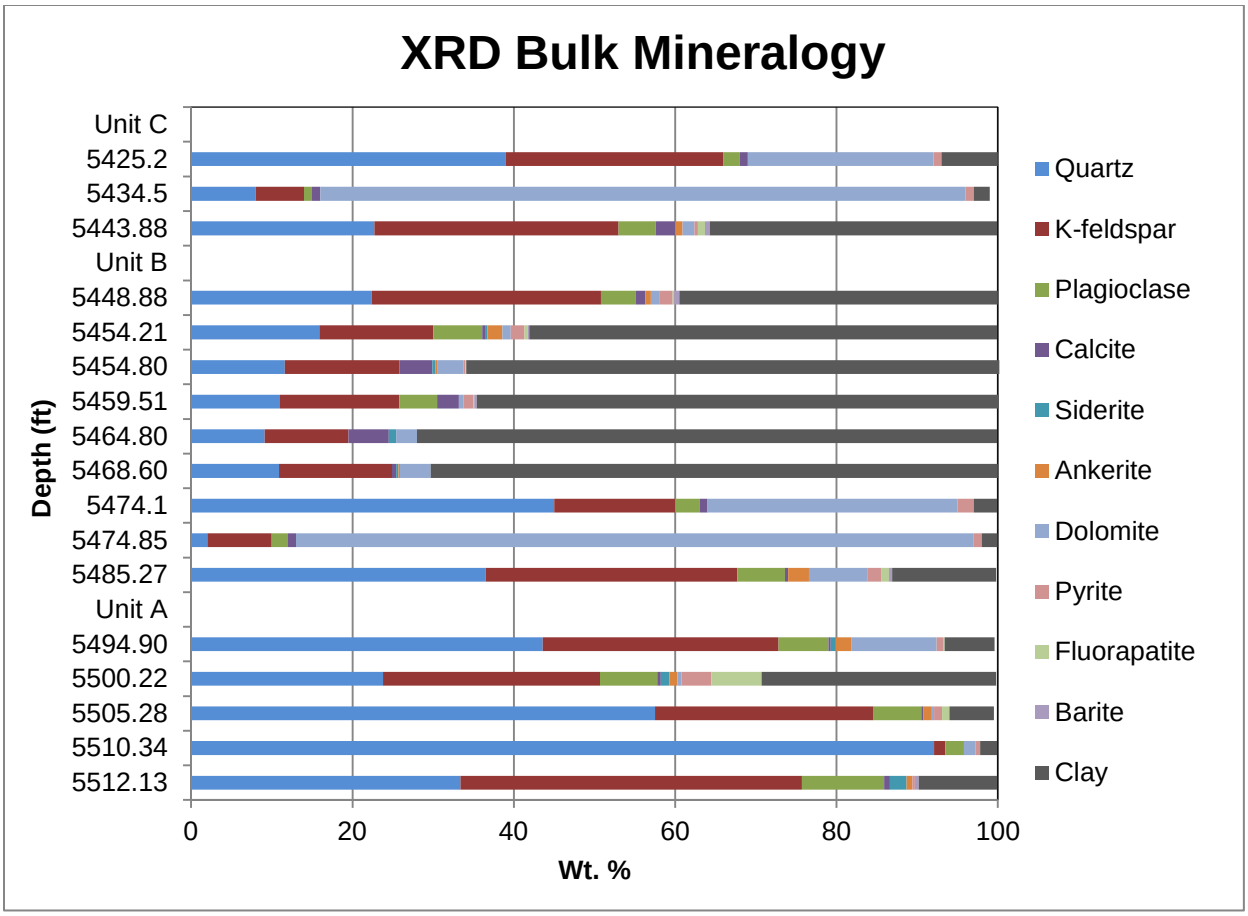

Fig. 4.12. XRD bulk mineralogy (sample depth vs. wt. %) for the Eau Claire Formation at the IBDP.

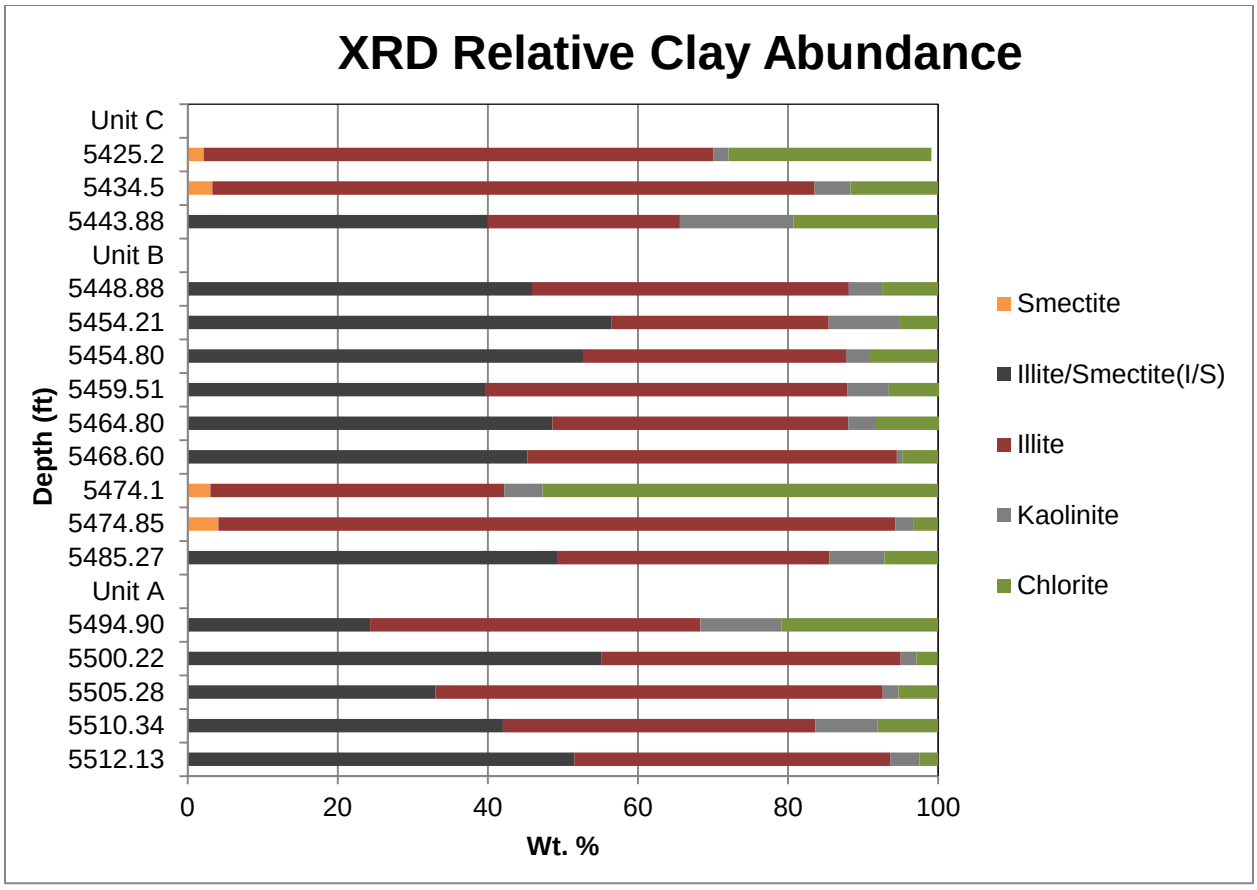

Fig. 4.13. XRD clay mineralogy (sample depth vs. wt. %) for the Eau Claire Formation at the IBDP.

Well and unit	Depth (ft)	Quartz	K-Feldspar	Pore	Glauc	Clay	Iron Oxide	Lithics	Carbonate	Total	Mean Grain Size (um)	Lithofacies	Depositional Environment
CCS#1													
D	**5022**	74.70%	0.81%	10.73%	0.00%	9.11%	0.00%	0.00%	4.66%	1.000			
	5040	54.86%	1.21%	5.87%	0.00%	0.81%	0.00%	0.00%	37.25%	1.000			
	5106	57.29%	3.24%	8.50%	0.00%	30.36%	0.00%	0.00%	0.61%	1.000			
	5120	36.23%	1.01%	0.40%	0.00%	7.89%	0.00%	0.00%	54.45%	1.000		Packstone	
	5132	65.79%	1.62%	3.04%	0.00%	1.01%	0.00%	0.00%	28.54%	1.000		Packstone	
	5140	19.64%	6.07%	0.81%	0.00%	5.87%	0.00%	0.00%	67.61%	1.000		Packstone	
	5190	0.00%	0.00%	0.00%	2.23%	3.64%	0.00%	0.00%	94.13%	1.000		Packstone	Ooid shoal
	5206	0.00%	0.00%	0.00%	0.00%	7.89%	0.61%	0.00%	91.50%	1.000		Packstone	Ooid shoal
VW#1													
D	**5036**	4.05%	2.23%	0.00%	0.00%	92.31%	0.00%	0.00%	1.42%	1.000	52.1		
	5036	6.07%	0.40%	0.00%	0.00%	90.49%	0.00%	0.00%	3.04%	1.000	<4	Shale	
	5078	81.98%	7.09%	6.07%	0.20%	2.23%	0.00%	1.42%	1.01%	1.000	42.1		
	5078	11.13%	2.02%	2.63%	0.00%	2.83%	0.00%	2.43%	78.95%	1.000		Packstone	
	5078	84.62%	3.04%	3.44%	0.00%	8.30%	0.00%	0.00%	0.61%	1.000			
	5078	13.36%	1.01%	0.20%	0.61%	17.81%	0.00%	0.00%	67.00%	1.000			
	5078	41.09%	0.00%	2.43%	0.00%	3.64%	0.00%	1.21%	51.62%	1.000			
	Average	36.72%	1.98%	2.94%	0.20%	18.95%	0.04%	0.34%	38.83%		47.1		

Table 4.4. Point count mineralogy, grain size, lithofacies and depositional environment for Unit D of the Eau Claire Formation, from the CCS#1 and VW#1 wells. All samples from Unit D are rotary sidewall cores. The average composition of the siliciclastic samples is a quartz wacke with an average grain size of 47 µm, while the average carbonate composition is a packstone. Glauc = Glauconite.

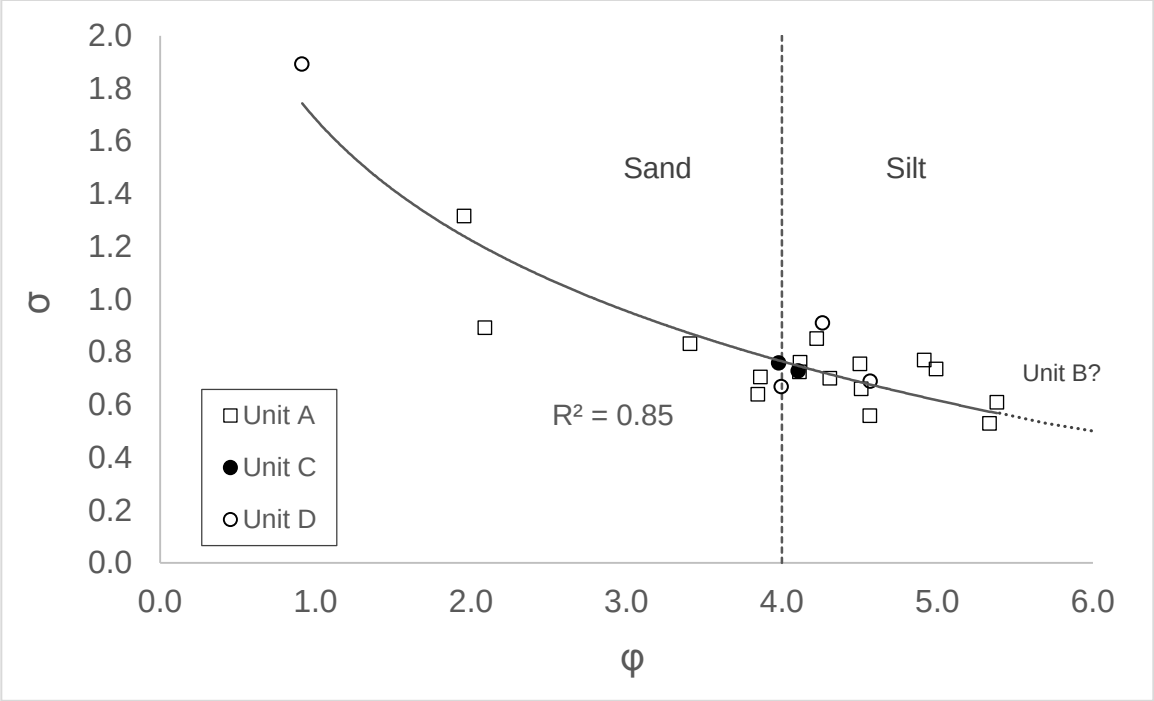

Fig. 4.14. σ (degree of sorting) vs. ϕ (grain size) for Units A,C and D in the Eau Claire Formation. Unit B is not included due to a lack of grain size data in samples containing clay size grains. Instead, its position is inferred based on the correlation for Units A,C and D.

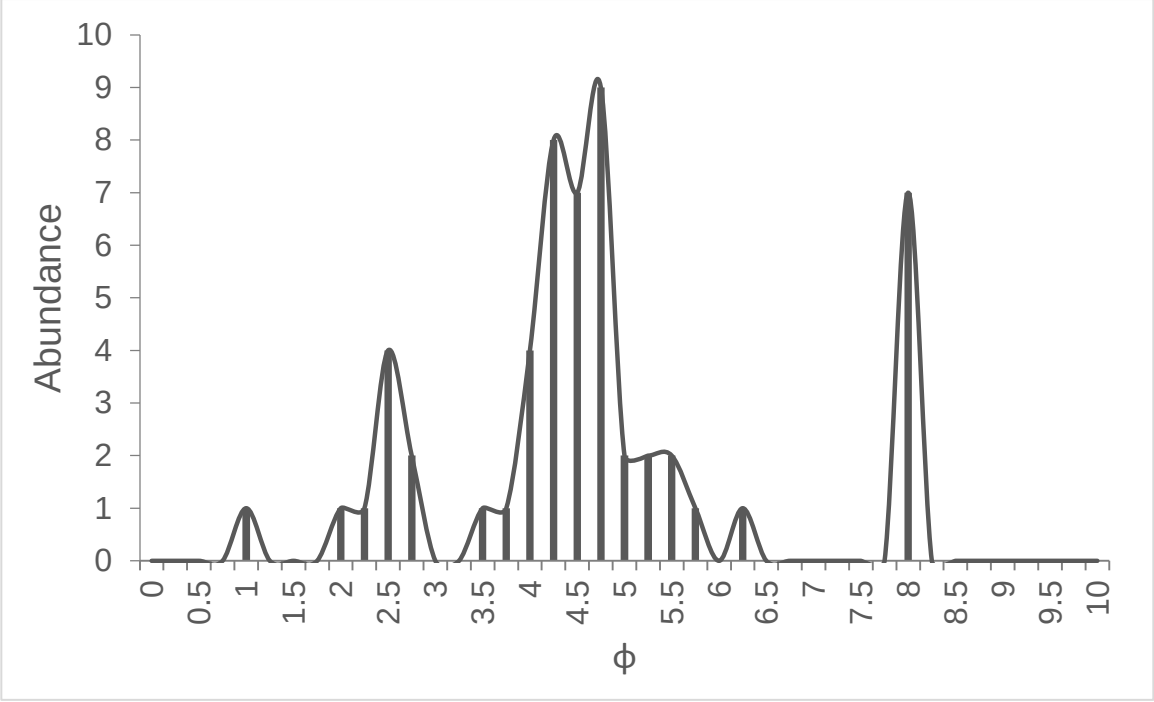

Fig. 4.15. Grain size histogram in ϕ units for all Units in the Eau Claire Formation.

Well	Depth (ft)	$\delta^{13}C_{VPDB}$	$\delta^{18}O_{VPDB}$	$^{87}Sr/^{86}Sr$	Formation	Unit	Sr Prep Method
CCS1	5000	3.4	-6.07		Eau Claire	Unit D	
CCS1	5040	4.64	-6.37		Eau Claire	Unit D	
CCS1	5120	0.86	-7.77	0.709642	Eau Claire	Unit D	HNO_3 Digestion
CCS1	5180	1.51	-7.53		Eau Claire	Unit D	
CCS1	5190	0.94	-7.7	0.709250	Eau Claire	Unit D	HNO_3 Digestion
CCS1	5206	0.53	-7.36	0.709208	Eau Claire	Unit D	HNO_3 Digestion
VW1	5425.2	-2.78	-7.625		Eau Claire	Unit C	
VW1	5434.5	-3.02	-7.78	0.710587	Eau Claire	Unit C	HNO_3 Digestion
VW1	5435.5			0.710515	Eau Claire	Unit C	HNO_3 Digestion
VW1	5440.25			0.73678995	Eau Claire	Unit C	NaOH fusion
VW1	5452.1			0.7710647	Eau Claire	Unit B	NaOH fusion
VW1	5464.8			0.745633	Eau Claire	Unit B	HNO_3 Digestion
VW1	5464.8			0.764460	Eau Claire	Unit B	NaOH fusion
VW1	5474.1			0.721120	Eau Claire	Unit B	HNO_3 Digestion
VW1	5474.1			0.735701	Eau Claire	Unit B	NaOH fusion
VW1	5474.4	-3.46	-7.725		Eau Claire	Unit B	
VW1	5474.85	-3.45	-7.3	0.718666	Eau Claire	Unit B	HNO_3 Digestion
VW1	5475.1	-3.46	-7.47		Eau Claire	Unit B	
VW1	5475.4	-3.79	-8.09		Eau Claire	Unit B	
VW1	5476.1	-3.36	-7.045	0.75648725	Eau Claire	Unit B	HNO_3 Digestion
VW1	5482.2			0.771930	Eau Claire	Unit B	NaOH fusion
VW1	5487.6	-4.28	-8.37	0.710234	Eau Claire	Unit A	HNO_3 Digestion
VW1	5495.6	-4.36	-9.15		Eau Claire	Unit A	
VW1	5496.42	-4.88	-10.96	0.709840	Eau Claire	Unit A	HNO_3 Digestion
VW1	5498.95	-4.31	-9.25		Eau Claire	Unit A	
VW1	5526.8			0.746581	Eau Claire	Unit A	HNO_3 Digestion
VW1	5526.8			0.756220	Eau Claire	Unit A	NaOH fusion
VW1	7062A			0.7118629	EGRP		NaOH fusion
VW1	7062B			0.7167868	EGRP		NaOH fusion
VW1	7066A			0.7275411	EGRP		NaOH fusion
Locality							
Silver Mines Granite				0.7341747	St. Francois		NaOH fusion
Knob Lick Granite				0.7419765	St. Francois		NaOH fusion
Johnsons Shut Ins Aplite				0.8676624	St. Francois		NaOH fusion
Johnsons Shut Ins Granite				0.9025629	St. Francois		NaOH fusion
Johnsons Shut Ins Rhyolite				1.107499	St. Francois		NaOH fusion
Elephant Rocks Granite				1.440842	St. Francois		NaOH fusion

Table 4.5. $\delta^{13}C$, $\delta^{18}O$ and $^{87}Sr/^{86}Sr$ for the Eau Claire Formation, basement rock at the IBDP site and the St. Francois region of Missouri. The basement rock at the IBDP site and samples from the St. Francois region of Missouri are both part of the EGRP.

CHAPTER 5: DISCUSSION

5.1 Unit A (VW#1 5,487–5,527 ft.) Depositional Environment

The intense bioturbation, paucity of glauconite and thick shale, interbedded sands/mud, and flaser/lenticular bedding indicates deposition on a near shore, tidally influenced, inter- to subtidal sand/mud flat environment **(Fig. 5.1).** The underlying upper unit of the Mt. Simon Sandstone represents a shift from a nearshore eolian environment with minor fluvial influence to a shallow marine environment, marking the beginning of the Sauk transgressive sequence (Sloss 1963; Freiburg et al. 2014). The clastic source supplying the Mt. Simon with detritus is gradually becoming more distal in Unit A, indicated by the reduction in grain size and evidence of decreasing energy. The small scale current ripples and bioturbated flaser/lenticular bedded siltstones and mudstones in Unit A are diagnostic of tidal flat deposits (Weimer 1982). Well sorted, well-rounded, cross-bedded quartz arenites occur periodically between tidal flat deposits, characteristic of tidal channel deposition **(Fig. 5.2)** (Weimer et al. 1982). Most of the tidal channels are small, representing no more than 1 ft. of deposition per channel as seen from the core, however at least one channel is greater than 2 ft. thick. The small size of the tidal channel deposits suggests lower energy and declining terrigeneous input from the land as the shoreline transgresses. Tidal channels are higher energy than the tidal flats that they cut across, allowing primarily suspended load deposition to occur. In a tidal flat, bioturbation is typically greatest in the intertidal zone, due to its low energy (Weimer et al. 1982, Desjardins et al. 2012). Unit A's extensive bioturbation occurs in its tidal flat deposits, representing the majority of this depositional unit. Most tidal flat deposition results from lateral accretion due to migrating tidal channels. However some vertical accretion occurs on the tidal flat portion of the environment. This migration is associated with progradation of the flats and point bars related with meandering tidal channels (Weimer et al. 1982). Numerous burrows exist that may be *planolites*, which are known to occur in shallow marine depositional environments (Alpert 1975). Glauconite is absent from the intertidal zone of Eau Claire's Unit A but present in the above units, suggesting deposition occurred closer towards the shore. The appearance of glauconite in overlying units is indicative of a marine transgression in the region. Glauconite requires fully saline conditions and typically occurs in water depths greater than 30m (Porrenga 1966). Glauconite also represents a low sedimentation rate, indicative of a lower energy depositional environment (Harris and Whiting 2000).

The upper section of Unit A (5487-5503 ft.) represents a subtidal environment within the tidal flat. A reduction in grain size, from fine sand to silt occurs across this transition and is characteristic of subtidal bedload deposition (Desjardins et al. 2012). Numerous wavy and ripple beds exist indicating this unit is still above the fair weather wave base (FWWB) (Longhitano et al. 2012). Sedimentation becomes more cyclic above a depth of 5503 ft., composed of interbedded siltstones and shales. This interbedding of higher energy siltstones/sandstones with shales is the classic tidal signature, and arguably the most diagnostic feature of a subtidal shoreface sequence (Weimer et al. 1982, Aigner 1985, Myrow and Southard 1996). A peculiar feature of the Eau Claire core from the VW#1 well is a flat pebble conglomerate that occurs around 5503 ft. Flat pebble conglomerates exist throughout the Phanerozoic, although they are particularly common in the early Paleozoic (Sepkoski 1982). Numerous theories exist pertaining to their formation (Myrow et al. 2004). However, the most commonly accepted hypothesis suggests these units form due to very high energy events (large storms) in a subtidal shelf succession (Pratt 2002). Thus, the flat pebble conglomerate bed likely marks the boundary of subtidal deposition for Unit A. Another indicator of subtidal deposition is the reduction of bioturbation that occurs above the flat pebble conglomerate bed.

5.1.1 Unit A Petrophysics

Unit A's porosity and permeability are the highest of the Eau Claire's measured units **(Figs. 4.3-4.4; Table D.1**) with values of 6.6% and 8.7 mD. Despite being the highest in the Eau Claire, Unit A's values are still quite low. Unit A's petrophysical properties do not meet the criteria laid out by previous authors (Fleury et al. 2010) for an effective caprock, i.e. a formation above the sequestration reservoir possessing nD ~ µD level permeability. Although 8.7 mD does not meet this requirement, it is not a value that is favorable for fluid flow and would likely inhibit CO_2 migration in the short term. Many interbedded mudstones exist within Unit A which would likely serve as impermeable baffles.

5.2 Unit B (VW#1 5,448-5,487 ft.) Depositional Environment

Water level continues to rise in central Illinois during deposition of the Eau Claire Formation's Unit B, indicated by the decreasing amount of sedimentary structures, finer grain size, and general lithologic dominance of dark grey shale throughout the unit **(Fig. 5.3).** Unit B is interpreted as having a depositional environment in the offshore transition zone, between the FWWB and storm wave base (SWB), also known as the lower shoreface **(Fig. 5.4)**. Interstratification and rippling of sand and mud are common in tidal deposits due to fluctuations of high/low energy (Weimer et al. 1982), however their absence in this case indicates deposition is occurring below the FWWB. Unit B is characterized by large amounts of dark grey shale with periodic occurrences of siltstone/clayey siltstone beds, and one relatively large (~1 ft. thick) silty dolostone bed that is interpreted as a storm deposit (tempesite) at 5,475 ft. (1668.8 m) in the VW#1 core. The bed averages 88% dolomite, 5% lithics, 4% glauconite, 1% quartz, 1% K-feldspar, and 1% hematite from point count mineralogy. Analysis of hand samples reveals disseminated pyrite and hematite throughout the bed. In sedimentary systems, both pyrite and hematite typically form through chemical processes in marine environments (Derry and Jacobsen 1990). The bed is interpreted as a tempesite because it has a sharp basal contact with the underlying shale and does not fit in with the low energy units above and below the bed. Tempesites are a diagonostic criteria of a subtidal shelf environment (Bouma et al. 1982) and by definition occur above the SWB. Unit B's Tempesite bed is easily identified by its unique gamma ray signature **(Fig. E.1)** and represents an important feature of the Unit which can be used as a marker bed in locations proximal to the IBDP site.

5.2.1 Unit B Petrophysics

Unit B is poorly represented in the core analysis dataset **(Figs. 4.3-4.4; Table D.1)** with 11 porosity values averaging 5.8% and no laboratory permeability data. The fissile nature of the shale makes sample preparation for core analysis of this unit impossible. However, four data points estimated from MICP data reveal an average permeability of 2.0×10^{-5} mD (20 nD) for Unit B. Although a more comprehensive assessment was not possible, shales are typically the favored caprock for carbon sequestration projects (Shukla et al. 2010) due to their low petrophysical values, and the estimated permeability values of Unit B exceed Fleury et al. (2010) petrophysical criteria of a suitable CCS seal.

5.3 Unit C (VW#1 5,355-5,448 ft.) Depositional Environment

Interstratified maroon – pink siltstones, grey clayey siltstones and dark grey shales represent the primary feature in the drill core available for Unit C, which is generally considered to be the diagnostic criteria of tidal deposition, also known as 'tidalites' (Klein 1963, Klein 1998, Coughenour et al. 2009, Steel et al. 2012). Unit C represents a subtidal upper shoreface environment between mean low tide and the FWWB **(Fig. 5.5).** These rhythmic changes in lithology represent the changes in energy that accompany ebb and flood deposition in a tidal system, and typically manifest in the form of interbedded sand and mud sized grains (**Fig. 5.6)** (Davis 2012). During high tide conditions (higher energy) bedload deposition forms planar to ripple bedforms on the surface, while low tide results in suspended load deposition of finer grains in the troughs, or overlying the bedforms, referred to as flaser bedding (mud within sand) or lenticular bedding (sand within mud) (Reineck and Wunderlich 1968). Typically, tidal deposits are thought of as being composed of interstratified sand/mud, however Unit C is less heterolithic than typical tidal deposits, being composed of primarily interbedded silt and mud. This is likely due to the Mt. Simon's clastic source drying up, causing a decrease in coarser detritus being supplied to the area. Further evidence for this is the overlying carbonate unit, indicating a complete cessation of clastic sediment to the area. Glauconite has a strong presence in Unit C, occurring rhythmically every 1-6 ft. in so-called 'greensand' beds **(Fig. A.2)**, indicating water depths of 30 m or greater (Porrenga 1966).

Planar bedding is the predominant sedimentary structure within Unit C. This feature, coupled with an average grain size of 49 µm **(Table 4.3)** alludes to lower energy, slack water deposition (Allen 1964, Best and Bridge 1992). However, a trace amount of ripple beds found throughout the Unit C core indicates it is being influenced by a weak amount of everyday tidal action. A depositional environment near the FWWB is likely, with planar bed deposition forming under normal tidal conditions and ripple beds forming during times of higher energy. The glauconite rich tempesite deposits found throughout Unit C do not appear to be related to the ripple beds in anyway. Given their cyclicity, these may indicate large scale super storm type events where the environment is shocked with a large amount of tidal energy. The maroon-pink color of Unit C's siltstones is a product of the high K-feldspar content, averaging 20.3% for the unit **(Table 4.3).**

5.4 Unit D (VW#1 5,010-5,355 ft.) Depositional Environment

Unit D reflects deposition slowly becoming more distal to the siliciclastic source supplying Units A-C, indicated by the gradual decrease in detrital material and increase in carbonate deposition (**Fig. 5.7)**. Log analysis indicates Unit D contains interbedded siliciclastic – carbonate deposits near its base, although the logs indicate basal lithology is not uniform across all three wells at the IBDP **(Fig. E.1)**. VW#1 contains considerable quartz, feldspar, and limited amounts of carbonate in the basal 100 ft. (30.5 m), while CCS#1 contains quartz, feldspar, calcite, dolomite, and a significant chlorite component. The VW#2 well is the only well with a significant carbonate component in the basal 100 ft. (30.5 m), which is comprised heavily of dolomite with lesser amounts of calcite. All three wells are located within 2 km (1.25 mi) of each other, and large lithologic changes between the three wells are not observed in underlying Units A-C. These large lithologic differences within a relatively short transect alludes to the possibility of a paleotopographic high within the Illinois Basin supplying sediment to the region (Leetaru and McBride, 2008).

5.5 Grain Size

Good correlation exists between sorting and grain size for the Eau Claire (R^2=0.85; **Fig. 4.14),** providing a first order approximation of the shallow marine depositional environment for the Eau Claire Formation. The sorting mechanisms within the terrestrial realm are quite different than those in the marine realm, often producing a wide range of grain sizes and grain sorting values (Rice and Church 1998). Fluvial deposits in braided rivers are created by lateral accretion as the channel avulses, producing fining upward sequences (Smith 1970). Therefore, a plot of sorting vs. grain size for a fluvial or alluvial formation would have a significantly lower correlation between sorting and grain size. Energy fluctuations can still be high in certain parts of the marine realm (Weimer et al. 1982), however the largely uniform grain size indicates deposition occurred in a shallow marine environment.

5.6 Carbon Isotopes

In the Eau Claire Formation, a +8‰ $\delta^{13}C$ excursion (R^2=0.97) occurs across the Eau Claire's 500 ft. (152.4 m) thickness at the IBDP site **(Fig. 5.8)**. At the base of the Eau Claire $\delta^{13}C$ values hover around -4‰. These values are expected due to their proximity to the Mt. Simon Sandstone, which exhibits a transgressive shift from terrestrial to shallow marine environment in its upper units (Freiburg et al. 2014). $\delta^{13}C$ values increase with shallower depth in the core, with a cluster of values at ~ +2‰ around 5200 ft., and values of +4‰ near 5000 ft. at the top of the Eau Claire. This positive isotopic excursion is likely indicative of increased organic carbon burial in proximal sediments and may relate to increased productivity, sedimentation or enhanced preservation under anoxic settings (Arthur et al. 1987; Derry et al. 1992; Schrag et al. 2002; Saltzmann and Thomas 2012). Although the qualitative evidence from the drill core indicates a marine transgression in the siliciclastic lower portion of the Eau Claire, the isotopic data cannot be inferred to compliment that. Instead, the author favors a marine transgression from Unit A to Unit B, a regression between Unit B and Unit C, and a relatively steady sea level throughout the remainder of the Eau Claire with a decrease of clastic sediment allowing carbonate production to flourish in the area. During the Cambrian, tectonic activity shifted from proto-Illinois Basin subsidence in the northeastern part of the state to rifting in the New Madrid Rift System at the southern edge of the state (Kolata and Nelson 2010). Isostatic adjustment of the crust is known to rearrange drainage networks (Liu 2014). This large tectonic shift would have caused a readjustment of drainage networks in subaerially exposed crust and is a plausible driving mechanism for declining clastic input throughout the Eau Claire in central Illinois.

Saltzmann and Thomas (2012) proposed a carbon isotope stratigraphy using $\delta^{13}C$ values plotted against U-Pb dates of interbedded volcanics. A major positive carbon isotope excursion that occurs in the Cambrian is referred to as the Steptoean Positive Carbon Isotope Excursion (SPICE), which occurred in the Dresbachian period approximately 501-497 Ma. In Iowa and Missouri, *Crepicephalus* and *Aphelaspis* zone trilobite fauna exist within the Eau Claire and laterally equivalent Bonneterre Formation, indicating an age of 500-495 Ma (Thompson 1995). Units A-C, the dominantly siliciclastic units also plot at isotopically lighter values than Unit D, representing a shift from a clastic to carbonate environment. The $\delta^{13}C$ values for the Eau Claire are consistent with a SPICE excursion, and coupled with the Dresbachian age of the Bonneterre/Eau Claire in bordering states provides compelling evidence that the Eau Claire within the Illinois Basin is also approximately 500 Ma.

5.7 Oxygen Isotopes

Traditionally, the ratio of ^{18}O to ^{16}O normalized to a standard ($\delta^{18}O$) is used to obtain paleotemperatures, assess polar ice volumes, and quantify diagenesis (Veizer and Hoefs 1976, Hoefs 1987, Veizer et al. 1997). More recently, $\delta^{18}O$ has been used as a form of chemical stratigraphy for carbonate rocks (Grossman 2012). Typical late Paleozoic values range from -6‰ to -9‰ (Veizer et al. 1997, Grossman 2012). In the Eau Claire, $\delta^{18}O$ exhibits a similar positive excursion from ~ -11‰ at the base to ~ -6‰ at the top of the formation. **(Fig. 5.9)**, complimenting trilobite zones in adjacent states and the $\delta^{13}C$ excursion in the Eau Claire of central Illinois.

Throughout geologic time, carbonate rocks tend to have lighter $\delta^{18}O$ values with increasing age throughout the Phanerozoic (Baertschi 1957, Clayton and Degens 1959, Degens and Epstein 1962, Keith and Weber 1964, Weber 1965, Dontsova et al. 1972, Perry and Tan 1972, Schidlowski et al. 1975 and many others) with an average value of ~ -8‰ in the Cambrian (Veizer et al. 1997). The origin and interpretation of Paleozoic $\delta^{18}O$ values is the topic of considerable debate. Are early Paleozoic rocks depleted in $\delta^{18}O$ due to diagenesis, or was the earth warmer in the Cambrian? Post depositional alteration is more common in older rocks, and usually results in an altered geochemical signal of the rock. Diagenesis typically leads to lighter $\delta^{18}O$ values, because the isotopically light pore waters exchange oxygen with the isotopically heavy bedrock (Veizer et al. 1997). However, diagenesis can only account for the overall trend of $\delta^{18}O$ depletion, not the continuous decline with age. If diagenesis was the sole contributor to the observed Phanerozoic $\delta^{18}O$ trend, calcite would likely exhibit different $\delta^{18}O$ values than other more resistant minerals such as chert or phosphorites. Chert is far more stable than calcite, and less susceptible to diagenetic alteration (Hoefs 1987). However, chert (Perry and Tan 1972, Knauth and Epstein 1976) and phosphorite minerals (Shemesh et al. 1983) exhibit the same $\delta^{18}O$ trend as calcite throughout the Phanerozoic. These three concurrent trends would seem to disprove the diagenesis hypothesis, instead favoring an alternative theory such as changes in oceanic temperature (Knauth and Epstein 1976, Hoefs 1987, Knauth 2005) or changes in the isotopic composition of the ocean (Perry 1967, Veizer and Hoefs 1976, Hoefs 1987, Veizer et al. 1999, Jaffres et al. 2007) during the early Phanerozoic.

In the rock record, heavier $\delta^{18}O$ values correlate with colder climatic conditions, while lighter $\delta^{18}O$ values indicate a warmer climate. The earth acts as a giant distillation apparatus, preferentially evaporating ^{16}O at the equator and depositing this ^{16}O as the moisture moves poleward. Due to the ice volume effect, heavier $\delta^{18}O$ values in

an oceanic drill core indicate more ^{16}O is locked up in polar ice. However, this inference is only very accurate for Cenozoic carbonates, due to the earth's conveyor belt system recycling oceanic crust every ~10^5 years (Emiliani 1955). Rocks older than Cenozoic age may reflect this ice volume effect assuming they were deposited in a marine environment, although validity must be assessed on a case-by-case basis. Laurentia was located on the equator at 500 Ma, and deposition occurred in a shallow marine environment indicating that an ice volume effect would be noticeable. The average $\delta^{18}O$ value at the equator today is 0‰, indicating Laurentia experienced either much warmer climatic conditions in the early Paleozoic or significant diagenesis afterwards. Due to the Eau Claire's relatively deep position within the Illinois Basin, it is likely that compaction and cementation had an effect on the $\delta^{18}O$, however most investigators favor increased oceanic temperatures (Knauth and Epstein 1976, Hoefs 1987, Knauth 2005), or a different isotopic composition of the ocean in the early Paleozoic (Perry 1967, Veizer and Hoefs 1976, Hoefs 1987, Veizer et al. 1999, Jaffres et al. 2007). Therefore, decoupling which effect is dominating the $\delta^{18}O$ signature is not a straightforward exercise with most samples due to the fine grained nature of the Eau Claire. Assuming the ice volume effect applies to Cambrian rocks, the $\delta^{18}O$ signature of the Eau Claire indicates a shift from extremely warm climatic conditions to cooler conditions that are still quite warm.

5.8 Provenance

In terms of provenance, the relatively high potassium feldspar content (12.4%) for Unit A directly contradicts the roundness of the quartz grains within the unit. Due to their frail nature, feldspars break down when transported over long distances. Therefore a sedimentary unit with a high feldspar content is likely near its source. Quartz grains within Unit A are well rounded, suggesting they have either traveled a long distance from their source to the Illinois Basin or were possibly reworked from the underlying Mt. Simon Sandstone. Wind transport is 10^2-10^3 times more effective at rounding grains than water transport (Kuenen 1959, 1960). Therefore it is possible that the sand sized quartz grains within Unit A are sourced from a nearby location and were transported to the Illinois basin by Eolian processes. When analyzed together, these two characteristics suggest more than one source of sediment for the Eau Claire's Unit A.

The Eau Claire Formation exhibits high $^{87}Sr/^{86}Sr$ isotope ratios (**Fig. 5.10)**, indicating that radiogenic grains within the Eau Claire might be sourced from a nearby terrane that has similar radiogenic $^{87}Sr/^{86}Sr$ isotope ratios. The nearby St. Francois igneous terrane in southeast Missouri exhibits very similar radiogenic values with an isochron age of 1.46 Ga. (**Fig. 5.11)**, and represents the best outcrop exposure of the EGRP. The EGRP trends northeast-southwest from Michigan to Oklahoma and exhibited significant relief on the Cambrian surface of Laurentia (Rudman et al. 1971; Leetaru and McBride 2008). Samples from two different locations exhibiting similar Sr isotope ratios may be genetically related (Revel et al. 1996), and due to the high K-feldspar content and the similarity of $^{87}Sr/^{86}Sr$ ratios the Eau Claire is possibly sourced from EGRP rocks. Note that the sedimentary rocks plotted on Fig. 5.11 cannot be used as an isochron, instead they are plotted to indicate their similarity to St. Francois samples. Three EGRP samples are available from basement rocks in the VW#1 well, and have similar radiogenic values averaging 0.71873 (**Table 4.5)**. Rocks of the EGRP are all 1.38-1.48 Ga and are derived from a similar magma source (Van Schmus et al. 1996), and therefore likely have similar strontium isotope ratios along its entire extent. However, the Ozark region of southeast Missouri likely did not contribute any sediment to the Illinois Basin during the late Cambrian, because the laterally equivalent Bonneterre Formation is a heavily dolomitized carbonate unit which nucleated around the exposed crust in southeast Missouri (Larsen 1977; Gregg 1985; Gregg and Shelton 1990). Any detritus weathering from the Ozark bedrock and heading northeast into the Illinois Basin would have choked out carbonate production and caused siliciclastic deposition to occur in the area. The Eau Claire of Indiana also contains high K-feldspar content (Liu et al. 2012), alluding to a nearby source terrane. A Canadian Shield provenance is also unlikely, as the distance between Illinois and northern Canada in the Cambrian would have been too great to preserve the high percentage of K-feldspar observed in the Eau Claire. Wisconsin in the Cambrian contained exposed continental crust, however it is part of the 1.8 Ga Penokean Province (Bickford et al. 1986) which contains Archean Gneisses, Paleoproterozoic igneous rocks, and metasedimentary rocks (Sims et al. 1980). Therefore, this study favors western Indiana as the most likely source of sediment, where a north-south transect of the EGRP was exposed 500 Ma (**Fig. 5.12)**(Blakely 2011) and the basement rocks are significantly closer to the surface (Rudman et al. 1971).

Unit A (5487-5527)
Mixed Sand/Mud Flat, Subtidal Upper Shoreface

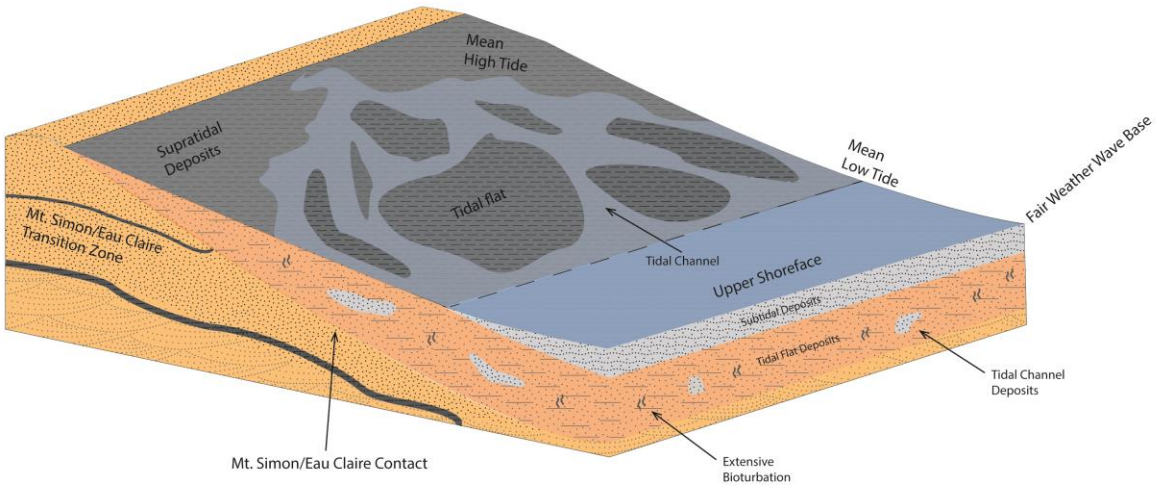

Fig. 5.1. Depositional block model for the Eau Claire Formation Unit A at the IBDP. Qualitatively, little change occurs across the Mt. Simon/Eau Claire contact in terms of lithology. Instead, the contact is defined by a change in gamma ray log signature that coincides with a color change between the Mt. Simon and Eau Claire sediments and a gradual decrease in grain size.

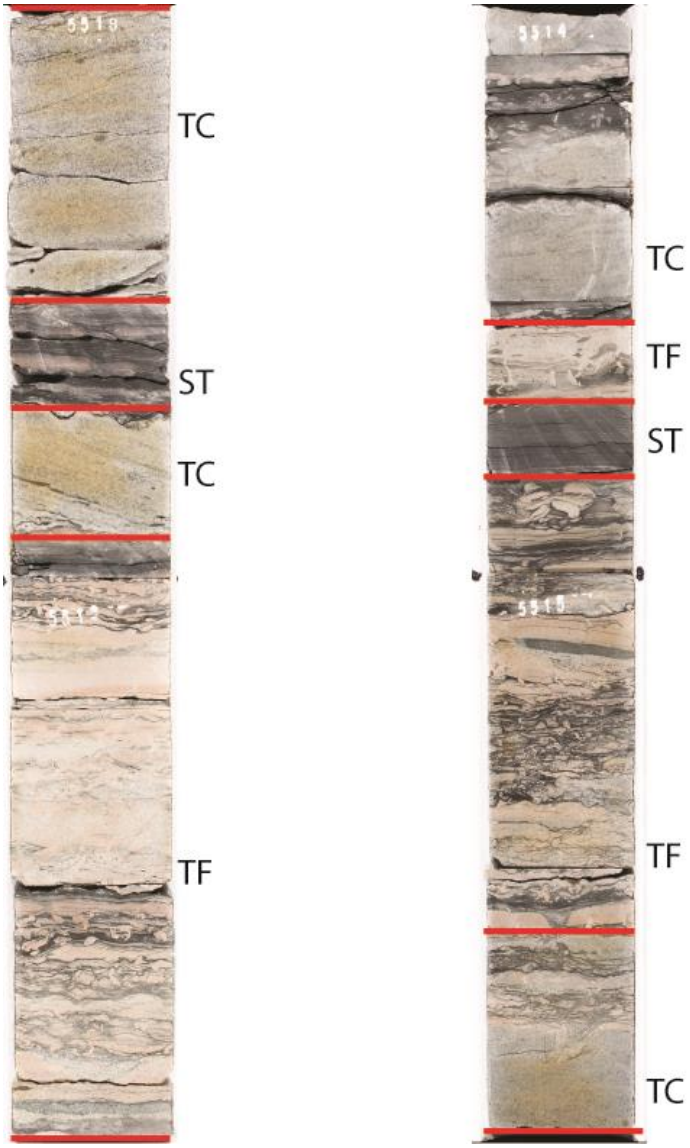

Fig. 5.2. Core photo of the Eau Claire Formation Unit A from the VW#1 well (Left core depth = 5518-5520 ft.; right core depth = 5514-5516 ft.). TC=tidal channel, TF= tidal flat and ST=supratidal.

Unit B (5447-5487)
Offshore Transition Zone
(Maximum Flooding Surface)

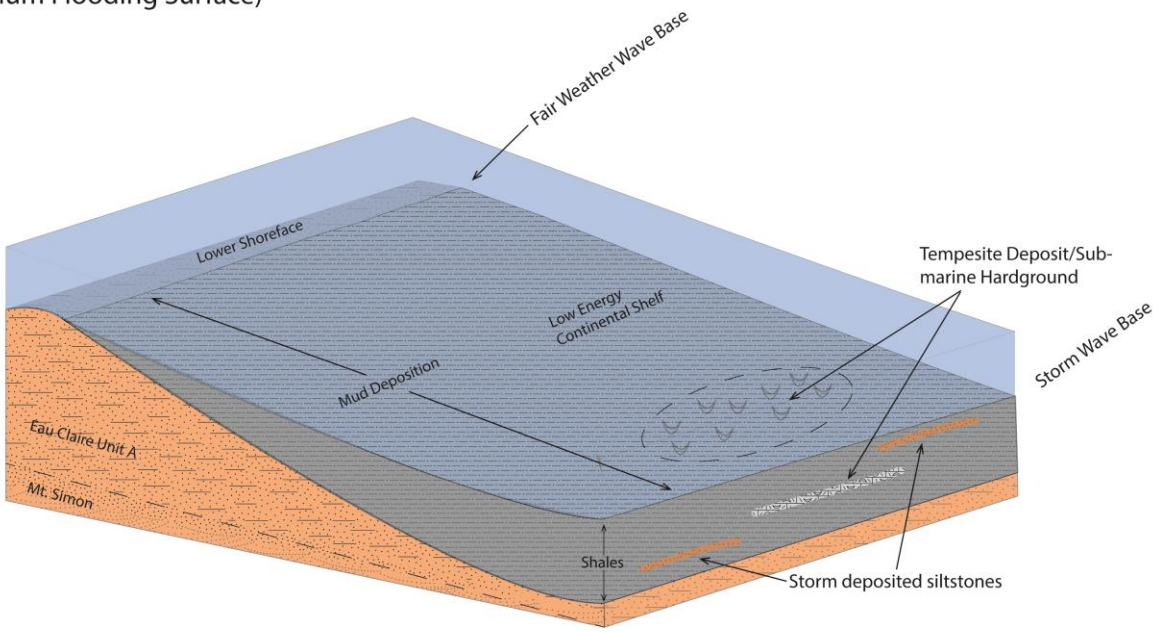

Fig. 5.3. Depositional block model for the Eau Claire Formation Unit B at the IBDP. Shoreline transgression occurred relative to Unit A, providing a deeper water, lower energy facies for unit B. The presence of a storm deposit (tempesite) indicates this facies is still above the SWB. The lack of ripple bedding suggests the unit lies below the FWWB.

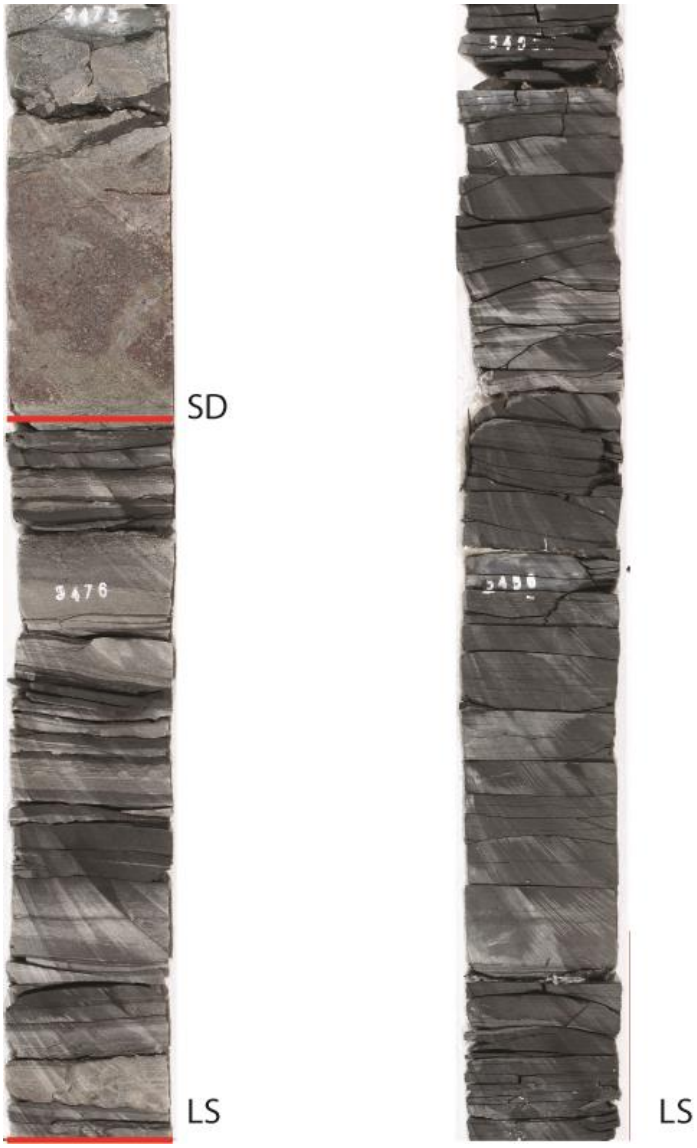

Fig. 5.4. Core photo of the Eau Claire Formation Unit B from the VW#1 well (left core depth = 5475-5477 ft.; right core depth = 5455-5457 ft.). LS= lower shoreface and SD=storm deposit. The boundary for unit B's storm bed has been placed slightly above the boundary to reveal the sharp basal contact.

Unit C (5350-5447)
Subtidal Shoreface
Deposits

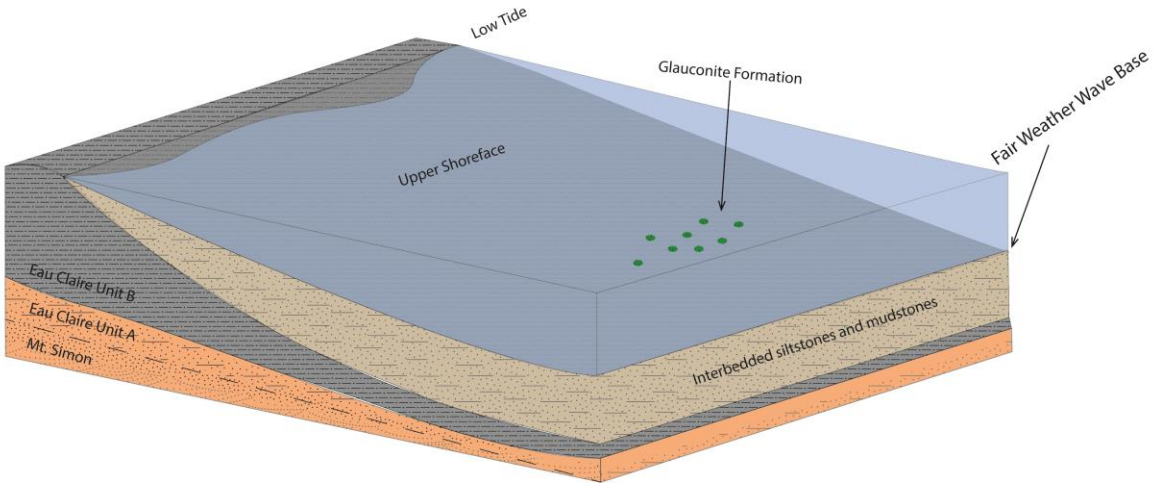

Fig. 5.5. Depositional block model for the Eau Claire Formation Unit C at the IBDP. Relative to unit B, shoreline regressions has occurred, situating this facies between the low tide mark and the FWWB, also known as the upper shoreface. Ripple bedding is a diagnostic indicator of deposition above the FWWB, and the presence of glauconite alludes to deposition closer towards the FWWB line.

Fig. 5.6. Core photo of the Eau Claire Formation Unit C from the VW#1 well (depth = 5425-5427 ft.). US=upper shoreface.

Unit D (5010-5350)
Carbonate Shelf
Deposits

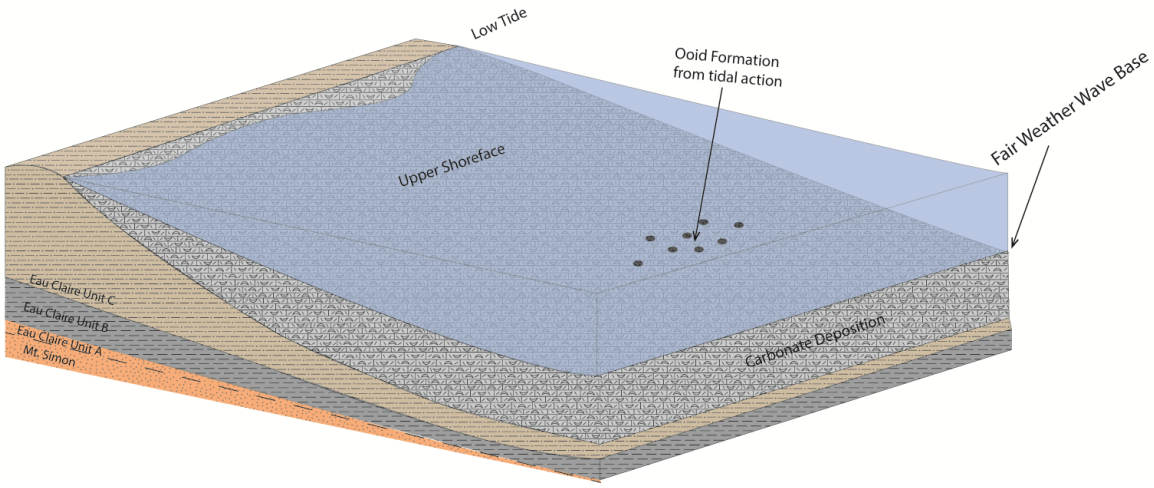

Fig. 5.7. Depositional block model for the Eau Claire Formation Unit D at the IBDP. No whole core is available for Unit D; therefore the block model was constructed entirely from wireline logs and RSWC's.

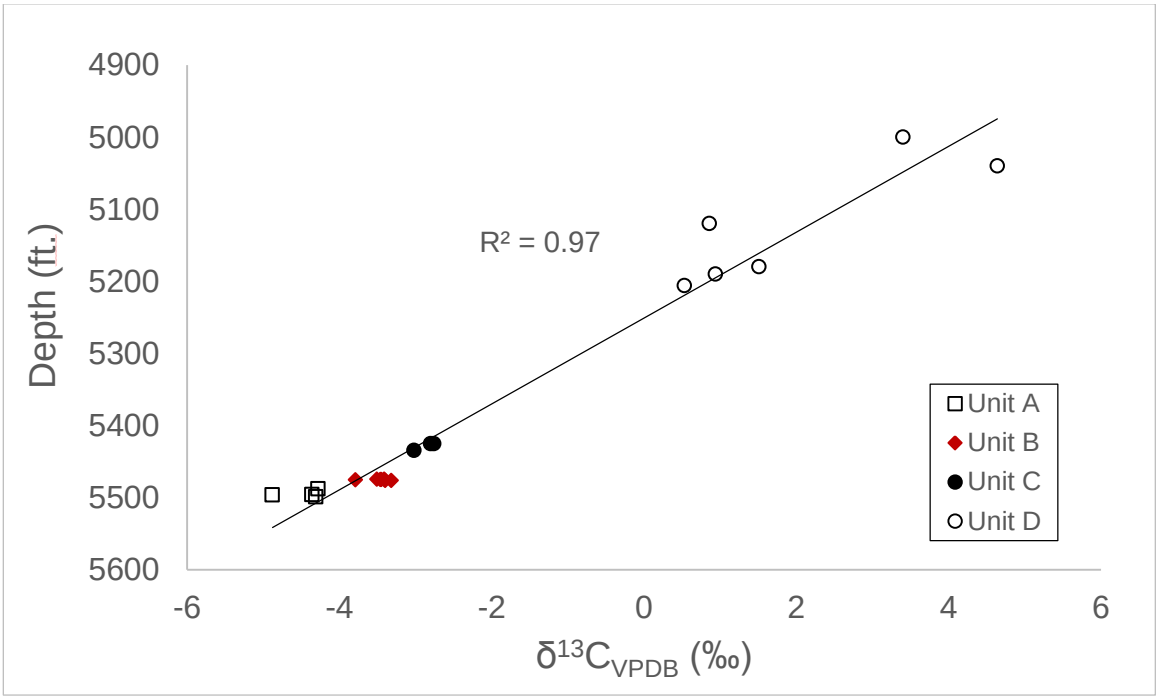

Fig 5.8. Depth (ft.) vs. $\delta^{13}C_{VPDB}$ for the Eau Claire formation.

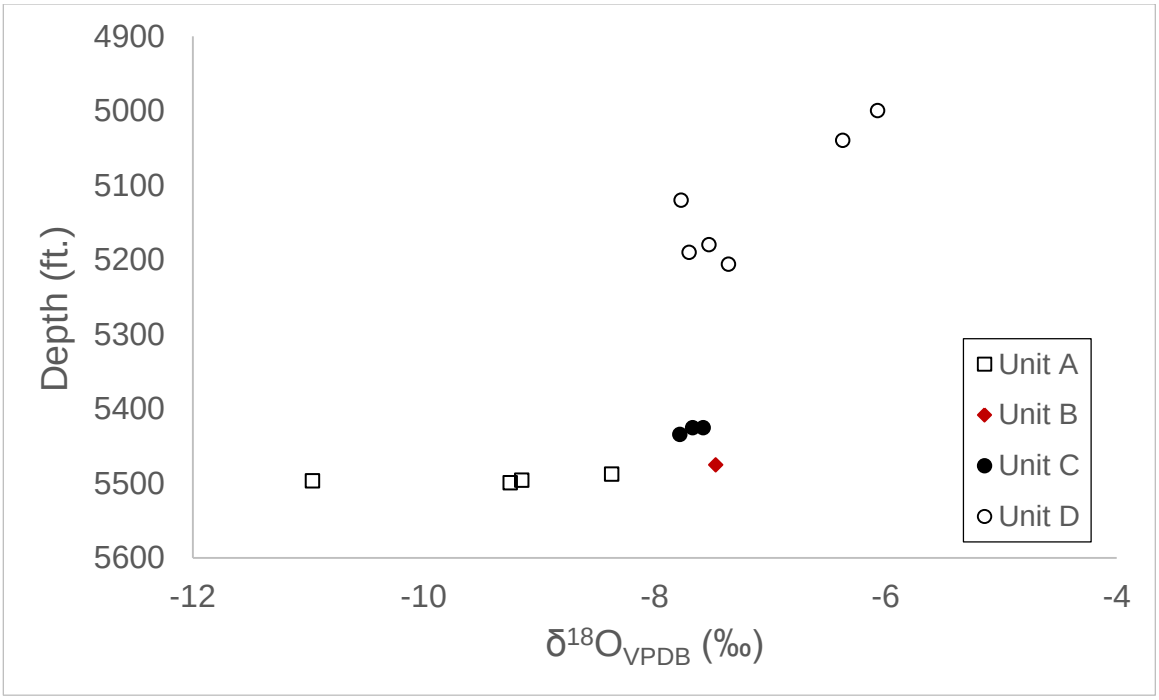

Fig. 5.9. Depth (ft.) vs. $\delta^{18}O_{VPDB}$ for the Eau Claire formation.

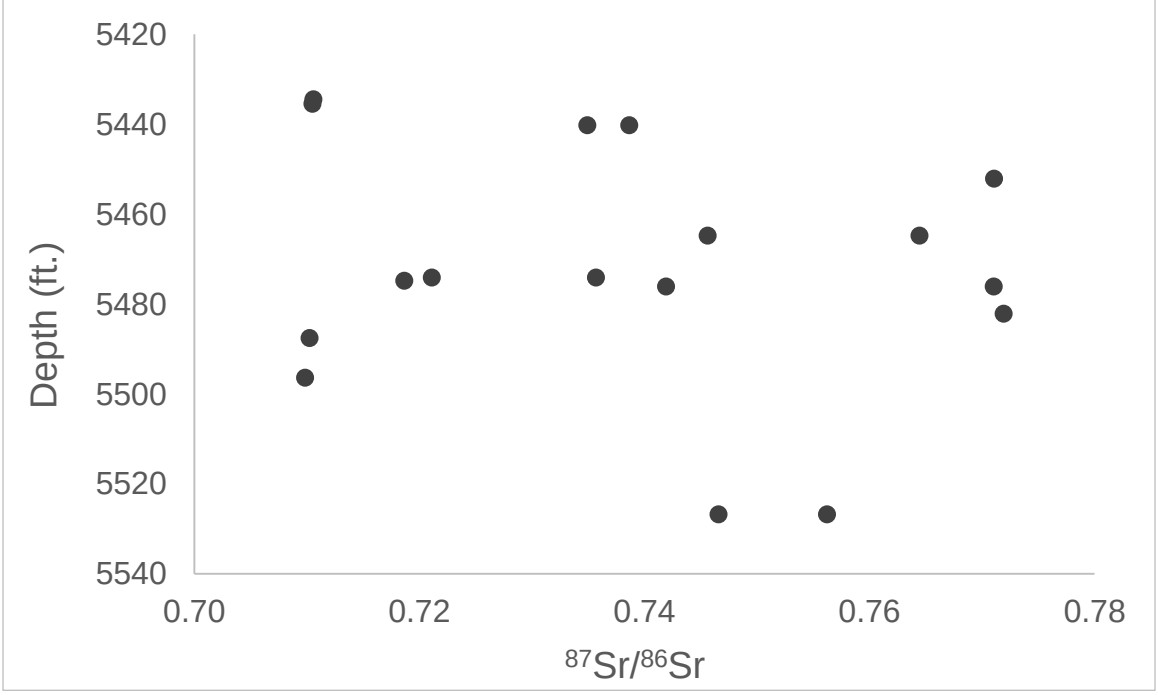

Fig. 5.10. Depth (ft.) vs. $^{87}Sr/^{86}Sr$ for the Eau Claire Formation.

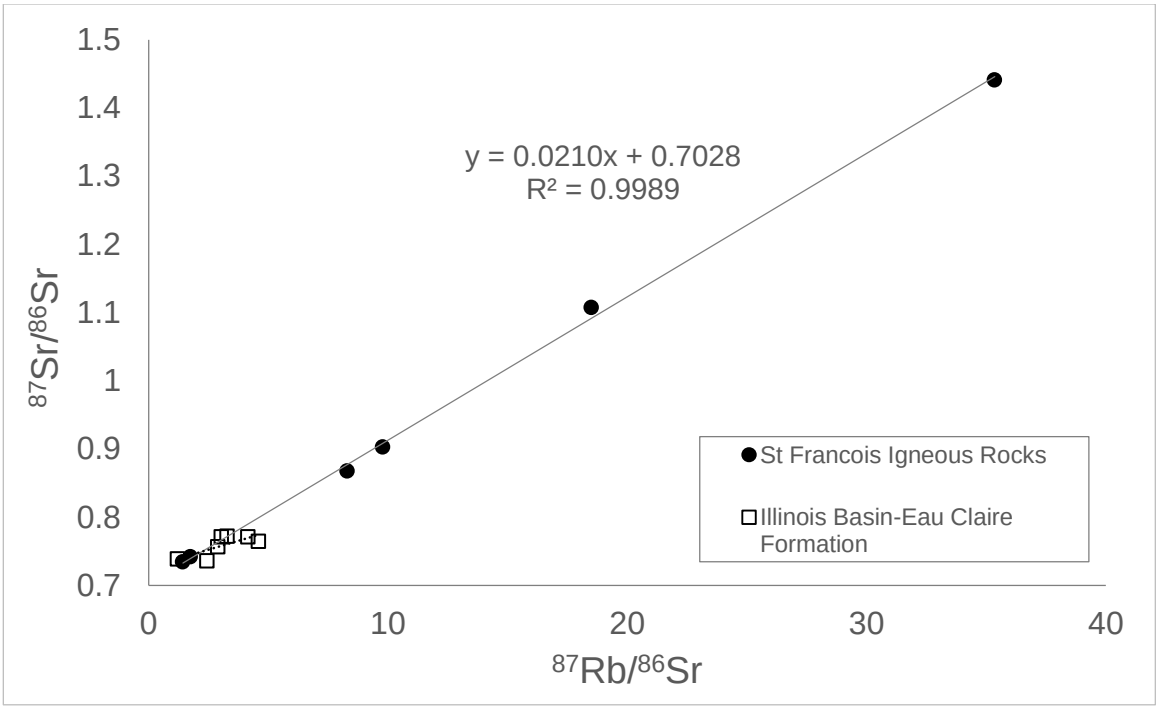

Fig. 5.11. $^{87}Sr/^{86}Sr$ vs. $^{87}Rb/^{86}Sr$ for St. Francois igneous rocks and the Eau Claire Formation in the Illinois Basin. The isochron age calculated for the St. Francois igneous rocks is 1.46 Ga.

Fig. 5.12. Cambrian Paleogeography showing possible source of sediment (present day Indiana) for the Eau Claire Formation. Modified from Blakely (2011).

CHAPTER 6: CONCLUSION

The Eau Claire Formation is a heterolithic unit at the IBDP site, spanning a range of siliciclastic and carbonate lithologies deposited within a shallow marine depositional environment. The formation can be divided into two broad lithostratigraphic components: a dominantly siliciclastic lower component (Units A-C) and a mixed siliciclastic/carbonate environment (Unit D). In terms of depositional environment, the formation can be separated into four primary depositional facies: (Unit A) intertidal mixed sand/mud flats and tidal channels of the foreshore environment; (Unit B) subtidal deposits of the lower shoreface (offshore transition zone); (Unit C) subtidal deposits of the upper shoreface environment; and (Unit D) subtidal mixed siliciclastic/carbonate deposits.

Within the Eau Claire, Unit B possesses the highest seal quality with 30.3 ft. (9 m) of shale and an average porosity and permeability of 5.8% and $2.0x10^{-5}$ mD (permeability estimated from MICP data). A permeability value of 20 nD exceeds the criteria for a suitable caprock (Fleury et al. 2010). Point count porosity for the unit is 0.01%, and shows no visible pore space or pore throat connectivity. The average clay content for Unit B is 43.1% from XRD and 42.5% from point count mineralogy. Unit B contains a 1 ft. (0.31 m) thick storm deposit, which can effectively serve as a marker bed for Unit B in locations proximal to the Decatur site.

The Eau Claire Formation exhibits a +8‰ (-4‰ to +4‰) $\delta^{13}C$ excursion at the IBDP site, possibly correlative with the late Cambrian SPICE event found worldwide 500-495 Ma. The SPICE event serves as an important stratigraphic marker that is dated with high precision by U-Pb dates of interbedded volcanic ash beds, and represents a defining feature of carbon isotope stratigraphy in the Cambrian. The Eau Claire contains *Crepicephalus* and *Aphelaspis* zone (501-497 Ma) trilobites in Iowa and Missouri (Thompson 1995), although no trilobites are found in the Eau Claire core from the IBDP site. At the IBDP site, the Eau Claire has $\delta^{18}O$ values of -6‰ to -11‰, concurrent with the range of $\delta^{18}O$ of -6‰ to -9‰ 500 Ma (Veizer et al. 1997; Grossman 2012). Therefore, the author favors an approximate age of 500 Ma for deposition of the Eau Claire in central Illinois.

In central Illinois, the Eau Claire is likely sourced from a nearby terrane due to the high K-feldspar content and its radiogenic $^{87}Sr/^{86}Sr$ ratios. The K-feldspar mode of the Eau Claire averages 8.7% for the formation and reaches an average of 20.3% in Unit C. $^{87}Sr/^{86}Sr$ ratios for the Eau Claire average 0.73436 and span a range of 0.70920 to 0.77193. Eastern Granite Rhyolite Province Samples from the nearby St. Francois region of Missouri

have similarly high values ranging from 0.73417 to 1.44084. The St. Francois region represents the best outcrop locality for the EGRP, an undeformed and unmetamorphosed felsic igneous terrane within the North American Craton that comprises the basement rock in a northeast – southwest trending line from Michigan to Oklahoma. Eastern Granite Rhyolite Province basement rocks from the VW#1 well have similar radiogenic values averaging 0.71873. Although the Ozark region of southeast Missouri was exposed during this time, it's unlikely that it was contributing detritus to the Illinois Basin because the laterally equivalent Bonneterre Formation is a heavily dolomitized carbonate shelf which nucleated around the paleotopography in southeast Missouri (Larsen 1977; Gregg 1985; Gregg and Shelton 1990). Due to the radiogenic $^{87}Sr/^{86}Sr$ values and the high K-feldspar mode, the author suggests a nearby provenance for the Eau Claire formation, such as Indiana. In Indiana, the EGRP is much closer to the surface than in Illinois in some locations (Rudman et al. 1971) and was likely subaerially exposed during deposition of the Eau Claire in the late Cambrian (**Fig. 5.11**).

Future CCS projects in the Illinois Basin that plan to utilize the Eau Claire – Mt. Simon system need to consider three criteria: the thickness of the Mt Simon Sandstone's reservoir quality lower unit, the thickness and lithology of the Eau Claire Formation's Unit B, and a viable CO_2 source to sequester CO_2. Meeting these criteria is complicated by the conflicting depocenters of the Mt Simon and the Eau Claire. The Mt. Simon depocenter is located in northeastern Illinois (Freiburg et al. 2014), while all overlying Paleozoic strata in the Illinois Basin have a depocenter in southeastern Illinois (Nelson 2010). However, the Mt. Simon is located closer to the surface at its depocenter and serves as a groundwater aquifer in the Chicago area, making the Mt. Simon an unsuitable target in northeastern Illinois. Although this is a site specific study, regional work on the Eau Claire in the future should utilize Unit B's gamma ray signature **(Fig. E.1)** and storm deposit (glauconitic dolostone) to identify the Eau Claire's Unit B, which has the highest seal quality within the unit. If core is not available, Unit B's storm deposit can be identified from its sharp negative gamma ray anomaly **(Fig. E.1)** to constrain the extent of the Eau Claire's highest seal quality facies.

REFERENCES

Aigner, T., 1985, Storm depositional systems; Dynamic stratigraphy in modern and ancient shallow marine sequences. Berlin, Springer, 174 p.

Allen, J.R.L., 1964, Primary current lineation in the Lower Old Red Sandstone (Devonian), Anglo-Welsh Basin. Sedimentology 3,89-108.

Alpert, S.P., 1975, *Planolites* and *Skolithos* from the upper Precambrian-lower Cambrian White-Inyo Mountains, California. Journal of Paleontology 49, 508-521.

Arthur, M.A., S.O. Schlanger, and H.C. Jenkyns, 1987, The Cenomanian-Turnian Oceanic Anoxic Event II: Paleooceanographic controls on organic-matter production and preservation. Marine petroleum source rocks, 401-420.

Aswasereelert, W., J.A. Simo, and D.L. Lepain, 2008, Deposition of the Cambrian Eau Claire Formation, Wisconsin: Hydrostratigraphic implications of fine grained Cratonic sandstone.: Geoscience Wisconsin 19, 1-21.

Avila, J., 1981, Regional setting of the Cambro-Ordovician in the Illinois Basin. Kentucky Geological Survey Special Publication 3, 60-76.

Babcock, L.E., 1994, Biostratigraphic significance and paleogeographic implications of Camrbian fossils from a deep core, Warren County, Ohio. Journal of Paleontology 68, 24-30.

Bachu, S., 2000, Sequestration of CO_2 in geological media: criteria and approach for site selection in response to climate change. Energy Conversion and Management 41, 953-970.

Bachu, S., 2003, Screening and ranking of sedimentary basins for sequestration of CO_2 in geological media in response to climate change: Environmental Geology 34, 277-289.

Bachu, S., 2008, CO_2 Storage in Geological Media: Role, Means, Status and Barriers to Deployment. Progress in Energy and Combustion Science, 34.2, p. 254-273.

Baertschi, P., 1957, Messung and Deutung relative Haufigskeitvariationen von O^{18} and C^{13} Karbongesteinen und Mineralien. Schweiz. Mineral. Petrog. Mitt. 37, 73-152.

Bandy, R.E., 2012, Geology of the Eau Claire Formation and Conasauga Group in part of Kentucky and analysis of their suitability as caprocks for deeper CO_2 sequestration: University of Kentucky Master's Thesis – Earth and Environmental Sciences. Paper 8. http://uknowledge.uky.edu/ees_etds/8 .

Becker, L.E., A.J. Hreha, and T.A. Dawson, 1978, Pre-Knox (Cambrian) stratigraphy in Indiana: Indiana Geological Survey Bulletin 57, 1-72.

Benson, S.M., and D.R. Cole, 2008, CO_2 Sequestration in Deep Sedimentary Formations. Elements 4, 325-331.

Best, J., and Bridge, J., 1992, The morphology and dynamics of low amplitude bedwaves upon upper stage plane beds and the preservation of planar laminae. Sedimentology 39, 737-752.

Bickford, M.E., W.R. Van Schmus, and I. Zietz, 1986, Proterozoic history of the midcontinent region of North America. Geology 14, 492-496, doi:10.1130/0091-7613(1986)14<492:PHOTMR>2.0.CO;2.

Blakely, R., 2011, Cambrian (505-495 Ma) Paleogeographic Map. Colorado Plateau Geosystems, Arizona, USA. http://cpgeosystems.com/namkeyframe.html

Bowen, B.B., R.I. Ochoa, N.D. Wilkens, J. Brophy, T.R. Lovell, N. Fischietto, C.R. Medina, and J.A. Rupp, 2011, Depositional and diagenetic variability within the Cambrian Mount Simon Sandstone: Implications for carbon dioxide sequestration. Environmental Geosciences 18, 69–89.

Bouma, A.H., H.L. Berryhill, R.L. Brenner, H.J. Knebel, 1981, Continental Shelf and Epicontinental Seaways, *in* Scholle, P.A. and D. Spearing, eds., Sandstone Depositional Environments: Tulsa, Oklahoma, AAPG Memoir 31, 281-327.

Bradbury, J.C., and E. Atherton, 1965, The Precambrian basement of Illinois: Illinois State Geological Survey Circular 382, 13 p.

Buschbach, T.C., 1964, Cambrian and Ordovician strata of northeastern Illinois: Illinois State Geological Survey, Report of Investigations 218, 90 p.

Buschbach, T.C., 1975, Cambrian system, *in* H.B. Willman, Atherton, E., Buschbach, T.C., Collinson, C., Frye, J.C., Hopkins, M.E., Lineback, J.A., and Simon, J.A., eds., Handbook of Illinois stratigraphy: Illinois State Geological Survey Bulletin 95, 34–46.

Clayton, R.N. and E.T. Degens, 1959, Use of C isotope analysis for differentiating fresh-water and marine sediments. AAPG Bulletin 42, 890-897.

Collinson, C., M.L. Sargent, and J.R. Jennings, 1988, Illinois Basin region. *in* Sloss, L.L., ed., Sedimentary Cover—North American Craton: U.S.: Boulder, Colorado, Geological Society of America, The Geology of North America D-2, 383 p.

Coughenour, C.L., A.W. Archer, and K.J. Lacovara, 2009, Tides, tidalites, and secular changes in the Earth – Moon system. Earth-Science Reviews 97, 59-79.

Davis, R.A., 2012, Tidal Signatures and Their Preservation Potential in Stratigraphic Sequences. *In* Davis, R.A. and Dalrymple, R.W. (Eds.), Principles of Tidal Sedimentology, 35-55.

Dastidar, R., C.H. Sondergeld, and C.S. Rai, 2007, An Improved Empirical Permeability Estimator from Mercury Injection for Tight Clastic Rocks. Petrophysics 48-3, 186-190.

Degens, E.T. and Epstein, S., 1962, Relationship between $^{18}O/^{16}O$ ratios in coexisting carbonates, cherts, and dolomites. AAPG Bulletin 46, 534-542.

Derry, L.A., and S.B. Jacobsen, 1990, The chemical evolution of Precambrian seawater: Evidence from REEs in banded iron formations. Geochimica et Cosmochimica Acta 54, 2965-2977.

Derry, L.A., A.J. Kaufman, and S.B. Jacobsen, 1992, Sedimentary cycling and environmental change in the Late Proterozoic: Evidence from stable and radiogenic isotopes. Geochimica et Cosmochimica Acta 56, 1317-1329.

Desjardins, P.R., L.A. Buatois, and M.G. Mangano, 2012, Tidal Flats and Subtidal Sand Bodies, *in* Knaust, D. and R.G. Bromley, Trace Fossils as Indicators of Sedimentary Environments. Developments in Sedimentology 64, 529-561.

DOE (Department of Energy) (2007)Carbon Sequestration Atlas of the United States and Canada Online. National Energy Technology Laboratory,Morgantown, WV, http://www.netl.doe.gov/technologies/carbon_seq/refshelf/atlas/index.html

Dontsova, E.I., A.A. Migdisov, and A.B. Ronov, 1972, On the causes of variation in oxygen isotopic composition in the carbonate strata of the sedimentary column. Geochemistry International 9, 885-891.

Dott, R.L., Jr., 1964, Wacke, greywacke, and matrix; what approach to sandstone classification? Journal of Sedimentary Petrology 34, 625–632.

Driese, S.G., C.W. Byers, and R.H. Dott Jr., 1981, Tidal deposition in the basal Upper Cambrian Mt. Simon Formation in Wisconsin. Journal of Sedimentary Petrology 51, 367–381.

Droste, J.B., and R.H. Shaver, 1983, Atlas of early and middle Paleozoic paleogeography of the southern Great Lakes area: Bloomington, Indiana Department of Natural Resources, Indiana Geological Survey Special Report 32.

Duffin, M.E., M. Lee, G.D. Klein, and R.L. Hay, 1989, Potassic diagenesis of Cambrian sandstones and Precambrian granitic basement in UPH-3 deep hole, Upper Mississippi Valley USA. Journal of Sedimentary Petrology 59, 848-861.

Emiliani, C., 1955, Pleistocene temperatures. Journal of Geology 63, 538-578.

Fleury, M., Pironon, J., Le Nindre, Y.M.m Bildstein, O., Berne, P., Laneau, V., Broseta, D., Pichery, T., 2010, Evaluating sealing efficiency of caprocks for CO_2 storage: an overview of the Geocarbone Integrity program and results: Oil and Gas Science Technology 65, p. 435-444.

Folk, R.L., 1980, The petrology of sedimentary rocks: Austin, Texas, Hemphill Publishing Company, 182 p.

Fischietto, N.E., 2009, Lithofacies and depositional environments of the Cambrian Mount Simon Sandstone in the northern Illinois Basin: Implications for CO2 sequestration: West Lafayette, Indiana, Purdue University, M.S. thesis, 114 p.

Freiburg, J.T., D.G. Morse, H.E. Leetaru, R.P. Hoss, and Yan, Q., 2014, A Depositional and Diagenetic Characterization of the Mt. Simon Sandstone at the Illinois Basin Decatur Project Carbon Capture and Storage Site, Decatur, Illinois, USA. Illinois State Geological Survey Circular 583, 1-43.

Gerdemann, P.E., and Myers, H.E., 1972, Relationships of carbonate facies patterns to ore distribution and to ore genesis in the Southeast Missouri lead district. Economic Geology 67, 426-433.

Grossman, E.L., 2012, Oxygen Isotope Stratigraphy. *In* Gradstein, F., J. Ogg, M. Schmitz, and G. Ogg (Eds.), The Geologis Time Scale 2012, 181-206.

Grebs, S.F., and Solis, 2009, Geologic carbon storage potential in Kentucky. *In* Parris, T.M., Greb, S.F., and Nuttall, B.C., (eds.), Evaluation of geologic CO_2 sequestration potential and CO_2 enhanced oil recovery in Kentucky. Final Report for the Kentucky Department for Energy Development and Independence. Kentucky Energy and Environment Cabinet Contract No. PO2-855-0700010071, 203 p.

Gregg, J. M., 1985, Regional epigenetic dolomitization in the Bonneterre Dolomite (Cambrian), southeastern Missouri: Geology, v. 13, p. 503–506, doi:10.1130/0091-7613(1985)132.0.CO;2.

Gregg, J.M., and Shelton, K.L., 1990, Dolomitization and dolomite noemorphism in the back reef facies of the Bonneterre and Davis formations (Cambrian), southeastern Missouri. Journal of Sedimentary Petrology 60, 549-562.

Gutstadt, A.M., 1958, Cambrian and Ordovician stratigraphy and oil and gas possibilities in Indiana: Indiana Geological Survey Bulletin 14, 103 p.

Harris, L.C., and B.M. Whiting, 2000, Sequence-stratigraphic significance of Miocene to Pliocene glauconite-rich layers, on- and offshore of the US Mid-Atlantic margin. Sedimentary Geology 134, 129-147.

Hoefs, J., 1987, Stable Isotope Geochemistry. Springer-Verlag, Berlin.

Hoholick, J.D., T. Metarko, and P.E. Potter, 1984, Regional variations of porosity and cement: St. Peter and Mount Simon Sandstones in Illinois Basin: AAPG Bulletin 68, 753–764.

Howe, W.B. and J.W. Koenig, 1961, The Stratigraphic Section in Missouri. Missouri Geological Survey, 15-18.

Huber, M.E., 1975, A paleoenvironmental interpretation of the Upper Cambrian Eau Claire Formation of west-central Wisconsin [unpub. M.S. thesis]. University of Wisconsin-Madison, 110 p.

Hughes, R.E., and R. Warren, 1989, Evaluation of the Economic Usefulness of Earth Materials by X-ray Diffraction: 23rd forum Geology Industrial Minerals; Hughes, R.E., and Bradbury, L.C., (Eds) Illinois State Geological Survey.

Hughes, R.E., D.M. Moore, and H.D. Glass, 1994, Qualitative and Quantitative analysis of clay minerals in soils. *In* Amonette, J.E., and Zelaney, L.W., (Eds): Quantitative Methods in Soil Mineralogy, SSSA Miscell. Pub., 330-59.

Jaffres, J.B.D., G.A. Shields, and K. Wallman, 2007, The oxygen isotope evolution of seawater: A critical review of a long-standing controversy and an improved geological water cycle model for the past 3.4 billion years. Earth-Science Reviews 83, 83-122.

Keith, M.L. and Weber, J.N., 1964, Carbon and oxygen isotopic composition of selected limestones and fossils. Geochimica et Cosmochimica Acta 28, 1787-1816.

Klein, G.D., 1963, Bay of Fundy intertidal zone sediments. Journal of Sedimentary Petrology 33, 844-854.

Klein, G.D., 1998, Clastic Tidalites – a partial retrospective view. *In* Alexander, C.R., R.A. Davis, V.J. Henry (Eds.), Tidalites: Processes and Products. SEPM Special Publication 61, 5-14.

Knauth, L.P., and S. Epstein, 1976, Hydrogen and oxygen isotope ratios in nodular and bedded cherts. Geochimica et Cosmochimica Acta 40, 1095-1108.

Knauth, L.P., 2005, Temperature and salinity history of the Precambrian ocean: Implications for the course of microbial evolution. Palaeogeography Palaeoclimatology Palaeoecology 219 (1-2), 53-69.

Kolata, D.R., 2010, Cambrian and Ordovician systems (Sauk Sequence and Tippecanoe I Subsequence). *In* D.R. Kolata and C.K. Nimz, eds., The Geology of Illinois: Illinois State Geological Survey.

Kolata, D.R., and W.J. Nelson, 1991, Tectonic history of the Illinois Basin. *In* M.W. Leighton, D.R. Kolata, D.F. Oltz, and J.J. Eidel (Eds.), Interior cratonic basins: Tulsa, Oklahoma, AAPG Memoir 51, 263–285.

Kolata, D.R., and W.J. Nelson, 2010, Tectonic history. *In* D.R. Kolata and C.K. Nimz, eds., The Geology of Illinois: Illinois State Geological Survey.

Kuenen, Ph. H, 1959, Experimental Abrasion, part 3: Fluviatile action on sand. American Journal of Science 257, 172-190.

Kuenen, Ph. H, 1960, Experimental Abrasion, part 4: Eolian action. Journal of Geology 68, 427-449.

Lahann, R., J. Rupp, and C. Medina, 2014, An evaluation of the seal capacity and CO_2 retention properties of the Eau Claire Formation (Cambrian). Environmental Geosciences 21, 83-106.

Larsen, K.G., 1977, Sedimentology of the Bonneterre Formation, Southeast Missouri. Economic Geology 72, 408-419.

Leetaru, H.E., 2015, Isopach map for the Eau Claire Formation. Unpublished Illinois State Geological Survey data.

Leetaru, H.E., and J.H. McBride, 2008, Reservoir uncertainty, Precambrian topography, and carbon sequestration in the Mt. Simon Sandstone, Illinois Basin. Environmental Geosciences 16-4, 235-243.

Leetaru, H.E., S. Frailey, D. Morse, R.J. Finley, J. Rupp, J.A. Drahozval, and J.H. McBride, 2008, Carbon sequestration in the Mt. Simon Sandstone saline reservoir, *in* M. Grobe, J.C. Pashin, and R.L. Dodge, eds., Carbon dioxide sequestration in geological media: State of the science: Tulsa, Oklahoma, American Association of Petroleum Geologists, AAPG Studies 59, 1–17.

Li, Z.X., S.V. Bogdanova, A.S. Collins, A. Davidson, B. De Waele, R.E. Ernst, I.C.W. FitzSimons, R.A. Fuck, D.P. Gladkochub, J. Jacobs, K.E. Karlstrom, S. Lu, L.M. Natapov, V. Pease, S.A. Pisarevsky, K. Thrane, and V. Vernikovsky, 2008, Assembly, configuration, and break-up history of Rodinia: A synthesis. Precambrian Research 160, 179-210.

Lidiak, E.G., 1996, Geochemistry of subsurface Proterozoic rocks in the eastern midcontinent of the United States: Further evidence for a within-plate tectonic setting. *In* B.A. van der Pluijm and P.A. Catacosinos (Eds.), Basement and basins of eastern North America: Boulder, Colorado, Geological Society of America, Special Paper 308, 45–66.

Liu, L., 2014, Rejuvenation of Appalachian topography caused by subsidence-induced differential erosion. Nature Geoscience 7, 518-523.

Liu, F., C. Griffith, S.W. Hedges, Y. Soong, H. Hellevang, C. and Zhu, 2012, CO_2-brine-caprock Interaction: Reactivity Experiments on Eau Claire Shale and a Review of Relevant Literature. International Journal of Greenhouse Gas Control 7, 153-167.

Longhitano, S.G., D. Mellere, R.J. Steel, and R.B. Ainsworth, 2012, Tidal depositonal systems in the rock record: A review and new insights. Sedimentary Geology 279, 2-22.

McBride, J.H., D.R. Kolata, and T.G. Hildenbrand, 2003, Geophysical Constraints on understanding the origin of the Illinois Basin and its underlying crust. Tectonophysics 363. 45-78.

McBride, J.H., D.R., Kolata, M.L. Sargent, and T.G. Hildenbrand, 2010, The Precambrian crust, *in* D.R. Kolata and C.K. Nimz, eds., The Geology of Illinois: Illinois State Geological Survey.

McKay, R.M., 1988, Stratigraphy and lithofacies of the Dresbachian (Upper Cambrian) Eau Claire Formation in the subsurface of eastern Iowa. *In* G.A. Ludvigson and B.J. Bunker, eds., New Perspective on the Paleozoic history of the Upper Mississippi Valley: Des Moines, Iowa, Iowa Department of Natural Resources, Geological Survey Guidebook 8, 33-53.

Medina, C.R., and J.A. Rupp, 2012, Reservoir characterization and lithostratigraphic division of the Mount Simon Sandstone (Cambrian): Implications for estimations of geologic sequestration storage capacity. Environmental Geosciences 19,1–15.

Medina, C.R., J. Rupp, K.L. Avery, E.R. Venteris, D.A. Barnes, J.A. Harper, S. Greb, B.E. Slater, A. Stolorow, and J. Sminchak, 2010, A regional characterization and assessment of geologic carbon sequestration opportunities in the Upper Cambrian Mount Simon Sandstone in the Midwest region: MRCSP Phase II Topical Report, October 2005–October 2010: Midwest Regional Carbon Sequestration Partnership.

Medina, C.R., J.A. Rupp, and D.A. Barnes, 2011, Effects of reduction in porosity and permeability with depth on storage capacity and injectivity in deep saline aquifers: A case study from the Mount Simon Sandstone aquifer. International Journal of Greenhouse Gas Control 5,146–156.

Miall, A.D., 1977, A review of the braided river depositional environment. Earth Science Reviews, 1–62.

Moore, D.M., and R.C. Reynolds, Jr., 1997, X-ray Diffraction and the Identification and the Identification and Analysis of Clay Minerals. 2nd edition. Oxford University Press, Oxford.

Morse, D.G., and H.E. Leetaru, 2005, Reservoir characterization and three-dimensional models of Mt. Simon gas storage fields in the Illinois Basin. Illinois State Geological Survey Circular 567.

Myrow, P.M., and J.B. Southard, 1996, Tempesite deposition. Journal of Sedimentary Research 66, 875-887.

Myrow, P.M., L. Tice, B. Archuleta, B. Clark, J.F. Taylor, and R.L. Ripperdan, 2004, Flat pebble conglomerate: Its multiple origins and relationship to metre-scale depositional cycles. Sedimentology 51, 973-996.

Nelson, W.J., and S. Marshak, 1996, Devonian Tectonism of the Illinois Basin region, U.S. continental interior. *In* B.A. van der Pluijm and P.A. Catacosinos, eds., Basement and basins of eastern North America: Boulder, Colorado, Geological Society of America, Special Paper 308, 169-180.

Nelson, W.J., 2010, Structural Features, *in* D.R. Kolata and C.K. Nimz, eds. The Geology of Illinois: Illinois State Geological Survey, 90-104.

Neufelder, R.J., B.B. Bowen, R.W. Lahann, and J.A. Rupp, 2012, Lithologic, mineralogical and petrophysical characteristics of the Eau Claire Formation: Complexities of a carbon storage system seal. Environmental Geosciences 19, 81-104.

Oelkers, E.H., and D.R. Cole, 2008, Carbon dioxide sequestration: a solution to a global problem. Elements 4, 305-310.

Ostrom, M.E., 1978, Stratigraphic relationships of lower Paleozoic rocks of Wisconsin: Wisconsin Geological and Natural History Survey Field Trip Guide Book 3, p. 3–22.

Pacala, S., and R. Socolow, 2004, Stabilization wedges: solving the climate problem for the next 50 years with current technologies. Science 305, 968–972.

Palmer, A.R., 1982, Fossils of Dresbachian and Franconian (Cambrian) age from the subsurface of west-central Indiana: Indiana Geological Survey Special Report 29, 12 p.

Perry Jr, E.C., 1967, The oxygen isotope chemistry of ancient cherts. Earth and Planetary Science Letters 3, 62-66.

Perry Jr, E.C., and Tan F.C., 1972, Significance of oxygen and carbon isotope variations in Early Precambrian cherts and carbonate rocks of southern Africa. GSA Bulletin 83, 647-664.

Porrenga, D.H., 1966, Glauconite and chamosite as depth indicators in the marine environment. Marine Geology 5, 495-501.

Pratt, B.R., 2002, Storms versus tsunamis: Dynamic interplay of sedimentary, diagenetic, and tectonic processes in the Cambrian of Montana. Geology 30, 423-426.

Reineck, H-E, and Wunderlich, F., 1968, Classification and origin of flaser and lenticular bedding. Sedimentology 11, 99-104.

Revel, M., J.A. Sinko, and F.E. Grousset, 1996, Sr and Nd isotopes as tracers of North Atlantic lithic particles: Paleoclimatic implications. Paleoceanography 11, 95-113.

Rice, S., and Church, M., 1998, Grain size along two gravel-bed rivers: statistical variation, spatial patter and sedimentary links. Earth Surface Processes and Landforms 23, 345-363.

Rudman, A.J., J. Mead, R.F. Blakely, and J.F. Whaley, 1971, Precambrian Geophysical Provinces in Indiana. AAPG Memoir 15, 1165-1218.

Saltzmann, M.R., and Thomas, E., 2012, Carbon Isotope Stratigraphy. *In* Gradstein, F., J. Ogg, M. Schmitz, and G. Ogg (Eds.), The Geologic Time Scale 2012: Elsevier, 207-232.

Sargent, M.L., 1991, Sauk Sequence: Cambrian System through Lower Ordovician Series. *In* M.W. Leighton, D.R. Kolata, D.F. Oltz, and J.J. Eidel, eds., Interior cratonic basins; Tulsa, Oklahoma, AAPG Memoir 51, 75-86.

Sargent, M.L., and Z. Lasemi, 1993, Tidally dominated depositional environment for the Mt. Simon Sandstone in central Illinois. Geological Society of America, Great Lakes Section, Abstracts and Programs 25, 78 p.

Schidlowski, M., R. Eichmann and E. Junge Ch., 1975, Precambrian sedimentary carbonates: carbon and oxygen isotope geochemistry and implications for the terrestrial oxygen budget. Precambrian research 2, 1-69.

Schrag, D.P., J.F. Adkins, K. McIntyre, J.L. Alexander, D.A. Hodell, and C.D. Charles, 2002, The oxygen isotopic composition of seatwater during the Last Glacial Maximum. Quaternary Science Reviews 21, 331-342.

Sepkoski Jr, J.J., 1982, Flat-Pebble Conglomerates, Storm Deposits, and the Cambrian Bottom Fauna. Cyclic and Event Stratification, 371-385.

Shemesh, A., Y. Kolodny and B. Luz, 1983, Oxygen isotope variations in phosphate of biogenic apatites, II. Phosphorite rocks. Earth and Planetary Science Letters 64, 405-416.

Shukla, R., P. Ranjith, A. Haque, and X. Choi, 2010, A review of studies on CO_2 sequestration and caprock integrity. Fuel 89, 2651-2664.

Sims, P.K., K.D. Card, G.B. Morey, and Z.E. Peterman, 1980, The Great Lakes tectonic zone – A major crustal structure in central North America. GSA Bulletin 12, 690-698.

Sloss, L.L., 1963, Sequences in the cratonic interior of North America. GSA Bulletin 74, 93–114.

Smith, N.D., 1970, The braided stream depositional environment: Comparison of the Platte river with some Silurian clastic rocks, north central Appalachians. GSA Bulletin 81, 2993-3014.

Steel, R.J., P. Plink-Bjorklund, J. Aschoff, 2012, Tidal deposits of the Campanian Western Interior Seaway, Wyoming, Utah, and Colorado, USA. *In* Davis, R.A. and Dalrymple, R.W. (Eds.), Principles of Tidal Sedimentology, 437-472.

Thompson, T.L., 1995, The stratigraphic succession in Missouri. Rolla, Missouri, Missouri Department of Natural Resources, Division of Geology and Land Survey 40, 190 p.

Treworgy, J.D., S.T. Whitaker, and Z. Lasemi, 1997, Structural cross section of the Paleozoic rocks in Illinois, Wayne County to Stephenson County. Illinois State Geological Survey, Illinois Map 7, 2 sheets.

Van Schmus, W.R., M.E. Bickford, and A. Turek, 1996, Proterozoic geology of the east-central midcontinent basement. *In* Van der Pluijm, B.A. and P.A. Catacosinos, eds., Basement and basins of eastern North America: Boulder, Colorado, GSA Special Paper 308, 7–32.

Veizer, J., and J. Hoefs, 1976, The nature of $^{18O}/^{16}O$ and $^{13}C/^{12}C$ secular trends in sedimentary carbonate rocks. Geochimica et Cosmochimica Acta 40, 1387-1395.

Veizer, J., P. Kruckschen, F. Pawellek, A. Diener, O. Podlaha, G.A.F. Carden, T. Jasper, C. Korte, H. Strauss, K. Azmy, and D. Ala, 1997, Oxygen isotope evolution of Phanerozoic seawater. Palaeo 132, 159-172.

Veizer, J., D. Ala, K. Azmy, P. Kruchschen, D. Buhl, F. Bruhn, G.A.F. Carden, A. Diener, S. Ebneth, Y. Godderis, T. Jasper, C. Korte, F. Pawallek, O.G. Podlaha, and H. Strauss, 1999, $^{87}Sr/^{86}Sr$, $\delta\,^{13}C$ and $\delta\,^{18}O$ evolution of Phanerozoic seawater. Chemical Geology 161 (1-3), 59-88.

Walcott, C. D., 1914, Cambrian geology and paleontology. Smithsonian Miscellaneous Collection 57, 345-412.

Weber, J.N., 1965, The $^{18}O/^{16}O$ ratio in ancient oceans. Geokhimija 6, 674-680.

Weimer, R.J., J.D. Howard, and D.R. Lindsay, 1982, Tidal Flats and Associated Tidal Channels. *In* Scholle, P.A. and D. Spearing, (Eds.), Sandstone Depositional Environments: Tulsa, Oklahoma, AAPG Memoir 31, 191-245.

Willman, H.B., E. Atherton, T.C. Buschbach, C. Collinson, J.C. Frye, M.E. Hopkins, J.A. Lineback, and J.A. Simon, eds., 1975, Handbook of Illinois stratigraphy. Illinois State Geological Survey Bulletin 95, 32–87.

Yochelson, E.L., 2006, The Lipalian interval: a forgotten, novel concept in the geologic column. Earth Sciences History 25, 251-269.

APPENDIX A: LITHOFACIES

Lithofacies

Ten lithofacies were observed in the cored interval (5,425 ft. to 5,527 ft.) of the VW#1 well for the Eau Claire formation, representing a range of marine depositional environments. Brief descriptions and a figure of each lithofacies are listed below and arranged from most to least common **(Figs A.1 and A.2)**.

Shale

Shale is the most common lithofacies within the VW#1 drill core, totaling 30.3 ft. (9.2 m). Shales are dark grey in color, highly fissile, and largely absent of any sedimentary structure. Abundant shale exists in depositional unit B, dominating the lithology of that unit. Slickensides exist within oblique fractures throughout the shale. The cored interval of the VW#1 well reveals numerous examples of shale interbedded with siltstone and sandstone. Occasional bands of maroon/pink siltstone and some coarser detritus exist throughout. Trace glauconite, pyrite, and bioturbation are found in Eau Claire shales. Throughout the large shale depositional facies, a few beds of fossiliferous clayey siltstone appear, as well as 1.1 ft. thick silty dolostone deposit.

Interbedded siltstone/shale

Interbedded siltstones and shales are maroon/pink to grey/tan in color, and interbedded with grey clayey siltstones and dark grey shales. The total thickness of this lithofacies is 26.3 ft. (8 m) in the VW#1 drill core. Composition is primarily subarkose-arkose arenite (siltstones), arkose wacke (clayey siltstones) and shale. Bedding is planar to ripple laminated, and bioturbation and brachiopod fragments commonly appear in this lithofacies.

Bioturbated siltstone-sandstone

This lithofacies is in the basal portion of the Eau Claire in unit A, near the contact with the Mt. Simon and is composed of grey/dark grey shales and clayey siltstones, to maroon/pink and grey/tan siltstones. The total thickness of this lithofacies is 17.7 ft. (5.4 m) within the VW#1 drill core. Composition ranges from quartz arenite to

arkosic wacke in this lithofacies. This facies is heavily bioturbated, although some primary bedding persists through in the form of ripple to planar bedding. A few beds contain iron oxide and pyrite cements, as well as some fine to medium grained quartz grains, which are both mono- and polycrystalline. Some segments are heavily cemented with dolomite. A flat pebble conglomerate exists within this lithofacies near 5502.9 ft. (1677.1 m).

Planar-bedded siltstone

This lithofacies is maroon/pink to grey/tan in color, and spans 7.7 ft. (2.3 m) within the VW#1 drill core. Maroon/pink beds of siltstone are largely subarkosic arenite in composition, while the grey/tan siltstone beds are arkosic arenite in composition and some may be arkosic wackes. Thin clay laminae cut across most beds defining the planar beds. Trace ripple beds exist although they are not prevalent. Some laminations are glauconite rich, and may be considered greensands. Some beds appear disturbed, and the clay takes on a flaser lamination. Trace skolithos burrows appear, and a few brecciated beds occur.

Homogeneous siltstone/sandstone

This facies is grey/tan in color, with very well sorted and well-rounded grains. The thickness of this lithofacies is 6.2 ft. (1.9 m) thick in the VW#1 core. The composition is quartz to subarkosic arenite. This lithofacies is primarily massive with a nearly complete lack of bedding with the exception of rare laminae composed predominantly of brachiopod fossils, shale lithic fragments, glauconite and larger quartz grains. Occurrence of this lithofacies is limited to Unit A, where it is associated with the bioturbated siltstone/sandstone facies.

Cross bedded sandstone

The observed cross bedded sandstones, limited to Unit A from the VW#1 core, are composed of maroon/pink siltstones, which are subarkose – arkose arenite in composition and attain a total thickness of 2.1 ft. (0.6 m) in the VW#1 core. Cross-beds are low angle and may contain disseminated pyrite. 93.7% of the grains within this lithofacies are quartz, and are generally well rounded. Abundant silica cement binds quartz grains

throughout the lithology. Overall, this lithofacies is texturally and compositionally mature, bound by the bioturbated siltstone-sandstone facies.

Mixed carbonate/siltstone

This facies is grey in color, containing 88% dolomite, 5% lithics, 4% glauconite, 1% quartz, 1% K-feldspar and 1% hematite. In hand sample, abundant brachiopod fossil fragments, glauconite, hematite and pyrite intersperse throughout a matrix of detrital silt-sized quartz grains. Mild brecciation occurs at the top of this bed, with a higher concentration of glauconite in this zone. Pyrite and hematite are concentrated in the basal half of the lithofacies and are largely unrepresented in the point count and XRD data.

Dolostone

Trace amounts of dolostone exist throughout the basal siliciclastic Eau Claire, while dolostone dominates the lithology of the upper Eau Claire. The abundance of dolostone in the upper Eau Claire is largely inferred from wireline logs and is confirmed from RSWC's and cuttings. The dolostones are dominantly packstone to grainstone with trace oolitic beds.

Greensands

Greensand beds are green to dark grey in color, highly mottled, and have a total thickness of 0.2 ft. (0.06 m) in the VW#1 core. Deposits of greensands occur rhythmically, appearing every 1-6 ft. in unit C. Thin section analysis reveals composition is primarily glauconite, brachiopod fossils, clay, quartz and K-feldspar. Not all greensands contain all aforementioned mineral phases; however, glauconite and clay minerals appear in all of the greensand beds.

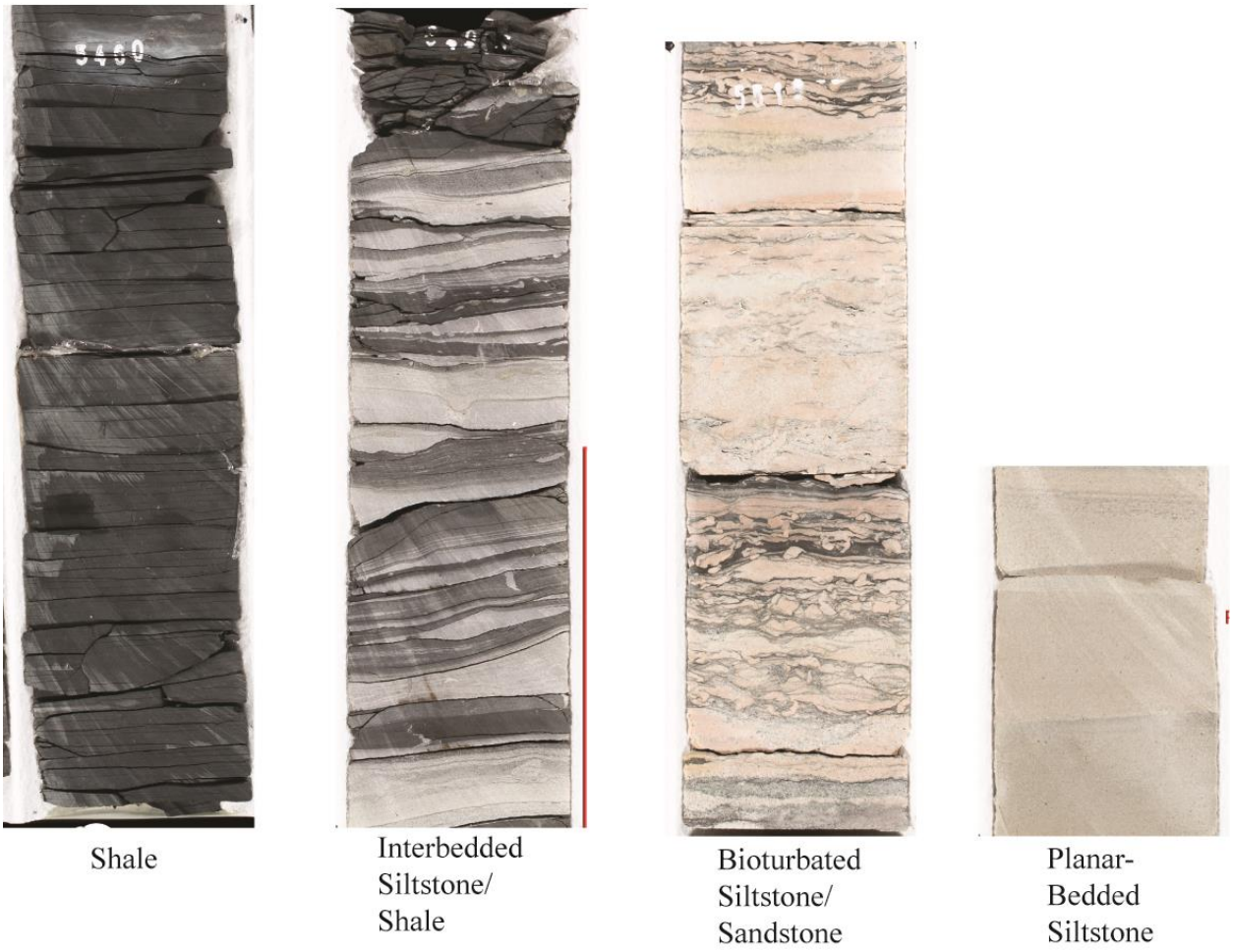

Fig. A.1. Lithofacies found in the Eau Claire drill core from the VW#1 well (Units A-C).

Fig A.2. Lithofacies found in the Eau Claire drill core from the VW#1 well (Units A-C).

APPENDIX B: X-RAY DIFFRACTION MINERALOGY

		Whole Rock Mineralogy (%)												
Unit	Depth (ft)	Quartz	K-feldspar	Plagio-clase	Calcite	Siderite	Ankerite/Fe-Dolomite	Dolomite	Pyrite	Fluorapatite	Barite	Total non-clay	Total clay	Grand total
C	**5425.2**	39	27	2	1	0	0	23	1	0	0	93.0	7.0	100
C	**5434.5**	8	6	1	1	0	0	80	1	0	0	97.0	2.0	99
C	5443.88	23	30	5	2	0	1	2	0	1	1	64.3	35.6	100
B	5448.88	22	28	4	1	0	1	1	2	0	1	60.5	39.5	100
B	5454.21	16	14	6	0	0	2	1	2	0	0	41.9	58.0	100
B	5454.80	12	14	0	4	0	0	3	0	0	0	34.1	66.1	100
B	5459.51	11	15	5	3	0	0	1	1	0	0	35.4	64.7	100
B	5464.80	9	10	0	5	1	0	3	0	0	0	28.0	71.9	100
B	5468.60	11	14	0	1	0	0	4	0	0	0	29.7	70.3	100
B	**5474.1**	45	15	3	1	0	0	31	2	0	0	97.0	2.9	100
B	**5474.85**	2	8	2	1	0	0	84	1	0	0	98.0	2.0	100
B	5485.27	37	31	6	0	0	3	7	2	1	0	86.9	12.9	100
A	5494.90	44	29	6	0	1	2	11	1	0	0	93.4	6.2	100
A	5500.22	24	27	7	0	1	1	1	4	6	0	70.7	29.1	100
A	5505.28	58	27	6	0	0	1	0	1	1	0	94.0	5.5	100
A	5510.34	92	1	2	0	0	0	1	1	0	0	97.8	2.1	100
A	5512.13	33	42	10	1	2	1	0	0	0	1	90.2	9.7	100
							Average							
	Unit A	50	25	6	0	1	1	3	1	1	0	89	11	
	Unit B	18	17	3	2	0	1	15	1	0	0	57	43	
	Unit C	23	21	3	1	0	0	35	1	0	0	85	15	

Table B.1. XRD Mineralogy for the Eau Claire Formation at the IBDP. Samples with bolded depths were run by the author at the ISGS XRD laboratory, while the remainder of the samples were analyzed by Schlumberger Carbon Services at their commercial laboratory.

Unit	Depth (ft)	Clay Mineralogy						
		% I/S expandability	Smectite	Illite/Smectite(I/S)	Illite	Kaolinite	Chlorite	Total Clay
C	**5425.2**		2.1	0.0	67.9	2.0	27.0	100
C	**5434.5**		3.3	0.0	80.2	4.8	11.7	100
C	5443.88	30	0.0	40.0	25.6	15.1	19.3	100
B	5448.88	30	0.0	45.9	42.2	4.4	7.5	100
B	5454.21	30	0.0	56.5	28.9	9.4	5.2	100
B	5454.80	25	0.0	52.8	34.9	3.2	9.1	100
B	5459.51	30	0.0	39.6	48.3	5.5	6.7	100
B	5464.80	25	0.0	48.6	39.4	3.7	8.4	100
B	5468.60	25	0.0	45.3	49.2	0.7	4.8	100
B	**5474.1**		3.0	0.0	39.1	5.1	52.7	100
B	**5474.85**		4.1	0.0	90.2	2.4	3.3	100
B	5485.27	30	0.0	49.2	36.3	7.3	7.2	100
A	5494.90	25	0.0	24.3	44.0	10.8	20.9	100
A	5500.22	30	0.0	55.1	39.9	2.1	2.8	100
A	5505.28	20	0.0	33.0	59.6	2.1	5.3	100
A	5510.34	20	0.0	42.0	41.6	8.3	8.1	100
A	5512.13	25	0.0	51.5	42.1	3.9	2.5	100

Table B.2. XRD clay mineralogy for the Eau Claire Formation at the IBDP. Samples with bolded depths were analyzed by the author at the ISGS XRD laboratory, while Schlumberger Carbon Services analyzed the rest of the samples at their commercial laboratory.

APPENDIX C: GRAIN SIZE

Well	Depth (ft)	Depth (m)	Grain Size (um)	φ	σ	Sorting	Unit
VW1	5036	1535.0	52.1	4.3	0.9	Moderately Sorted	D
VW1	5078	1547.8	42.1	4.6	0.7	Moderately Well Sorted	D
VW1	5078B	1547.8	530.9	0.9	1.9	Poorly Sorted	D
VW1	5350	1630.7	62.6	4.0	0.7	Moderately Well Sorted	D
VW1	5367	1635.9	63.4	4.0	0.8	Moderately Sorted	C
VW1	5378	1639.2	58.1	4.1	0.7	Moderately Sorted	C
VW1	5418	1651.4	42.4	4.6			C
VW1	5425.2	1653.6	53.9	4.2			C
VW1	5430.6	1655.2	31.2	5.0			C
VW1	5434.1	1656.3	42.0	4.6			C
VW1	5434.5	1656.4	42.0	4.6			C
VW1	5441.4	1658.5	48.8	4.4			C
VW1	5452	1661.8	51.5	4.3			B
VW1	5452	1661.8	4.0	8.0			B
VW1	5452	1661.8	4.0	8.0			B
VW1	5452.3	1661.9	43.4	4.5			B
VW1	5454.6	1662.6	21.6	5.5			B
VW1	5459.9	1664.2	14.5	6.1			B
VW1	5464.8	1665.7	4.0	8.0			B
VW1	5468.6	1666.8	4.0	8.0			B
VW1	5474	1668.5	53.1	4.2			B
VW1	5474	1668.5	4.0	8.0			B
VW1	5474.4	1668.6	47.8	4.4			B
VW1	5474.9	1668.7	4.0	8.0			B
VW1	5475.35	1668.9	4.0	8.0			B
VW1	5486.4	1672.3	26.8	5.2			B
VW1	5491.97	1674.0	40.2	4.6			A
VW1	5494.19	1674.6	47.1	4.4			A
VW1	5501.3	1676.8	195.0	2.4			A
VW1	5502.9	1677.3	149.3	2.7			A
VW1	5503.3	1677.4	52.9	4.2			A
VW1	5503.9	1677.6	56.2	4.2			A
VW1	5512.1	1680.1	81.0	3.6			A
VW1	5513.2	1680.4	168.4	2.6			A
VW1	5515.8	1681.2	192.1	2.4			A
VW1	5516.4	1681.4	201.2	2.3			A
VW1	5518.8	1682.1	183.1	2.4			A
VW2	5390.9	1643.1	53.5	4.2	0.9	Moderately Sorted	A
VW2	5391.62	1643.4	43.8	4.5	0.7	Moderately Well Sorted	A

VW2	5393.55	1644.0	44.1	4.5	0.8	Moderately Sorted	A
VW2	5396.65	1644.9	257.7	2.0	1.3	Poorly Sorted	A
VW2	5401.35	1646.3	57.6	4.1	0.8	Moderately Sorted	A
VW2	5414.65	1650.4	235.0	2.1	0.9	Moderately Sorted	A
VW2	5415	1650.5	68.7	3.9	0.7	Moderately Well Sorted	A
VW2	5416.12	1650.8	57.8	4.1	0.7	Moderately Sorted	A
VW2	5423.25	1653.0	50.4	4.3	0.7	Moderately Well Sorted	A
VW2	5423.4	1653.1	94.1	3.4	0.8	Moderately Sorted	A
VW2	5423.6	1653.1	31.4	5.0	0.7	Moderately Sorted	A
VW2	5425.25	1653.6	50.4	4.3			A
VW2	5449.9	1661.1	42.2	4.6	0.6	Moderately Well Sorted	A
VW2	5455	1662.7	69.5	3.8	0.6	Moderately Well Sorted	A
VW2	5460	1664.2	24.0	5.4	0.6	Moderately Well Sorted	A
VW2	5495	1674.9	24.7	5.3	0.5	Moderately Well Sorted	A
VW2	5505	1677.9	33.1	4.9	0.8	Moderately Sorted	A
Average			73.4				

Table C.1. Grain size for the Eau Claire Formation from all three wells at the IBDP site. $\phi = -\log_2$(grain size in mm). σ is the standard deviation of ϕ, and represents the degree of sorting of the sample.

APPENDIX D: POROSITY AND PERMEABILITY

Routine Core Analysis, Eau Claire Formation, IBDP

Depth (ft)	Length (cm)	Diameter (cm)	Grain Density (g/cm3)	Helium Porosity (%)	Air Permeability (mD)	Notes	Depositional Unit
VW#2							
5390.25	5.268	3.797	2.64	16.35	0.405		
5391.00	5.204	3.799	2.66	10.76	0.473		
5392.75	5.177	3.797	2.62	8.70	0.235		
5393.20	5.334	3.803	2.66	8.16	0.103		
5396.70	5.192	3.800	3.02	6.71	0.036		
5397.25	5.279	3.799	2.62	10.22	0.111		
5398.85	5.317	3.799	2.66	7.86	0.120		
5399.40	5.245	3.794	2.70	4.58	0.939		
5401.28	5.346	3.800	2.64	9.37	0.079		
5401.83	5.227	3.799	2.68	7.55	0.080		
5402.44	5.321	3.781	2.67	6.51	0.013		
5403.95	5.217	3.796	2.62	8.33	0.134		
5404.90	5.273	3.786	2.67	6.73	0.040		
5405.60	5.212	2.571	2.62	11.18	0.028		
5407.70	5.215	2.576	2.65	10.07	9.349		
5408.45	5.188	3.792	2.64	8.69	0.356		
5409.80	5.219	3.796	2.63	10.34	0.324		
5410.5	5.224	3.804	2.72	6.31	0.024	Schlumberger Analysis	Unit C
5410.85	5.190	2.579	2.65	11.83	6.058		
5411.53	5.146	2.556	2.70	7.75	0.006		
5412.25	5.210	3.797	2.64	9.69	0.351		
5414.55	5.250	3.791	2.91	2.72	0.004		
5416.20	5.208	3.805	2.66	7.79	0.144		
5417.22	4.960	3.805	2.64	9.47	0.137		
5418.25	4.988	3.801	2.67	9.54	0.164		
5419.33	5.196	3.804	2.70	7.35	0.111		
5421.70	5.304	3.804	2.62	9.66	0.121		
5423.30	5.264	3.803	2.65	7.72	0.084		
5424.30	5.203	2.577	2.65	8.07	0.011		
5425.55	5.345	3.801	2.68	3.28	0.015		
5426.70	5.209	3.805	2.69	6.99	0.062		
5427.52	5.148	2.568	2.65	10.80	0.042		
5428.37	4.987	3.793	2.68	11.45	0.149		
5429.10	5.215	2.581	2.63	8.03	2.098		
5429.67	6.387	3.793	2.98	5.59	0.004		
5432.95	4.992	3.809	2.65	4.10	0.231		
5449.9	3.004	2.315	2.64	16.04	0.039		
CCS#1							
5474.80				9.92	0.133	Weatherford Analysis	Unit C
5475.55				8.72	0.053		
5476.40				15.36	0.326		
5480.60				12.50	0.054		
5474.70				10.88	0.064		
5475.45				8.50	0.026		

5476.45				13.35	0.009	Weatherford Analysis	
5480.50				12.62	0.008		
VW#1							
5350.00	0.92	0.91	2.62	10.08	0.03	Schlumberger Analysis	
5367.00	1.10	0.92	2.68	6.46	8.24		
5378.00	0.98	0.92	2.66	12.84	0.22		
5418.00	0.37	0.89	2.65	5.70	12.39		
5426.60	6.65	2.53		12.25		ISGS Analysis	Unit C
5430.65	5.43	2.53		13.74			
5433.90	6.65	2.53		9.96			
5437.75			2.65	11.20	0.28	Schlumberger Analysis	
5439.60	6.92	2.53		15.57		ISGS Analysis	
5443.90			2.68	5.98	1.62E-04	Approx. from MICP	
5445.30	6.87	2.53		11.83		ISGS Analysis	
5448.90			2.67	2.57	1.55E-05	Approx. from MICP	Unit B
5454.20			1.74	2.19	1.00E-05		
5459.50			2.75	3.02	3.43E-05		
5473.50	7.00	2.53		3.29		ISGS Analysis	
5481.10	7.00	2.53		0.88		ISGS Analysis	
5485.30			2.69	3.07	1.64E-05	Approx. from MICP	
5488.50	7.15	2.53		2.29		ISGS Analysis	Unit A
5493.00			2.67	9.30	0.24	Schlumberger Analysis	
5494.70	4.88	2.53		7.68		ISGS Analysis	
5504.40	7.11	2.53		3.21			
5507.20	7.20	2.53		5.79			
5510.65			2.66	5.90	16.72	Schlumberger Analysis	
5511.70	7.35	2.53		4.60		ISGS Analysis	
5514.10			2.68		3.30	Weatherford Analysis	
5515.00			2.66		7.50		
5516.30			2.62		10.90		
5517.00	6.98	2.53		13.22		ISGS Analysis	
5518.50			2.67	3.90	0.19	Weatherford Analysis	
5519.20			2.63	10.70	2.32		
5520.25			2.65	7.70	17.74		
5521.05			2.64	7.60	15.76		
5522.30			2.64	6.10	12.92		
5523.35			2.65	4.60	1.61		
5524.15			2.64	6.30	9.67		
5525.40			2.65	8.70	21.44		
5526.15			2.65	5.90	0.88		

Averages	**Porosity**	**Permeability**
Unit A	6.7%	8.7mD
Unit B	2.5%	19 nD
Unit C	9.4%	0.9 mD

Table D.1. Porosity and permeability data for the Eau Claire formation from 3 wells at the IBDP.

APPENDIX E: WIRELINE LOGS

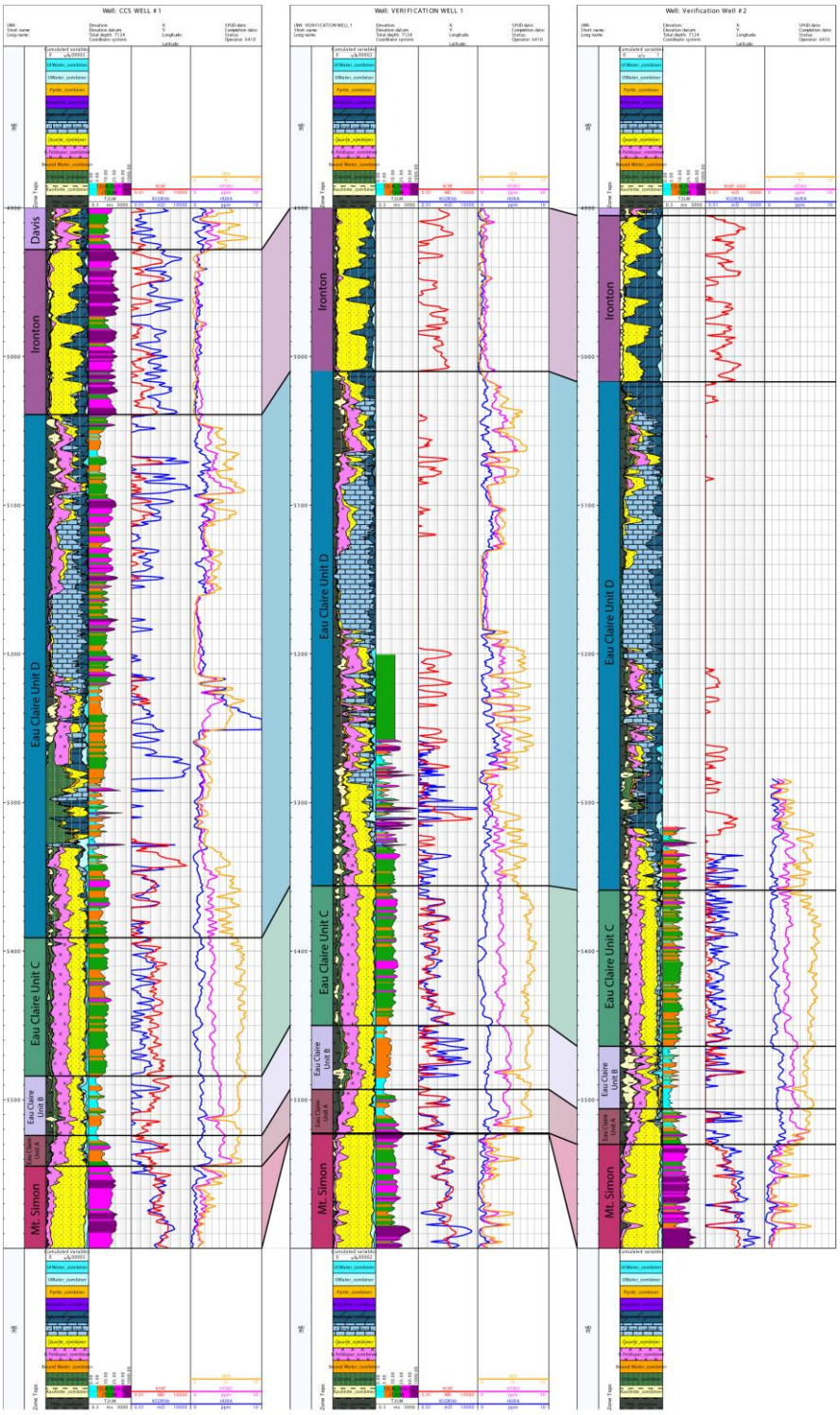

Fig. E.1. Wireline log for the Eau Claire formation from the CCS#1, VW#1 and VW#2 wells. Logs include a spectral gamma ray log, permeability, and two logs computed by proprietary Schlumberger algorithms (Elemental analysis and facies logs).